



DOCTORAL THESIS

Presented to the Department of Pharmacy  
Graduate School of Pharmaceutical Science

The University of Naples Federico II  
For the Degree of

**DOCTOR OF PHILOSOPHY**

**ADVANCED TARGETING APPROACHES  
TO DRIVE NANOPARTICLES INSIDE THE BODY**

by

ALESSANDRO VENUTA

APPROVED BY

Supervisor: Prof. Fabiana Quaglia, PhD

PhD Program Coordinator: Prof. MariaValeria D'Auria, PhD

University of Napoli Federico II, Napoli, Italy

March 2018

## Abstract

The development of new chemical entities is expensive and time consuming. Therefore, the path taken by research into the last century was directed to find new methods to exploit the already existing pharmaceutical tools. “There’s plenty of room at the bottom” was the title of a lecture delivered in 1959 by Richard Feynman, who introduced the concept of nanotechnology as an important field for future research. This novel science covers areas of biomedical disciplines and engineering involved in the development of materials and devices in the [nanometer scale](#). These systems is nowadays drawing major attention in the medical field for the delivery of therapeutics, especially in the treatment of complex diseases such as cancer. In fact, this malignancy possesses unique features that perfectly suits the concepts underlying nano delivery. Amongst all, the enhanced and permeability retention effect (EPR) certainly is widely recognized as the rational basis for using nanotherapeutics in the treatment of cancer. EPR is phenomenon by which macromolecules preferentially accumulate in tumor tissues due to immature, tortuous, and multi-fenestrated cancer vessels. Moreover, the opportunity to improve drug pharmacokinetics without affecting the chemical features of the carried molecules, provides not only the ability to overcome several biological obstacles that normally reduce the accumulation of therapeutics into the target area but also to increase their therapeutic impact.

The general aim of this thesis was to develop different strategies for the delivery of conventional chemotherapeutics in the field of cancer therapies.

In fact, different nanocarriers for cancer treatment have been developed so far basically differing for composition, size and shape, as well as stiffness. Particularly promising are those based on amphiphilic block polyester copolymers (NPs). Polymeric NPs of poly( $\epsilon$ -caprolactone) (PCL) covered with a hydrophilic poly(ethylene glycol) (PEG) can be employed as passive delivery system and possibly decorated with targeting ligands such as folate to accumulate in cancerous tissue. However, the density and conformation of PEG on the surface affect the exposition of small targeting ligands and the receptor mediated cell uptake. In this context Chapter 3 – *Shedding light on surface exposition of poly(ethylene glycol) and folate targeting units on nanoparticles of poly( $\epsilon$ -caprolactone) diblock copolymers: beyond a paradigm* – is dedicated to PEG-PCL NPs targeted to folate receptor. The impact of preparation method on PEGylation extent and folate surface exposition is fully addressed in the attempt to relate quality attributes of NPs to biological behavior.

Although the EPR effect has been postulated to carry NPs and spread inside the cancer tissue, only a small percentage (0.7% median) of the total administered nanoparticle dose is usually able to reach a solid tumor. New strategies based on the microscale and combining different disciplines together such as biology, chemistry, physics and engineering has been proposed to address this issue. The multistage vector (MSV) is a platform that combine nano and microcarriers conceived to overcome the biological obstacles in a sequentially manner. This platform consists of three components. The first stage is a discoidal porous silicon microparticles designed to navigate into the circulatory stream and preferentially adhere to the tumor abnormal endothelial wall. Depending on the application, different types of NPs can be loaded into the pores of the microparticle as second stage. In contrast to the discoidal microparticle, the second stage enter into the cells by exploiting the fenestrature of vascular endothelium and finally releases the third stage, i.e. the therapeutic agent that can be freely selected depending on the application. In addition to this general concept, a new generation of MSV that display additional properties was developed in the attempt to improve the therapeutic performance of the platform. As an example MSV that possesses a biomimetic coating, novel approaches to load multiple types of nanotherapeutics inside the microdiscoidal carrier and more recently the application of this platform to cancer immunotherapy have been proposed. Despite all these applications, this versatile vector has not yet been used to treat brain disease. This is because brain represent a major challenge in drug delivery due to the presence of the Blood Brain Barrier (BBB). Within this framework the aim of the project described in Chapter 4 – *Strategies to overcome the Blood Brain Barrier (BBB)* – is the development of novel approaches based on the combination of micro- and nano-delivery systems to treat brain metastases arisen from primary tumors as melanoma and breast cancer. The idea is to functionalize the micro-vector surface to promote preferential accumulation at the brain microvasculature and after obtaining the intended accumulation, near the endothelial wall, the capacity of transporting simultaneously more than one active component in the porous micro particle. The concept is validated by the development of in vitro and in vivo models. Despite the considerable progress made with NPs, only a limited number of NPs have been approved for clinical use. As an example, Doxil<sup>®</sup> the first FDA approved formulation for the delivery of Doxorubicin (Dox) is able to reduced systemic side effects compared to the free drugs but not to significantly improve the antitumor effects into the metastatic diseases. This clinical evidence suggests that further delivery approaches needs to be developed and that there is a need for an in depth study of the anatomical knowledge of

the EPR. In this context, the aim of the work described in Chapter 2 – *Synthesis and characterization of rationally-designed Dextran-Doxorubicin conjugate: a novel strategy to improve the antitumor efficacy of doxorubicin in multiple breast cancer liver metastases* – is to develop a rationally-designed Dox-dextran conjugate with appropriate molecular weight (MW) based on estimated EPR effect in established liver metastases to overcome the limited clinical efficacy of PEGylated liposomes and Dox.

In the two annexes the development of a novel antibacterial polymeric film of poly(lactic-co-glycolic acid) (PLGA) for the release of nitric oxide (NO) under visible light is reported (Annex I) and a study of the growth of the drug delivery literature published during 1974-2015 was discussed (Annex II).

<b>CHAPTER 1</b>	<b>4</b>
<b>INTRODUCTION AND AIM</b>	<b>4</b>
<b>1. Disadvantages of standard chemotherapy</b>	<b>5</b>
<b>2. Fundamentals of Nanotechnology</b>	<b>6</b>
2.1 Nanotechnology and cancer	7
2.2 Polymers in cancer	11
2.3 Drug Conjugates	11
2.4 Physical entrapment: Polymeric nanoparticles (NPs)	16
<b>3 Microsized drug delivery systems</b>	<b>25</b>
3.1 Multistage vector (MSV)	25
3.2 Fabrication of MSV	27
3.3 Second generation of MSV	28
<b>4 Brain therapy</b>	<b>32</b>
<b>5 Aim of the work</b>	<b>33</b>
<b>CHAPTER 2</b>	<b>35</b>
<b>SYNTHESIS AND CHARACTERIZATION OF RATIONALLY-DESIGNED DEXTRAN-DOXORUBICIN CONJUGATE: A NOVEL STRATEGY TO IMPROVE THE ANTITUMOR EFFICACY OF DOXORUBICIN IN MULTIPLE BREAST CANCER LIVER METASTASES.</b>	<b>35</b>
<b>1 Introduction</b>	<b>36</b>
<b>2 Experimental section</b>	<b>37</b>
2.1 Materials	37
2.2 Synthesis of Dextran <sub>10k</sub> -Doxorubicin (Dex-Dox)	38
2.3 Cancer cell preparation	39
2.4 Cell cytotoxicity	39
2.5 In Vivo Model of Breast Cancer Liver Metastasis	40
2.6 Models of breast and lung cancer liver metastasis and primary breast tumor	40
2.7 Intravital microscopy analysis	40
<b>3 Results and discussion</b>	<b>41</b>
3.1 Molecular weight dependent tumors accumulation of dextrans	41
3.2 Synthetic strategy	42
3.3 Cell proliferation assay	43
<b>4 Conclusions</b>	<b>44</b>
<b>CHAPTER 3</b>	<b>48</b>

<b>SHEDDING LIGHT ON SURFACE EXPOSITION OF POLY(ETHYLENE GLYCOL) AND FOLATE TARGETING UNITS ON NANOPARTICLES OF POLY(E-CAPROLACTONE) DIBLOCK COPOLYMERS: BEYOND A PARADIGM</b>	<b>48</b>
<b>1. Introduction</b>	<b>50</b>
<b>2 Experimental section</b>	<b>51</b>
2.1 Materials	51
2.2 Copolymer characterization	52
2.3 Synthesis of MPEG <sub>s</sub> -PCL and MPEG <sub>L</sub> -PCL	52
2.4 Synthesis of Fol-PEG-PCL	53
2.5 Preparation and characterization of nanoparticles	54
2.6 Intracellular uptake of NPs in cancer cells	55
2.7 Capture of NPs by human macrophages	56
2.8 Statistical analysis:	57
<b>3 Results and discussion</b>	<b>57</b>
3.1 Synthetic strategy	57
3.2 Influence of PEG length on nanoparticle shell	60
3.3 Interaction of nanoparticles with HSA	63
3.4 Interaction of nanoparticles with human macrophages	64
3.5 Cellular uptake of nanoparticles in KB cancer cells	65
3.6 Modulating degree of valency in folate-decorated nanoparticles based on PCL-mPEG <sub>s</sub>	67
<b>4 Conclusions</b>	<b>69</b>
<b>5 Acknowledgments</b>	<b>69</b>
<b>CHAPTER 4</b>	<b>74</b>
<b>STRATEGIES TO OVERCOME THE BLOOD BRAIN BARRIER (BBB)</b>	<b>74</b>
<b>1 Introduction</b>	<b>75</b>
<b>2 Experimental section</b>	<b>77</b>
2.1 Materials	77
2.2 Oxidation and APTES modification of MSV	77
2.3 Polysorbate 80 (Tween 80) coating	77
2.4 Conjugation of holo-Transferrin human (hTf) to MSV	77
2.5 Fluorescent particles	78
<b>3 In Vivo Studies</b>	<b>78</b>
3.1 Inductively coupled plasma mass spectroscopy (ICP-MS)	79
3.2 Immunohistochemistry (IHC)	79
3.3 Intravital Microscopy (IVM)	80
3.4 In Vivo Imaging Systems (IVIS)	80
<b>4 Result and discussion</b>	<b>81</b>
4.1 Particles characterization	81

4.2 Brain accumulation	83
<b>5 Conclusion</b>	<b>87</b>
<b>GENERAL CONCLUSIONS</b>	<b>95</b>
<b>ANNEX-I</b>	<b>98</b>
<b>PHOTO-ANTIMICROBIAL POLYMERIC FILMS RELEASING NITRIC OXIDE WITH FLUORESCENCE REPORTING UNDER VISIBLE LIGHT</b>	<b>98</b>
<b>ANNEX-II</b>	<b>115</b>
<b>EVOLUTION OF THE SCIENTIFIC LITERATURE ON DRUG DELIVERY: A 1974- 2015 BIBLIOMETRIC STUDY</b>	<b>115</b>



## ABBREVIATIONS

ABC	ATP-binding cassettes
BBB	Blood brain barrier
BRAF	B-Raf proto-oncogene serine/threonine kinase
CNS	Central nervous system
CYPs	Cytochromes
DC	Dendritic cells
DCC	Dicyclohexyl carbodiimide
DDS	Drug delivery system
DLS	Dynamic light scattering
DNA	Deoxyribonucleic Acid
ECM	Extracellular matrix
EMA	European Medicines Agency
EPR	Enhanced permeability and retention
ER	Estrogen receptor
EU	European Union
FDA	Food and Drugs Administration
FRs	Folate receptors
GLUT-1	Glucose transporter 1
GPCRs	G protein coupled receptors
GPI	Glycosylphosphatidylinositol
HER2	Human epidermal growth factor
HHA	6- hydroxyhexanoic acid
HPMA	N-(2-hydroxypropyl)methacrylamide
IFN-I	Type I interferons
INPG	Injectable nanoparticle generator

LA	Lactic acid
MDR1	Multidrug resistance protein 1
MHCs	Major histocompatibility complexes
MMP2	Metalloproteinase-2
mPEG-OH	Monomethoxy poly(ethyleneglycol)
MPS	Mononuclear phagocyte system
MSV	Multi stage vector
MW	Molecular weight
NCI	National Cancer Institute
NCL	Nanotechnology Characterization Laboratory
NIST	National Institute of Standards and Technology
NPs	Nanoparticles
PCFT	Proton coupled folate transporter
PCL	Poly( $\epsilon$ -caprolactone)
PEG	Polyethylene glycol
PGA	Polyglycolides
Pgp	P-glycoprotein
PLA	Poly lactides
PLGA	Poly(lactic-co-glycolic acid)
PR	Progesteron receptor
PVP	Polyvinylpyrrolidone
RFC	Reduced folate carrier
RGD	Arginylglycylaspartic acid
ROP	Ring-opening polymerization
ROS	Reactive oxygen species
SEM	Scanning electron microscopy
siRNA	Small interfering RNA

SLC	Solute carrier
SRS	Stereotactic radiosurgery
TEM	Transmission electron microscopy
TJ	Tight Junctions
TNBC	Triple negative breast cancer
TNF- $\alpha$	Tumor necrosis factor
TfRs	Transferrin receptors
US	United States
VEGF	Vascular endothelial growth factor
WBRT	Whole brain radiotherapy

# **Chapter 1**

## **Introduction and aim**

## ***1. Disadvantages of standard chemotherapy***

Cancer can be defined as a heterogeneous disease and one of the leading cause of death worldwide.<sup>1</sup> Cancer can generate from different tissues but the common features is the loss of cell-proliferation control with an abnormal growth of the diseased tissue. Furthermore the formation of metastasis, a secondary cancer that spreads in the body and leads to multiple organ failure and death, is a recurring event.<sup>2</sup> The origin and type of cancer are important elements for the choice of the best treatment for a cancer patient. Currently the treatment of cancer is based on a combination of drugs therapy (chemotherapy), surgery, radiotherapy and immunotherapy. However, these approaches present some drawbacks such as the high cost of the therapy for the radio or the limitation of the surgery to treat only well localized tumor mass. The chemotherapy provides an opportunity to decrease the costs of treatment and to reach also metastasis but is associated to many side effects due to the inability of the drugs to kill only the cancerous cells or to accumulate only at the target site. Other limitations come from the route of administration. Usually chemotherapeutic agents are administered by intravenous route but most of them are poorly water-soluble and need toxic vehicles for administration (Chremophor®, ethanol, surfactants). The effectiveness of a chemotherapy is also limited by intrinsic or acquired drug resistance. The most common forms of chemoresistance are drug inactivation, drug target alteration, drug efflux, DNA damage repair and cell death inhibition.<sup>3</sup> Different strategies have been tried in order to improve the quality and reduce the side effects of the systemic administration of the chemotherapeutic agents such as the chemical modification of the drug itself but the most promising seems to be the application of nanotechnology.

---

<sup>1</sup> Fitzmaurice, C., Dicker, D., Pain, A., Hamavid, H., Moradi-Lakeh, M., MacIntyre, M. F., et al. (2015). The Global Burden of Cancer 2013. *JAMA Oncol*, 1(4), 505-527.

<sup>2</sup> Mehlen, P., & Puisieux, A. (2006). Metastasis: a question of life or death. *Nat Rev Cancer*, 6(6), 449-458.

<sup>3</sup> Wilson, T. R., Longley, D. B., & Johnston, P. G. (2006). Chemoresistance in solid tumours. *Ann Oncol*, 17 Suppl 10, x315-324.

## 2. Fundamentals of Nanotechnology

Nanotechnology is referred to materials and healthcare products engineered at the molecular scale approximately in the size range from 1 nm to 100 nm (Figure 1).<sup>4</sup>

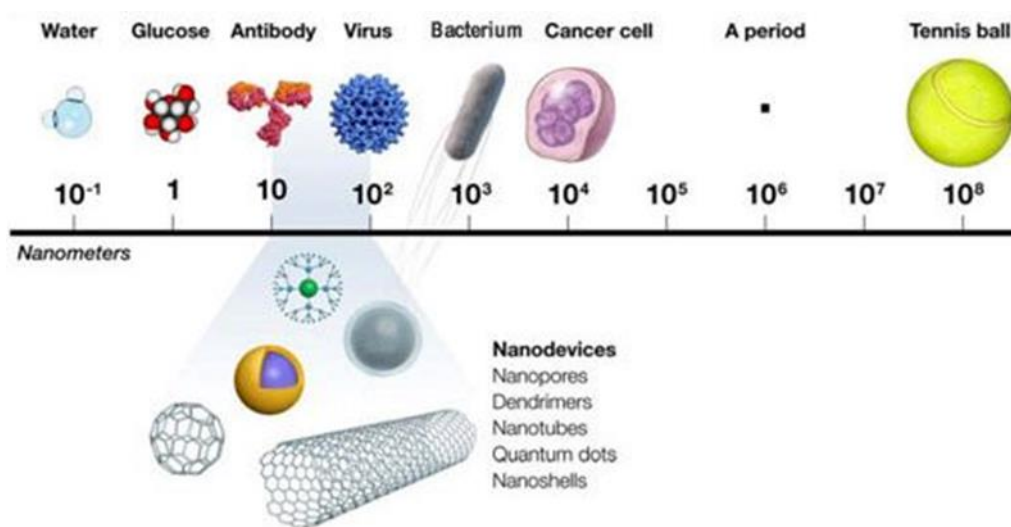


**Figure 1.** Comparison of various biological assemblies and nanodevices.

The application of nanotechnology into the medical field is called nanomedicine. The European Medicines Agency (EMA) had outlined a working definition of nanomedicine based on three points: i) systems designed for clinical applications, ii) at least one component at nano-scale and iii) resulting in specific properties and characteristics [related to the specific nanotechnology application and characteristics for the intended use (route of admin and dose) or associated with the expected clinical advantages of nano- (e.g. preferential organ/tissue distribution)]. As well the Food and Drug Administration (FDA) in the United States (US) defined as products that contain or are manufactured using materials in the nano-scale range or products that contain or are manufactured using certain materials that exhibit related dimension-dependent properties or phenomena. The word “products” (or “FDA-regulated products”) is referred to materials or other substances regulated by FDA, including drugs, biological products, medical devices, food substances (including food for animals) and cosmetic products.<sup>5</sup> This technology arise to aid

<sup>4</sup> De Jong, W. H., & Borm, P. J. (2008). Drug delivery and nanoparticles: applications and hazards. *Int J Nanomedicine*, 3(2), 133-149.

<sup>5</sup> US FDA. Considering Whether an FDA-Regulated Product Involves the Application of Nanotechnology. <http://www.fda.gov/RegulatoryInformation/Guidances/ucm257698.htm>.

molecules that cannot be used due to own toxicity by increasing their therapeutic efficacy. However, these products are not regulated by a specific legislation in the European Union (EU) and in the US since they are included in the regulatory system of medical products as is stands. The high standards of the medical product are difficult to achieve by this new nano sized carriers due to size related physicochemical properties and unexpected biological effects. For this reason they require additional quality control compared to standard products. Accurate parameters such as stability, size, physical morphology, solubility, etc have to be identified and translated into standardised and regulatory accepted development methods. In order to ensure the safety of nanodevices the National Cancer Institute (NCI) together with the National Institute of Standards and Technology (NIST) and the FDA established the Nanotechnology Characterization Laboratory (NCI-NCL) to perform preclinical efficacy and toxicity testing. Recently, also the EU founded the European Nanotechnology Characterisation Laboratory (EU-NCL) that work in close partnership with the NCI. The NCLs accelerates the transition of basic nanoscale particles and devices into clinical applications. Therefore, the application of these nanotherapeutics is retarded by the lack of a specific regulatory system but despite this the great potential to improve medical treatments of disease such as cancer resulted in the last few decades in a tremendous impact on the field of research.

## **2.1 Nanotechnology and cancer**

Nanocarriers are expected (i) to protect drug cargo and to improve its pharmacokinetics; (ii) to provide the drugs with the ability to overcome several biological obstacles that normally reduce the accumulation of therapeutics into the target area; (iii) to provide multifunctionality by loading various compounds such as two different drugs or a drug with an imaging agent; (iv) to increase the therapeutic impact by interacting with specific tissues and cells through surface functionalization; (v) to impact clinical application of several drugs or potential drugs. Several types of nanovectors such as liposomes<sup>6</sup>, polymeric nanoparticles<sup>7,8</sup>, micelles<sup>9</sup>, and inorganic nanoparticles<sup>10,11</sup> have been exploited, being the intravenous injection the preferred route of

---

<sup>6</sup> Akbarzadeh, A., Rezaei-Sadabady, R., Davaran, S., Joo, S. W., Zarghami, N., Hanifehpour, Y., et al. (2013). Liposome: classification, preparation, and applications. *Nanoscale Res Lett*, 8(1), 102.

<sup>7</sup> Banik, B. L., Fattahi, P., & Brown, J. L. (2016). Polymeric nanoparticles: the future of nanomedicine. *Wiley Interdiscip Rev Nanomed Nanobiotechnol*, 8(2), 271-299.

<sup>8</sup> Grottkau, B. E., Cai, X., Wang, J., Yang, X., & Lin, Y. (2013). Polymeric nanoparticles for a drug delivery system. *Curr Drug Metab*, 14(8), 840-846.

<sup>9</sup> Croy, S. R., & Kwon, G. S. (2006). Polymeric micelles for drug delivery. *Curr Pharm Des*, 12(36), 4669-4684.

<sup>10</sup> Ali, A., Zafar, H., Zia, M., Ul Haq, I., Phull, A. R., Ali, J. S., et al. (2016). Synthesis, characterization, applications, and challenges of iron oxide nanoparticles. *Nanotechnol Sci Appl*, 9, 49-67.

<sup>11</sup> Arvizo, R., Bhattacharya, R., & Mukherjee, P. (2010). Gold nanoparticles: opportunities and challenges in nanomedicine. *Expert Opin Drug Deliv*, 7(6), 753-763.

entry in the body. Since a solid tumor has an abnormal vasculature conformation, its hypoxic environment stimulates pathways resulting in the release of growth factors such as the vascular endothelial growth factor (VEGF) which leads to immature, tortuous, and multi-fenestrated vessels.<sup>12</sup> This unique architecture was observed from Maeda and his colleagues that found that molecules with molecular weight larger than 40-50 kDa showed selective accumulation in tumor tissues and they retained in tumor tissues for long periods.<sup>13</sup> This concept is known as enhanced permeability and retention (EPR) effect and lays the basis for the mechanism of passive accumulation of drugs into the tumor exploited also by nanotherapeutics. It should also be considered that the tumor interstitium has an impaired lymphatic drainage that decreases the clearance of macromolecules. This is due to mechanical forces generated by the growing tumor that deforms the normal tissue and indirectly by warps capillaries and lymphatic vessels.<sup>14</sup> However, progress in developing effective drugs using this approach has been hampered by heterogeneity of EPR effect in different tumor animal models as an example very aggressive tumors that are highly vascularized such as carcinomas showed more blood vessels and the leakage of the particles is higher, while other tumors are characterized by a slower growth resulting in an ineffective accumulation of particles.<sup>15,16</sup>

This evidence paved the way to a novel reductionist approach in drug development to the nanometric level. Reductionism studies a phenomenon separating it in its elementary parts in that a complex system is nothing if not the sum of its parts. In the case of drug delivery the simplistic view of a system that accumulates in tumors only exploiting the anatomical architecture of cancer vessels is not satisfactory because the route of access of nanoparticles is dynamically remodelled. Tumour is a complex entity and all the single variables must be considered such as rates of extravasation, binding or uptake by tumour cells, release from binding, rate of elimination from blood, as well as plasma volume, tumour interstitial volume, tumour cellular volume and tumour vascular and some of this cannot be studied *in vivo*.<sup>17</sup>

---

<sup>12</sup> Lee, S. H., Jeong, D., Han, Y. S., & Baek, M. J. (2015). Pivotal role of vascular endothelial growth factor pathway in tumor angiogenesis. *Ann Surg Treat Res*, 89(1), 1-8.

<sup>13</sup> Matsumura, Y., & Maeda, H. (1986). A new concept for macromolecular therapeutics in cancer chemotherapy: mechanism of tumor-tropic accumulation of proteins and the antitumor agent smancs. *Cancer Res*, 46(12 Pt 1), 6387-6392.

<sup>14</sup> Jain, R. K., Martin, J. D., & Stylianopoulos, T. (2014). The role of mechanical forces in tumor growth and therapy. *Annu Rev Biomed Eng*, 16, 321-346.

<sup>15</sup> Hansen, A. E., Petersen, A. L., Henriksen, J. R., Boerresen, B., Rasmussen, P., Elema, D. R., et al. (2015). Positron Emission Tomography Based Elucidation of the Enhanced Permeability and Retention Effect in Dogs with Cancer Using Copper-64 Liposomes. *ACS Nano*, 9(7), 6985-6995.

<sup>16</sup> Wang, A. Z. (2015). EPR or no EPR? The billion-dollar question. [10.1126/scitranslmed.aac8108]. *Science Translational Medicine*, 7(294), 294ec112.

<sup>17</sup> Florence, A. T. (2012). Reductionism and complexity in nanoparticle-vector drug targeting. *J Control Release*, 161(2), 399-402.

In any case, efforts in the field of research have been made to increase the accumulation of nanotherapeutics in cancer tissue by EPR.

Nanoparticles may be recognized by the host immune system particularly the mononuclear phagocyte system (MPS) which rapidly clear-up nanoparticles from the circulation and accumulate them into liver, spleen and bone marrow. Hydrophobicity of the surface determine the quantity of blood components that bind the carrier. Therefore to minimize the opsonization and to evade the uptake from the MPS several strategies have been tried to make the particles “stealth”. Coating with hydrophilic polymers or surfactants can prevent complement activation and impart long-circulating properties. However, these coating polymers may also greatly decrease the cellular uptake efficiency of nanoparticles. For this reason, novel approaches were developed by taking advantage of the opportunity of modifying the surface and the physico-chemical properties of the nanovectors, such as the active targeting approach and the stimuli-responsive particles. The active strategies requires on the surface of the nanoparticles the conjugation of several moieties that are able to bind receptors mainly expressed on cancer cells like the G protein coupled receptors (GPCRs), integrins, folate receptors (FRs) and transferrin receptors (TfRs).<sup>18</sup> In addition to the cellular target another promising approach is the vascular target. Integrins are a family of heterodimeric transmembrane glycoproteins involved in a wide range of cell-to-extracellular matrix (ECM) and cell-to-cell interactions. As cell surface receptors, integrins readily interact with extracellular ligands and play a vital role in angiogenesis, leukocytes function and tumor development, which sets up integrins as an excellent target for chemotherapy treatment. The peptide ligands containing the arginine-glycine-aspartic acid (RGD), which displays a strong binding affinity and selectivity to integrins, particularly to integrin  $\alpha\beta3$ , have been developed to conjugate with various conventional chemotherapeutic agents, such as small molecules, peptides and proteins, and nanoparticle-carried drugs for integrin targeted therapeutic studies. The RGD-decorated nano delivery systems have been extensively investigated in that after bearing multiple RGD-peptides, can be more readily internalized via receptor-mediated endocytosis. Instead the stimuli-responsive nanoparticles can release their cargo in two different ways or exploiting the physical features of the tumor environment such as the low pH or through external stimuli such

---

<sup>18</sup> Akhtar, M. J., Ahamed, M., Alhadlaq, H. A., Alrokayan, S. A., & Kumar, S. (2014). Targeted anticancer therapy: overexpressed receptors and nanotechnology. *Clin Chim Acta*, 436, 78-92.

as light and magnetic field and temperature.<sup>19,20</sup> Actually, there are several nanotherapeutics that have been approved for clinical use by the FDA in the United States and by EMA in European countries (Table 1). The first FDA-approved nanoformulation was Doxil®.<sup>21</sup> Doxil® is a PEGylated liposome encapsulating doxorubicin that minimizes side effects, such as cardiotoxicity associated to the drug. All these systems are liposome based formulations except for Abraxane® that consists of human serum albumin bound to paclitaxel and allows to deliver paclitaxel, that is the standard treatment for metastatic breast cancer, without using solvents as vehicles that cause severe toxicity.<sup>22</sup> It is also noteworthy that most of these formulations are non-PEGylated and all of them are supposed to accumulate through the passive mechanisms.

**Table 1** FDA and EMA-approved nanoformulations.

Name	Particle type/drug	Approved application	Approval (year)
<b>Doxil®/Caelyx®</b>	Liposomal doxorubicin (PEGylated)	Ovarian cancer HIV-associated Kaposi's sarcoma Multiple myeloma	FDA (1995) EMA (1996)
<b>DaunoXome®</b>	Liposomal doxorubicin (non-PEGylated)	HIV-associated Kaposi's sarcoma	FDA (1996)
<b>Myocet®</b>	Liposomal doxorubicin (non-PEGylated)	Metastatic breast cancer	EMA (2000)
<b>Abraxane®</b>	Albumin bound paclitaxel	Advanced non-small cell lung cancer Metastatic breast cancer Metastatic pancreatic cancer	FDA (2005) EMA (2008)
<b>Mepact®</b>	Liposomal mifamurtide (non-PEGylated)	Osteosarcoma	EMA (2009)
<b>Marqibo®</b>	Liposomal vincristine (non-PEGylated)	Philadelphia chromosome-negative acute lymphoblastic leukemia	FDA (2012)
<b>Onivyde®</b>	Liposomal irinotecan (PEGylated)	Metastatic pancreatic cancer	FDA (2015)

<sup>19</sup> Shen, Y., Tang, H., Radosz, M., Van Kirk, E., & Murdoch, W. J. (2008). pH-responsive nanoparticles for cancer drug delivery. *Methods Mol Biol*, 437, 183-216.

<sup>20</sup> Torchilin, V. (2009). Multifunctional and stimuli-sensitive pharmaceutical nanocarriers. *Eur J Pharm Biopharm*, 71(3), 431-444.

<sup>21</sup> Barenholz, Y. (2012). Doxil®--the first FDA-approved nano-drug: lessons learned. *J Control Release*, 160(2), 117-134.

<sup>22</sup> Gradishar, W. J. (2006). Albumin-bound paclitaxel: a next-generation taxane. *Expert Opin Pharmacother*, 7(8), 1041-1053.

## ***2.2 Polymers in cancer***

Chemotherapy is based on the use of anti-cancer drugs that inhibit the fast proliferation of cancer cells but at the same time acting on healthy cells causing several systemic adverse side effects. Furthermore, due to their chemical structure and size, drugs also show low half-life times in the circulation and a low bioavailability. In order to address that drawbacks the use of carriers for the conventional chemotherapeutics can offer significant benefits in the field of cancer therapy. The drugs carriers allow to delivery an active compound in a controlled way (time and release rate) improving the therapeutic window. Among the many approaches for drug delivery the use of polymers have been widely explored in the development of drug carriers due to their versatility. Natural polymers are highly biocompatible and biodegradable and present functional groups (e.g., -COOH, -NH<sub>2</sub>) that can be exploited for further modification. Secondly, synthetic polymers can be simply prepared in term of compositions and properties for a specific application. In particular, the production of biodegradable materials that can be metabolized in the biological environment marked a change in the field of drug delivery. The natural polymers mainly consist of proteins (i.e., albumin and gelatin) and polysaccharides (i.e., hyaluronic acid, chitosan and dextran). The bioabsorbable materials that are commonly used in cancer therapy are polyesters, polyanhydrides, polyphosphoesters. Poly(lactic acid) (PLA), poly(lactic-co-glycolic acid) (PLGA), and poly( $\epsilon$ -caprolactone) (PCL) are the most widely synthetic polymers used for the delivery of anti-cancer drugs. PLGA is obtained through the copolymerization of lactic acid (LA) and glycolic acid, PCL is synthesized by the ROP of  $\epsilon$ -caprolactone ( $\epsilon$ -CL) and PLA can be obtained either from the polycondensation of LA or by the ring opening polymerization (ROP) of lactide. Poly(ethyleneglycol) (PEG) is the most commonly used nonionic polymer in the field of polymer-based drug delivery. Due to high aqueous solubility, PEG polymer is considered as a versatile candidate for the prodrug conjugation. The drugs can be chemically conjugated to the polymer or physically entrapped within the core of polymeric structure formed in aqueous media.

## ***2.3 Drug Conjugates***

Low-molecular weight chemotherapeutics typically spread throughout the body, and this often leads to systemic side effects. In the 1975, Ringsdorf proposed a polymer–drug conjugate model that could enhance the delivery of an anti cancer drug to a tumor.<sup>23</sup> The clinical purpose

---

<sup>23</sup> Ringsdorf, H. (1975), Structure and properties of pharmacologically active polymers. J. polym. sci., C Polym. symp., 51: 135–153. doi:10.1002/polc.5070510111

of polymer–drug conjugate is to produce long-circulating conjugates to taking advantage of passive tumour targeting (EPR), improve drug accumulation to the tumour, reduce drug toxicity and to overcome the mechanisms of drug resistance. Nevertheless, conjugation to hydrophilic polymer can also improve the water solubility of hydrophobic drugs such as doxorubicin and paclitaxel. To develop an optimal polymer conjugate carrier is crucial consider the physiopathology of tumors (e.g., location and vascularization) and the properties of the drug that will be bound to the polymer. Other important aspect is the choice of the polymer–drug linkers. If is too stable could prevent drug release but instead if degrades quickly in aqueous media leads to premature drug release. The polymer must be non-toxic, non-immunogenic and must be able to carry an adequate drug payload. Indeed, many polymers have been used as drug carriers but due to these issues only few have been tested in clinical studies. As an example PEG has been used in the development of drug conjugates<sup>24</sup> but it posses only two terminal groups exploitable for conjugation and this limits the drug-loading. N-(2-hydroxypropyl)methacrylamide (HPMA) copolymers were active against numerous cancer models and are in clinical trials.<sup>25,26</sup> A dextran–doxorubicin conjugate (AD-70) with a molecular weight (MW) of ~70,000 containing drug bound to oxidized dextran was used in a phase I trial and also another dextran-conjugate was clinically tested suggest that natural polymers are suitable for drug delivery.<sup>27,28</sup>

### ***2.3.1 Polymers based conjugate***

An ideal polymeric conjugate consists of i) a polymeric backbone, ii) one or more than one therapeutic component, iii) a spacer that ensures the release of the bioactive molecules and facilitates the conjugation and further iv) an imaging agent and v) a targeting moiety.

---

<sup>24</sup> Greenwald, R. B., Choe, Y. H., McGuire, J., & Conover, C. D. (2003). Effective drug delivery by PEGylated drug conjugates. *Adv Drug Deliv Rev*, 55(2), 217-250.

<sup>25</sup> Bissett, D., Cassidy, J., de Bono, J. S., Muirhead, F., Main, M., Robson, L., et al. (2004). Phase I and pharmacokinetic (PK) study of MAG-CPT (PNU 166148): a polymeric derivative of camptothecin (CPT). *Br J Cancer*, 91(1), 50-55.

<sup>26</sup> Vasey, P. A., Kaye, S. B., Morrison, R., Twelves, C., Wilson, P., Duncan, R., et al. (1999). Phase I clinical and pharmacokinetic study of PK1 [N-(2-hydroxypropyl)methacrylamide copolymer doxorubicin]: first member of a new class of chemotherapeutic agents-drug-polymer conjugates. Cancer Research Campaign Phase I/II Committee. *Clin Cancer Res*, 5(1), 83-94.

<sup>27</sup> Danhauser-Riedl, S., Hausmann, E., Schick, H. D., Bender, R., Dietzfelbinger, H., Rastetter, J., et al. (1993). Phase I clinical and pharmacokinetic trial of dextran conjugated doxorubicin (AD-70, DOX-OXD). *Invest New Drugs*, 11(2-3), 187-195.

<sup>28</sup> Kumazawa, E. and Ochi, Y. (2004), DE-310, a novel macromolecular carrier system for the camptothecin analog DX-8951f: Potent antitumor activities in various murine tumor models. *Cancer Science*, 95: 168–175. doi:10.1111/j.1349-7006.2004.tb03199.x

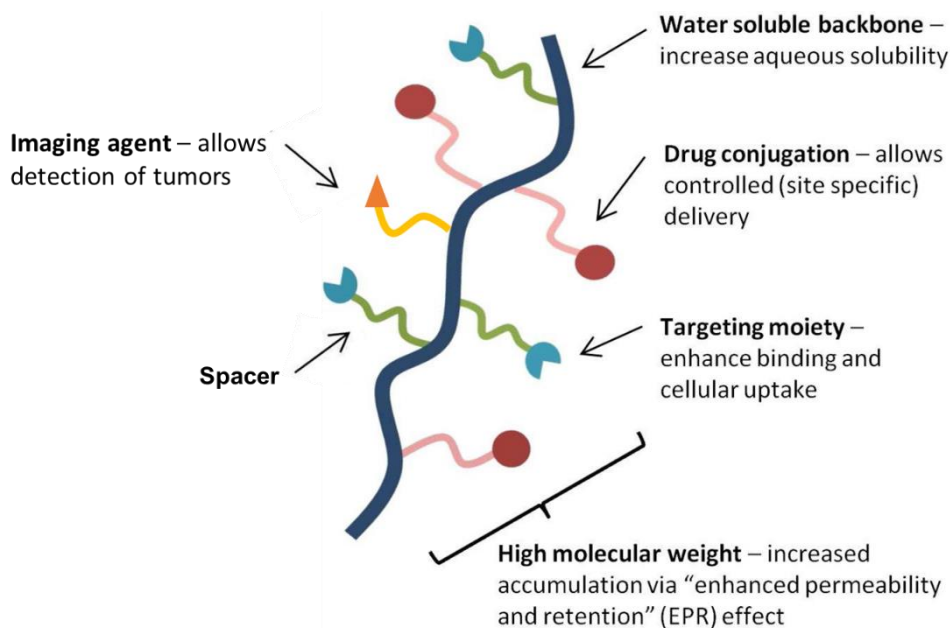


**Figure 2.** Schematic representation of an ideal polymeric conjugate.

Many different drug conjugates have been synthesized utilizing water soluble polymers such as Polyvinylpyrrolidone (PVP)<sup>29</sup>, poly(vinyl alcohol)<sup>30</sup>, poly-L-glutamic acid<sup>31</sup>, poly(ethylene glycol) (PEG)<sup>32,33</sup> and N-(2-hydroxypropyl)methacrylamide (HPMA)<sup>34</sup>. In this systems the drugs have been fixed directly or through a spacer group onto the polymer backbone. An important aspect is that a proper selection of the spacer provides the possibility of controlling the site and rate of release of drug from conjugate by hydrolytic or enzymatic cleavage. The choice of linkers depends on the stability in the physiological pH and on the ability to release the therapeutic agent at an appropriate site of action. Successful conjugation is correlated to the chemical structure especially both chemicals need to possess a reactive or functional groups such as  $-\text{COOH}$ ,  $-\text{OH}$ ,  $-\text{SH}$  or  $-\text{NH}_2$ , while also molecular weight and steric hindrance are important aspects. Often the conjugation leads to the formation of stable bonds such as ester, amide, and disulphide. Commonly, the conjugation is performed by coupling the drugs to the end chains

<sup>29</sup> D'Souza, A. J., Schowen, R. L., & Topp, E. M. (2004). Polyvinylpyrrolidone-drug conjugate: synthesis and release mechanism. *J Control Release*, 94(1), 91-100.

<sup>30</sup> Kakinoki, A., Kaneo, Y., Ikeda, Y., Tanaka, T., & Fujita, K. (2008). Synthesis of poly(vinyl alcohol)-doxorubicin conjugates containing cis-aconityl acid-cleavable bond and its isomer dependent doxorubicin release. *Biol Pharm Bull*, 31(1), 103-110.

<sup>31</sup> Li, C. (2002). Poly(L-glutamic acid)-anticancer drug conjugates. *Adv Drug Deliv Rev*, 54(5), 695-713.

<sup>32</sup> Greenwald, R. B., Choe, Y. H., McGuire, J., & Conover, C. D. (2003). Effective drug delivery by PEGylated drug conjugates. *Ibid.*, 55(2), 217-250.

<sup>33</sup> Banerjee, S. S., Aher, N., Patil, R., & Khandare, J. (2012). Poly(ethylene glycol)-Prodrug Conjugates: Concept, Design, and Applications. *Journal of Drug Delivery*, 2012, 17.

<sup>34</sup> Kopeček, J., Kopecková, P., Minko, T., & Lu, Z. (2000). HPMA copolymer-anticancer drug conjugates: design, activity, and mechanism of action. *Eur J Pharm Biopharm*, 50(1), 61-81.

of the polymers but another opportunity comes from “click” chemistry<sup>35</sup>. A click reaction is a highly specific, possesses a high yield of conjugation and the waste products are easily removed. Usually coupling agents such as dicyclohexyl carbodiimide (DCC) and 1-ethyl-3-(3-dimethylaminopropyl)carbodiimide or use of N-hydroxysuccinimide esters are employed for the activation of chemical groups. Monomethoxy poly(ethyleneglycol) (mPEG–OH) is one of the most widely used polymer in delivering anticancer drugs but its use is strictly limited by conjugation capacity since only one terminal functional group exists at the end of the polymer chain, which can be functionalized and conjugated to the drugs. Synthetic poly( $\alpha$ -amino acids) like poly(L-lysine), poly(L-glutamic acid), and poly((N-hydroxyalkyl) glutamines) have functionalities in their side groups (amine, hydroxyl, and carboxyl) that allow covalent coupling with drug molecules. HPMA is also a well studied polymer due to its versatility as a vehicle. Various functionalities may be incorporated into HPMA copolymers side chains and several have been used in clinical trials. Dendritic polymers are emerging as potentially ideal drug delivery vehicles because they are easily manipulated and they provide a large density of functional groups. In contrast with the linear polymers, dendritic micelles are more stable to various environmental effects, such as dilution, shear force, and pH value due to structural advantages. Common drawback is that all polymers exhibit some degree of heterogeneity despite the well defined chemical structures of conventional small molecular therapeutics and also the macroscale architecture of polymers causes steric hindrance. Steric hindrance describes how molecular groups interfere with other groups in the structure or other molecules during chemical conjugation. This effect drives chemical conformations and may affect the chemical conjugation with molecules.

### ***2.3.2 Polysaccharides based conjugate***

Amongst the polysaccharides, dextrans, due to their excellent physico-chemical properties and physiological compliance, are one of the most promising carrier candidates for a wide variety of therapeutic agents. Dextran possesses multiple primary and secondary hydroxyl groups and therefore can be easily conjugated either by direct conjugation or by incorporation of a spacer arm.

---

<sup>35</sup> Thirumurugan, P., Matosiuk, D., & Jozwiak, K. (2013). Click Chemistry for Drug Development and Diverse Chemical–Biology Applications. *Chemical Reviews*, 113(7), 4905-4979.

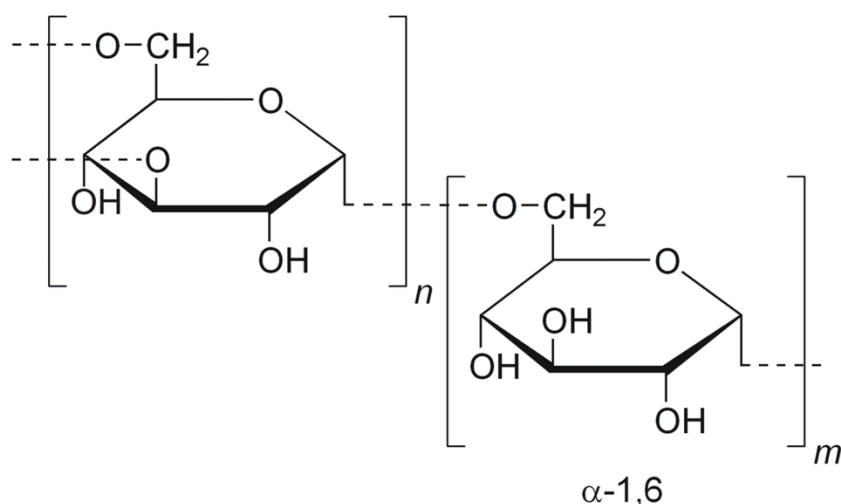


**Figure 3.** General structure of dextrans.

Dextrans might be linked irreversibly or reversibly to the therapeutic agents through direct linkage or by using a spacer arm. The widely used methods for the synthesis of dextran conjugates include direct esterification (ref), carbonate ester method in which an hydroxyl group belonging to the drugs is coupled to the polymer by forming a carbonate ester linkage, oxidation method that allows to obtain a dialdehyde dextran that can interact with amino compounds yielding Schiff bases, carbamate ester method and the cyanogen bromide activation of dextrans. Dextrans once internalized are exposed in the endosomal or lysosomal compartment to acid pH (~4.5-5.5). Using a pH-sensitive spacers like hydrazon spacer and N-cis-aconityl spacer one can ensure a controlled intracellular drug release especially in the case tumor characterized by acid environment that could be exploited to increase the accumulation of the drugs only at the targeted site. Also one of the major problem in cancer drug delivery is the development of multidrug resistance which occurs mainly due to over-expression of the P-glycoprotein (Pgp). This transmembrane glycoprotein reduces the intracellular accumulation of anticancer drugs because the free drugs enter the cell by diffusion through the plasma membrane. When the drugs are conjugated to macromolecular carriers, the drug-conjugate is taken up by endocytosis and subsequently efflux pumps are circumvented in turn reducing the multidrug resistance and increasing drug influx. However this drug delivery approach is limited by the amount of the conjugated therapeutics or by a premature release of it in the blood and this results in a low concentration into the cancerous cells not sufficient to be effective.

## 2.4 Physical entrapment: Polymeric nanoparticles (NPs)

Polymeric nanoparticles (NPs) are one of the most studied approaches in nanomedicine. The research of an ideal system for the delivery of therapeutics was the major challenge in nanomedicine and the evolution of the nano polymeric carriers brought to different generation of NPs. The first attempts were focused on the biocompatibility and non toxicity of materials, after that more effort have been made to optimize particles surface to increase stability, to give to NPs stealth properties and also to improve cellular uptake of the NPs using targeting moieties, most recent in the last generation of NPs arise the idea of dynamic carriers that can exploit the cellular enviroment to improve the therapeutic efficiency, the stimuli-responsive NPs. One of the most important biomedical applications of biodegradable polymeric particles is the delivery of conventional chemotherapeutics to improve drug efficacy in cancerous cells. These polymeric NPs decrease the drug toxicity, increase aqueous solubility of anticancer agents, overcome multidrug resistance of tumors, provided a controlled release and enhanced the cell cytotoxicity. Polymeric NPs also provide the opportunity to monitor tumor activity by tracking NP kinetics and can be used as theranostics agents for simultaneous cancer targeted imaging and therapy.

There are some requirements to consider in order to achieve successfully the release of drug payloads to the target site. Particle size and size distribution are the most important characteristics of these carriers that determine the *in vivo* distribution and toxicity. Nanoparticles need to avoid renal excretion, which depends on molecular weight: broadly molecules with a diameter over 15 nm own prolonged half-life in the blood.<sup>36</sup> The size affects also the degradation rate generally smaller particles degrade slower than the big ones<sup>37</sup> and this influences the release rate of the cargo.

A valuable drug delivery system (DDS) needs also a high-drug loading capacity that is the drug amount associated to the nanoparticle mass which is an important aspect in the manufacturing process of nanotherapeutics. Association of a drug to a nanocarrier can be performed in two distinctive ways: the incorporation method in which the drug is integrated during the manufacturing process and the adsorption method in which the drug is incubated with the particles already assembled. Another interesting aspect of the DDS is the opportunity to obtain

---

<sup>36</sup> Choi, H. S., Liu, W., Misra, P., Tanaka, E., Zimmer, J. P., Ity Ipe, B., et al. (2007). Renal clearance of quantum dots. *Nat Biotechnol*, 25(10), 1165-1170.

<sup>37</sup> Dunne, M., Corrigan, I., & Ramtoola, Z. (2000). Influence of particle size and dissolution conditions on the degradation properties of polylactide-co-glycolide particles. *Biomaterials*, 21(16), 1659-1668.

a prolonged release of their cargo potentially reducing the number of administration and increasing patient compliance. The release depends on the solubility of the drug, or on the diffusion of the drug through the material forming the DDS or on the degradation of the DDS itself. DDS potentially are important tools in cancer therapy for optimizing the effect of drugs and reducing side effects for this reason nanotechnology has become one of the most growing research area. Most recently polymer-based nanoparticles drew attention due to the possibility of manipulate their properties thanks to the progress made by polymer chemistry.<sup>38</sup>

Due to the wide variety of materials and drugs that can be used in the production of NPs the choice of a proper method for their fabrication is of crucial importance and depends on the chemical features of the polymer and the drug that must be loaded. Solvent evaporation, emulsification, nanoprecipitation and salting out are the widely used technique for the preparation of NPs. These method are based on the dispersion of preformed polymers involving an organic solution (e.g., dichloromethane, chloroform, ethyl acetate, acetone) containing the nanoparticle components and an aqueous solution containing stabilizers that will constitute the dispersion medium. The volatile organic solvent is removed by continuous stirring or by reducing the pressure. This leads to the formation of polymeric NPs with an efficient encapsulation of the lipophilic compound that finally are collected by ultra-centrifugation. Particullary, in the solvent diffusion method (nanoprecipitation) the polymer and the drug are solubilized into a water-miscible organic solvent such as acetone. The organic phase is added dropwise to a stirred aqueous solution and the fast diffusion of the organic solvent into the aqueous medium causes the instantianous formation of NPs. This is due to the interaction of the polymer with the two different phases. The solvent is removed under reduced pressure. This method is limited to the water-miscible solvents but ensures high reproducibility and high encapsulation efficacy.

Once formulated particles are characterized to ensure that the system is suitable to deliver the drug into the body. Dynamic light scattering (DLS) that utilizes the interaction of light with suspended particles under Brownian motion is the most used technique to obtain their hydrodynamic size. Particles are also imaged via Transmission Electron Microscopy (TEM) and Scanning Electron Microscopy (SEM). The two microscopes differ in which the SEM collects the secondary electrons that bounce back from the sample creating a well-rounded image while the TEM collects the electrons that pass through the sample generating just a

---

<sup>38</sup> Binder, W. H. and Sachsenhofer, R. (2008), 'Click' Chemistry in Polymer and Material Science: An Update. *Macromol. Rapid Commun.*, 29: 952–981. doi:10.1002/marc.200800089

shadow of the sample. Surface charge of the particles is another fundamental parameter that is related to suspension stability and particle surface morphology. The widespread technique to determine the surface charge is the measurement of the electric potential away from the particle surface in the diffuse layer. This location is known as slipping or shear plane and the potential measured at this plane is called zeta potential ( $\zeta$ ).

#### ***2.4.1 Stealth nanoparticles: poly(ethylene glycol) (PEG)***

Materials employed for NPs production have the fundamental requirement to be biodegradable. A biodegradable material is cleaved in the human body by several mechanisms such as hydrolysis (reaction with water), oxidation (due to oxidants produced by tissues) and enzymatic degradation and then reabsorbed or excreted without any adverse effects. A material for systemic use should be also biocompatible. Biocompatibility is defined as the capacity of a material to be in contact with a living system without producing any adverse effect such as host immune system response. Different strategies have been adopted so far to fabricate “stealth” NPs. The most widely used is coating the surface with polyethylene glycol (PEG) that minimizes the absorption of plasma proteins by creating a hindrance layer on the surface of NPs. The PEG layer can assume two different shape depending on the surface density. When PEG density is low, a mushroom like structure is formed while as PEG density increases, the chains reach out to not overlap and a brush structure is established (Figure 2).

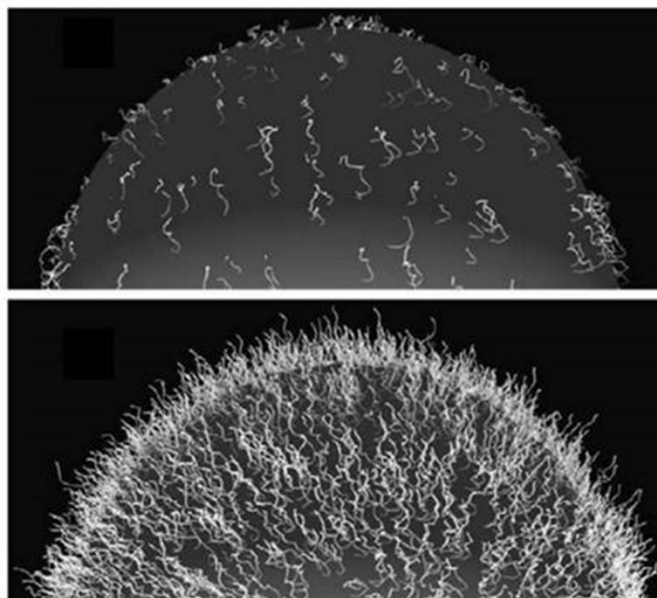


**Figure 4.** Representations of different PEG conformations top: the low density surface coverage of PEG chains leads to the “mushroom” configuration where most of the chains are located closer to the particles surface. Bottom: the high density surface coverage of the PEG chains leads to the “brush” configuration where most of the chains are extended away from the surface.

Functionalization of the particles surface can be done pre- or post-assembly. In pre-assembly approach, the ligand is incorporated with the NPs building blocks before NPs are formed. This is done by conjugating the ligand to the employed polymer, or by adding the ligand with NPs components in the solution. In post-assembly approach, the ligand is attached to pre-formed NPs by establishing a strong, covalent or non-covalent, interaction between the ligand and the NPs surface (Figure 3). PEG can be occasionally incorporated through both approaches, not only as stealth molecules, but also as a ‘spacer’ that separate ligands on NPs surface, therefore reducing the steric interference and allowing higher targeting efficiency.<sup>39</sup> Polymeric NPs should be rationally designed to have optimum size, surface properties, drug loading and cellular interactions, and then appropriately characterized and tested in vitro and in vivo.

---

<sup>39</sup> Abd Ellah, N. H., & Abouelmagd, S. A. (2017). Surface functionalization of polymeric nanoparticles for tumor drug delivery: approaches and challenges. *Expert Opin Drug Deliv*, 14(2), 201-214.

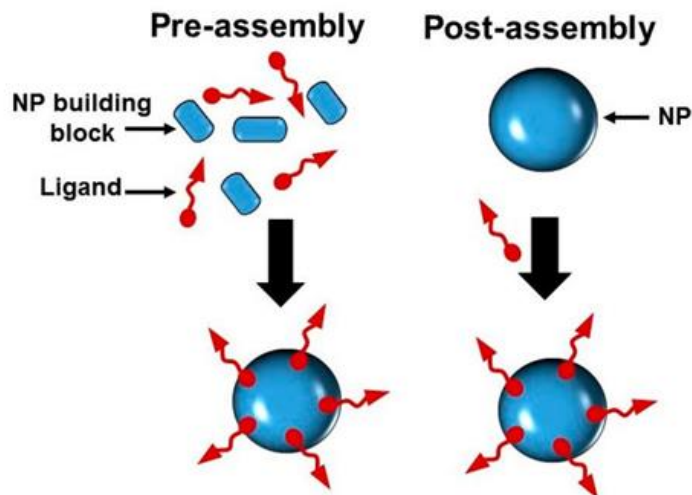


**Figure 5.** Pre- and post-assembly approaches for functionalization of polymeric NPs

### 2.4.2 Amphiphilic block copolymers

Amphiphilic block copolymers have unique properties and numerous potential applications due to the ability to form various types of self-assembling structures. Novel synthetic techniques allows to obtain block copolymers with well-defined compositions and molecular weights depending on the intended application. These copolymers are produced throughout the polymerization process. Basically two or more chemically different monomers, usually one hydrophobic and the other hydrophilic, are linked together by covalent bonds. The versatility of block copolymers is enhanced by the possibility to incorporate functional groups that allow further chemical modification after polymer formation. Basically, these process could be based on covalent or non covalent bonds. The formation of covalent bonds between a polymer backbone and functionalized moieties has been the most commonly used method to modify polymer chains. This postmodification facilitates the production of multiple block architectures. The different architectures are shown in Figure 4. The simplest is AB-type, while other architecture can be formed from two B units connected to A or conversely and this is the ABA or BAB triblock. More configurations are the multiblock in which the two units are bounded  $n$  times and the star shape block copolymers.

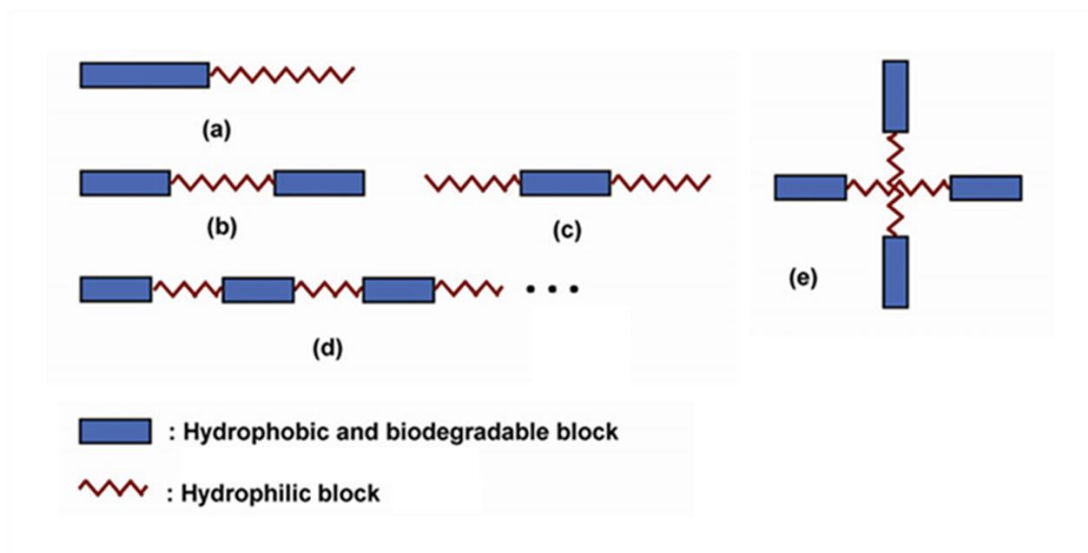


**Figure 6.** Schematic representation of block copolymer structures: (a) A-B diblock, (b) A-B-A triblock, (c) B-A-B triblock, (d)  $AB_n$  multiblock and (e) AB star shape.

The most common and extensively studied are linear amphiphilic block copolymers. The linear diblock are capable to self-assembly in aqueous media into spherical structures with an oil or aqueous core surrounded by a polymeric shell. The hydrophilic shell serves as an interface between the hydrophobic core and the environment. This unique architecture enables polymeric particles to serve as depots for poorly water-soluble compounds. There are many synthetic polymers used for the fabrication of polymeric nanoparticles like. Amid them, polyesters such as PLGA and PCL are the most widely used. PCL can be synthesized by ROP of monomeric unit of  $\epsilon$ -caprolactone (Figure 5).

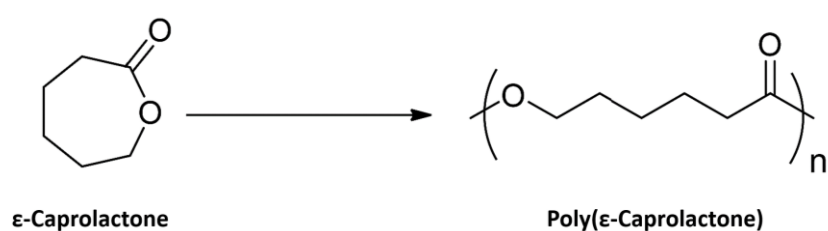


**Figure 7.** Ring opening polymerization method (ROP). ROP is a chain-growth polymerization in which the terminal end group of a polymer chain acts as a reactive center where further cyclic monomers can be added by ring-opening and addition of the broken bond.

This hydrophobic, semicrystalline polymer has been extensively explored because it is soluble in numerous organic solvents, has a low melting point (59-64°C) and can be bound with a wide range of polymers. In aqueous medium PCL is degraded by hydrolytic scission of ester bonds

and the degradation product is the non-toxic 6- hydroxyhexanoic acid (HHA). Due to this slow degradation and safety PCL was used in the biomedical field and has already been approved by the U.S. FDA.<sup>40</sup>

As stated above, linear diblocks in aqueous media can self-assemble into spherical structures with a hydrophilic shell and a hydrophobic core that can be exploited to deliver poorly water soluble drugs (Figure 6).

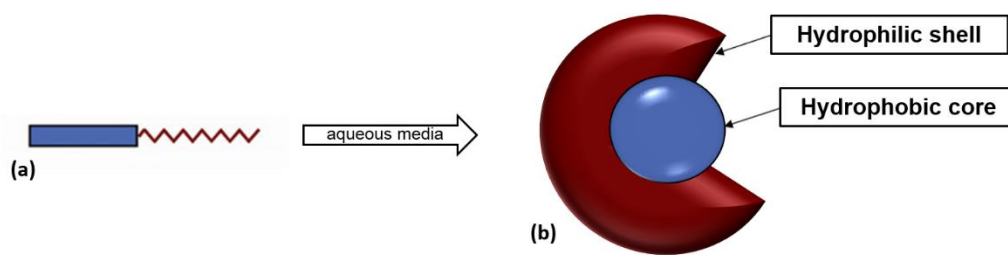


**Figure 8.** Schematic representation of core-shell self-assembled nanoparticle (b) from a hydrophilic/hydrophobic polymer diblock (a). The hydrophobic side of the diblock sets as the core of the particle appropriate for the loading of poorly water soluble molecules although the other half formed an hydrophilic shell serving as interface for the delivery into aqueous media

Polymer based nanoparticles have a great potential in the field of nanomedicine, especially polymeric nanoparticles made of PEG-PCL diblock. PEG-PCL copolymers combine the features of the single unit yielding a new promising biomedical material with amphiphilicity, biodegradability and biocompatibility. Particles generated from this diblock are composed of a hydrophobic core formed by PCL and the external shell made by water soluble group of PEG. Poorly water-soluble drugs have been successfully loaded

<sup>40</sup> Ulery, B. D., Nair, L. S., & Laurencin, C. T. (2011). Biomedical Applications of Biodegradable Polymers. *J Polym Sci B Polym Phys*, 49(12), 832-864.

inside these particles such as curcumin<sup>41,42</sup>, indomethacin<sup>43</sup>, rapamycin<sup>44</sup>, paclitaxel<sup>45,46</sup> and docetaxel<sup>47,48</sup>.

### 2.4.3 Active folate targeting

The efficiency of nanotherapeutics shall be measured by the amount of cancerous cells recognised and killed without damaging healthy cells. In order to increase the ability of these vectors to bind solely the diseased cells one of the most promising strategies is the decoration of the surface of the particles with moieties that recognized receptors overexpressed at the tumor site, known as active targeting. An increased action specificity and improved internalization through endocytosis mechanism can improve the effectiveness of treatment and decrease the possibility of serious side effects. Among the targeted receptors, folate drew considerable attention. Folate are part of the family of vitamins B and require specific transport systems to be delivered to systemic tissues include the reduced folate carrier (RFC) (SLC19A1), the proton coupled folate transporter (PCFT) (SLC46A1) and four isoforms of folate receptors (FR $\alpha$ , FR $\beta$ , FR $\gamma$  and FR $\delta$ ). RFC, the major transporter of reduced folate, is an organic anion antiporter that utilizes the transmembrane phosphate gradient to transport folate into cells. PCFT also belong to the solute carrier (SLC) group of transporters but differs from RFC in that works optimally at acid pH (~5.5) rather than neutral as the RFC and furthermore it shows differences in binding various anti folate substrates. The folate receptors (FRs) are expressed at the cell surface, anchored in the cell membrane by a glycosylphosphoinositol (GPI) domain. Distribution of the isoforms is different. FR $\alpha$  is expressed on epithelial tissues and it is even more expressed in various tumors still of epithelial origin (ovarian, mammary, lungs, kidney, bladder, cervical,

---

<sup>41</sup> Bisht, S., Feldmann, G., Soni, S., Ravi, R., Karikar, C., & Maitra, A. (2007). Polymeric nanoparticle-encapsulated curcumin ("nanocurcumin"): a novel strategy for human cancer therapy. *J Nanobiotechnology*, 5, 3.

<sup>42</sup> Udornpormmongkol, P., & Chiang, B. H. (2015). Curcumin-loaded polymeric nanoparticles for enhanced anti-colorectal cancer applications. *J Biomater Appl*, 30(5), 537-546.

<sup>43</sup> Rezaei Mokarram, A., Kebriaee Zadeh, A., Keshavarz, M., Ahmadi, A., & Mohtat, B. (2010). Preparation and in-vitro evaluation of indomethacin nanoparticles. *Daru*, 18(3), 185-192.

<sup>44</sup> Bisht, S., Feldmann, G., Koorstra, J. B., Mullendore, M., Alvarez, H., Karikari, C., et al. (2008). In vivo characterization of a polymeric nanoparticle platform with potential oral drug delivery capabilities. *Mol Cancer Ther*, 7(12), 3878-3888.

<sup>45</sup> Zhang, L., He, Y., Yu, M., & Song, C. (2011). Paclitaxel-loaded polymeric nanoparticles based on PCL-PEG-PCL: preparation, in vitro and in vivo evaluation. *J Control Release*, 152 Suppl 1, e114-116.

<sup>46</sup> Hu, J., Fu, S., Peng, Q., Han, Y., Xie, J., Zan, N., et al. (2017). Paclitaxel-loaded polymeric nanoparticles combined with chronomodulated chemotherapy on lung cancer: In vitro and in vivo evaluation. *Int J Pharm*, 516(1-2), 313-322.

<sup>47</sup> Maiolino, S., Russo, A., Pagliara, V., Conte, C., Ungaro, F., Russo, G., et al. (2015). Biodegradable nanoparticles sequentially decorated with Polyethyleneimine and Hyaluronan for the targeted delivery of docetaxel to airway cancer cells. *J Nanobiotechnology*, 13, 29.

<sup>48</sup> Ungaro, F., Conte, C., Ostacolo, L., Maglio, G., Barbieri, A., Arra, C., et al. (2012). Core-shell biodegradable nanoassemblies for the passive targeting of docetaxel: features, antiproliferative activity and in vivo toxicity. *Nanomedicine-Nanotechnology Biology and Medicine*, 8(5), 637-646.

endometrial and brain).<sup>49</sup> The function of the folate in tumor progression is unknown and therefore the reason of overexpression of the FR $\alpha$  is not clear. Folic acid is involved in DNA synthesis, cell division and growth possibly. FR $\alpha$  might confer a growth advantage to the tumor by modulating folate uptake from serum or by generating regulatory signals. The role of targeted drug delivery systems is improved efficacy by increasing drug concentration at a desired site and simultaneously reducing toxicity. This technology did not give the expected results and several factors need to be considered in the development of future targeted nanocarriers generation. The current targeted nanoparticles are developed to treat cancer by intravenous administration route and this constitutes an issue for the desired cellular selectivity in that it is almost impossible to reach only one cellular population even with a driving molecule. Moreover, the biodistribution profiles showed that these carriers accumulate in liver and spleen also when this accumulation is not sought. Probably, this is due to the surface adsorption of serum proteins that lead to interaction with the MPS. Also the formed protein corona causes a reduction in the exposition of ligands. Even more, the cellular uptake is sensitive to the physicochemical features of the particles such as size, surface charge and shape and the decoration with these molecules negatively affects the therapeutic impact of the NPs with a lower accumulation through passive mechanisms (Figure 7). There are also important temporal aspects affected by targeting including the relationship between pharmacokinetics, drug release kinetics and the therapeutic window for effective disease treatment. A correct approach will focus attention first on the biological features that define a disease and then on nanoparticles development to design a targeting system that is specifically tailored to these characteristics.<sup>50</sup>

---

<sup>49</sup> Parker, N., Turk, M. J., Westrick, E., Lewis, J. D., Low, P. S., & Leamon, C. P. (2005). Folate receptor expression in carcinomas and normal tissues determined by a quantitative radioligand binding assay. *Anal Biochem*, 338(2), 284-293.

<sup>50</sup> Cheng, C. J., Tietjen, G. T., Saucier-Sawyer, J. K., & Saltzman, W. M. (2015). A holistic approach to targeting disease with polymeric nanoparticles. *Nat Rev Drug Discov*, 14(4), 239-247.

Issue	Contributing factors	Potential solution
<i>Factors affecting targeting specificity</i>		
Unintended nanoparticle uptake	Nanoparticle size, shape, charge and cell-specific uptake properties	Inert particle coatings (for example, PEG and HPG)
Protein corona	Unintentional receptor-mediated uptake and steric hindrance	Composition characterization and control by nanoparticle formulation
Receptor identification	Lack of unique targets for cells of interest	Combine with local delivery
<i>Factors affecting therapeutic efficacy</i>		
Reduced passive targeting	Increased immunogenicity and shorter circulation time	Control ligand density to maximize avidity and minimize immunogenicity
Intracellular fate	Endosomal entrapment and lysosomal degradation	Combine with endosomal escape ligands (for example, CPP)

CPP, cell-penetrating peptide; HPG, hyperbranched polyglycerol; PEG, polyethylene glycol.

**Figure 9.** Selected challenges facing molecular targeting of polymeric NPs

### 3 Microsized drug delivery systems

#### 3.1 Multistage vector (MSV)

Despite nanotechnology brought innovation and new strategies are still developing this field did not achieve the expected results, indeed Wilhelm et al showed that only a small portion of the injected dose reaches the site of action.<sup>51</sup> This could be due to the presence of multiple biological barriers including enzymatic degradation, uptake by the immune system, renal clearance throughout their passage in the circulatory system, cell membranes and various efflux pumps once the particles reach the cells. This represents major obstacles for the delivery of therapeutic compounds.<sup>52</sup> Newly research efforts has been made based on the micro scale by combining different disciplines together such as biology, chemistry, physics and engineering. The multistage vector (MSV) is an innovative platform that combine nano and micro technology to overcome the biological obstacles in a sequentially manner (Figure 8).<sup>53</sup> This platform consists of three components. The first stage is a discoidal porous silicon microparticles designed to adhere to the tumor abnormal endothelial wall. To achieve this the

<sup>51</sup> Wilhelm S. , T. A. J., Dai Q. , Ohta S. , Audet J. , Dvorak H.F. & Chan W. (2016). Analysis of nanoparticle delivery to tumors. *Nature Reviews Material*.

<sup>52</sup> Blanco, E., Shen, H., & Ferrari, M. (2015). Principles of nanoparticle design for overcoming biological barriers to drug delivery. *Nat Biotechnol*, 33(9), 941-951.

<sup>53</sup> Venuta, A., Wolfram, J., Shen, H., & Ferrari, M. (2017). Post-nano strategies for drug delivery: multistage porous silicon microvectors. [10.1039/C6TB01978A]. *Journal of Materials Chemistry B*, 5(2), 207-219.

discoidal shape plays a fundamental role because previous study showed that discoidal particles marginate against the vascular wall better than spherical particles<sup>54</sup> also the red blood cells push the microparticles towards the vasculature due to shape interactions.<sup>55</sup> Even more the nature of the tumor environment promotes the accumulation of the microparticles due to the low shear rates<sup>56</sup> and increases the degradation through presence of reactive oxygen species (ROS).<sup>57</sup> With these features the microvectors arise as an excellent vehicle for the second nanostage. Depending on the application, different types of nanoparticles can be loaded into the pores of the microparticle, including liposomes<sup>58,59</sup>, polymeric nanoparticles<sup>60,61,62</sup>, micelles<sup>63</sup>, and gold nanoparticles.<sup>64</sup> The second stage (nanoparticle) enters into the cells by exploiting the fenestrated vascular endothelium and the third stage, the therapeutic agent, is released.

---

<sup>54</sup> Gentile, F., Chiappini, C., Fine, D., Bhavane, R. C., Peluccio, M. S., Cheng, M. M., et al. (2008). The effect of shape on the margination dynamics of non-neutrally buoyant particles in two-dimensional shear flows. *J Biomech*, 41(10), 2312-2318.

<sup>55</sup> Lee, T. R., Choi, M., Kopacz, A. M., Yun, S. H., Liu, W. K., & Decuzzi, P. (2013). On the near-wall accumulation of injectable particles in the microcirculation: smaller is not better. *Sci Rep*, 3, 2079.

<sup>56</sup> Jain, R. K., Martin, J. D., & Stylianopoulos, T. (2014). The role of mechanical forces in tumor growth and therapy. *Annu Rev Biomed Eng*, 16, 321-346.

<sup>57</sup> Liou, G. Y., & Storz, P. (2010). Reactive oxygen species in cancer. *Free Radic Res*, 44(5), 479-496.

<sup>58</sup> Shen, H., Rodriguez-Aguayo, C., Xu, R., Gonzalez-Villasana, V., Mai, J., Huang, Y., et al. (2013). Enhancing chemotherapy response with sustained EphA2 silencing using multistage vector delivery. *Clin Cancer Res*, 19(7), 1806-1815.

<sup>59</sup> Tanaka, T., Mangala, L. S., Vivas-Mejia, P. E., Nieves-Alicea, R., Mann, A. P., Mora, E., et al. (2010). Sustained small interfering RNA delivery by mesoporous silicon particles. *Cancer Res*, 70(9), 3687-3696.

<sup>60</sup> Shen, J., Wu, X., Lee, Y., Wolfram, J., Yang, Z., Mao, Z. W., et al. (2015). Porous silicon microparticles for delivery of siRNA therapeutics. *J Vis Exp*(95), 52075.

<sup>61</sup> Blanco, E., Sangai, T., Hsiao, A., Ferrati, S., Bai, L., Liu, X., et al. (2013). Multistage delivery of chemotherapeutic nanoparticles for breast cancer treatment. *Cancer Lett*, 334(2), 245-252.

<sup>62</sup> Zhang, M., Xu, R., Xia, X., Yang, Y., Gu, J., Qin, G., et al. (2014). Polycation-functionalized nanoporous silicon particles for gene silencing on breast cancer cells. *Biomaterials*, 35(1), 423-431.

<sup>63</sup> Martinez, J. O., Evangelopoulos, M., Bhavane, R., Acciardo, S., Salvatore, F., Liu, X., et al. (2015). Multistage Nanovectors Enhance the Delivery of Free and Encapsulated Drugs. *Curr Drug Targets*, 16(14), 1582-1590.

<sup>64</sup> Shen, H., You, J., Zhang, G., Ziemys, A., Li, Q., Bai, L., et al. (2012). Cooperative, nanoparticle-enabled thermal therapy of breast cancer. *Adv Healthc Mater*, 1(1), 84-89.

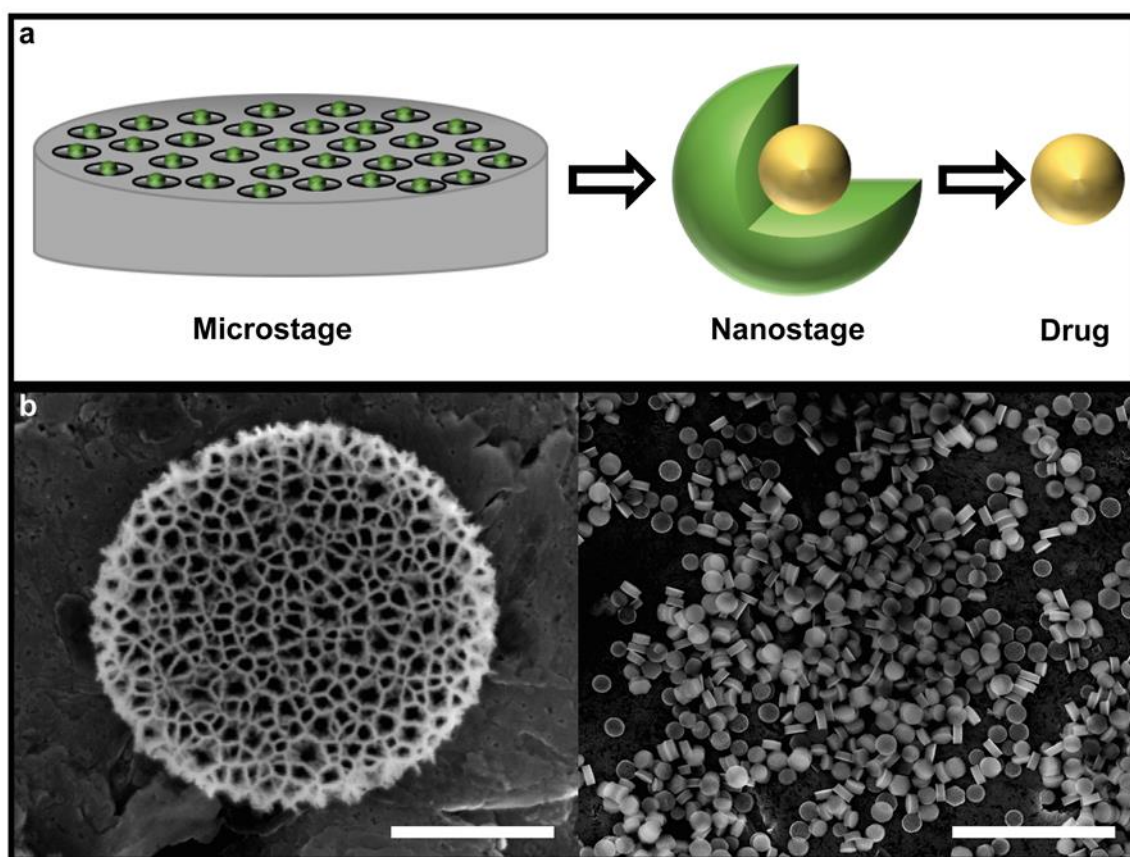


**Figure 10.** The multistage vector (MSV) a) Schematic representation of the MSV, which is composed of three components. The first stage vector is a biodegradable porous silicon microparticle that can be loaded with second stage nanoparticles, which encapsulate third stage therapeutic agents. The microstage, nanostage, and drug component are sequentially utilized to overcome biological barriers in the body. b) Scanning electron microscopy (SEM) images of MSVs. Scale bar, 500 nm (left), 10  $\mu$ m (right).

### 3.2 Fabrication of MSV

Silicon has been widely used for implantable biomedical applications<sup>65</sup> and for injectable drug delivery systems<sup>66,67,68</sup> possessing several advantages including biodegradability<sup>69,70</sup>, the

<sup>65</sup> Coffey, J. L., Whitehead, M. A., Nagesha, D. K., Mukherjee, P., Akkaraju, G., Totolici, M., et al. (2005). Porous silicon-based scaffolds for tissue engineering and other biomedical applications. *physica status solidi (a)*, 202(8), 1451-1455.

<sup>66</sup> Anglin, E. J., Cheng, L., Freeman, W. R., & Sailor, M. J. (2008). Porous silicon in drug delivery devices and materials. *Adv Drug Deliv Rev*, 60(11), 1266-1277.

<sup>67</sup> Santos, H. A., Mäkilä, E., Airaksinen, A. J., Bimbo, L. M., & Hirvonen, J. (2014). Porous silicon nanoparticles for nanomedicine: preparation and biomedical applications. *Nanomedicine (Lond)*, 9(4), 535-554.

<sup>68</sup> Wang, C. F., Sarparanta, M. P., Mäkilä, E. M., Hyvönen, M. L., Laakkonen, P. M., Salonen, J. J., et al. (2015). Multifunctional porous silicon nanoparticles for cancer theranostics. *Biomaterials*, 48, 108-118.

<sup>69</sup> Park, J. H., Gu, L., von Maltzahn, G., Ruoslahti, E., Bhatia, S. N., & Sailor, M. J. (2009). Biodegradable luminescent porous silicon nanoparticles for in vivo applications. *Nat Mater*, 8(4), 331-336.

<sup>70</sup> Godin, B., Gu, J., Serda, R. E., Bhavane, R., Tasciotti, E., Chiappini, C., et al. (2010). Tailoring the degradation kinetics of mesoporous silicon structures through PEGylation. *J Biomed Mater Res A*, 94(4), 1236-1243.

opportunity to control shape, size and porosity through different fabrication protocols<sup>71</sup> and biocompatibility. Numerous studies based on the administration of silicon microparticles revealed the absence of toxicity.<sup>72,73,74,75</sup> Additionally humans have several grams of silicon distributed throughout the body, primarily in the bones, nails, and kidneys. The fabrication of MSV consists of two major steps: a silicon wafer is shaped by photolithography and subsequently an electrochemical etch formed porous silicon particles of desired porosity pore size and thickness. The silicon particles are suspended in isopropyl alcohol (IPA) and stored at 20°C. Mostly microparticles are made in two sizes a small one (1 µm x 400 nm) and a bigger one (2 µm x 700 nm). These differ in pore size and more important for the biodistribution profiles in that both accumulate in liver and spleen but only the bigger one accumulates into the lungs aiming to specific application.

### **3.3 Second generation of MSV**

In addition to the general application a new generation of MSV that displays additional properties was developed in seeking to improve the therapeutic performance of this platform. As an example MSV-based strategies that exploit biomimetic coating to overcome biological barriers or novel approaches to load inside the micro discoidal particles different nanotherapeutics were developed.

#### **3.3.1 MSV for combination therapy**

Often the combination therapy can be more effective than the conventional single treatment.<sup>76,77</sup> Difficulty arises from physicochemical properties of the drugs, because if they are too different it is really hard to deliver them simultaneously with the same nanovector.

---

<sup>71</sup> Tasciotti, E., Liu, X., Bhavane, R., Plant, K., Leonard, A. D., Price, B. K., et al. (2008). Mesoporous silicon particles as a multistage delivery system for imaging and therapeutic applications. *Nat Nanotechnol*, 3(3), 151-157.

<sup>72</sup> Mai, J., Huang, Y., Mu, C., Zhang, G., Xu, R., Guo, X., et al. (2014). Bone marrow endothelium-targeted therapeutics for metastatic breast cancer. *J Control Release*, 187, 22-29.

<sup>73</sup> Tanaka, T., Godin, B., Bhavane, R., Nieves-Alicea, R., Gu, J., Liu, X., et al. (2010). In vivo evaluation of safety of nanoporous silicon carriers following single and multiple dose intravenous administrations in mice. *Int J Pharm*, 402(1-2), 190-197.

<sup>74</sup> Shen, J., Xu, R., Mai, J., Kim, H. C., Guo, X., Qin, G., et al. (2013). High capacity nanoporous silicon carrier for systemic delivery of gene silencing therapeutics. *ACS Nano*, 7(11), 9867-9880.

<sup>75</sup> Xu, R., Huang, Y., Mai, J., Zhang, G., Guo, X., Xia, X., et al. (2013). Multistage vectored siRNA targeting ataxia-telangiectasia mutated for breast cancer therapy. *Small*, 9(9-10), 1799-1808.

<sup>76</sup> Bayat Mokhtari, R., Homayouni, T. S., Baluch, N., Morgatskaya, E., Kumar, S., Das, B., et al. (2017). Combination therapy in combating cancer. *Oncotarget*, 8(23), 38022-38043.

<sup>77</sup> Fossati, R., Confalonieri, C., Torri, V., Ghislandi, E., Penna, A., Pistotti, V., et al. (1998). Cytotoxic and hormonal treatment for metastatic breast cancer: a systematic review of published randomized trials involving 31,510 women. *J Clin Oncol*, 16(10), 3439-3460.

Thereby MSV result very useful since nanotherapeutics with distinct physical features can be loaded into them. For example MSV was used to deliver siRNA loaded liposomes and docetaxel polymeric nanoparticles to treat metastatic melanoma lesions in the lungs.<sup>78</sup> The most common mutation in metastatic melanoma is the B-Raf proto-oncogene serine/threonine kinase (BRAF) V600E, which is strongly correlated with reduced survival rates.<sup>79</sup> The use of a BRAF inhibitors such as vemurafenib and dabrafenib had a positive impact in the treatment of metastatic melanoma.<sup>80</sup> Drug resistance develops over time against the BRAF inhibitors so the use of combination therapy that can suppress tumor growth through multiple mechanisms is used to improve the anticancer efficacy.<sup>81</sup> Against that background the MSV aims at delivering all the therapeutics into an ideal platform for combination therapy. Also spontaneous accumulation of the larger particles at the tumor metastasis site as the lungs makes them even more suitable. In fact *Mi et al.*<sup>54</sup> showed that the survival rate of melanoma tumor mice increase of ~60% in the group treated with MSV loaded with NPs and liposomes despite the group treated with NPs or monotherapy.

### 3.3.2 Stimuli responsive MSV

The microdevice can exploit the tumor environment to release the cargo like the stimuli responsive NPs that release the therapeutics under specific condition. Metalloproteinase-2 (MMP2) play a major role in tissue penetration by cancer cells and the secretion is elevated in numerous human cancer and thus may be used as target to improve the accumulation into diseased tissues. Polymeric NPs bound to the MSV surface through a peptide substrate linker responsive to MMP2 get a chance to exploit this cancer feature and the biodistribution profile of the silicon vectors.<sup>82</sup> The work show a major difference in the NPs release profiles from the silicon surface in presence or in absence of MMP2 proving that MSV could be used as a stimuli responsive platform.

### 3.3.3 Biomimetic MSV

---

<sup>78</sup> Mi, Y., Mu, C., Wolfram, J., Deng, Z., Hu, T. Y., Liu, X., et al. (2016). A Micro/Nano Composite for Combination Treatment of Melanoma Lung Metastasis. *Adv Healthc Mater*, 5(8), 936-946.

<sup>79</sup> Ascierto, P. A., Kirkwood, J. M., Grob, J. J., Simeone, E., Grimaldi, A. M., Maio, M., et al. (2012). The role of BRAF V600 mutation in melanoma. *J Transl Med*, 10, 85.

<sup>80</sup> Spagnolo, F., Ghiorzo, P., Orgiano, L., Pastorino, L., Picasso, V., Tornari, E., et al. (2015). BRAF-mutant melanoma: treatment approaches, resistance mechanisms, and diagnostic strategies. *Onco Targets Ther*, 8, 157-168.

<sup>81</sup> Queirolo, P., Picasso, V., & Spagnolo, F. (2015). Combined BRAF and MEK inhibition for the treatment of BRAF-mutated metastatic melanoma. *Cancer Treat Rev*, 41(6), 519-526.

<sup>82</sup> Y, M., C, M., J, W., Z, D., Y, H. T., X, L., et al. (2016). Enzyme-responsive multistage vector for drug delivery to tumor tissue.

Other interesting application of the MSV is in the field of biomimetic strategies for drug delivery. Synthetic systems that mimic the function or the structure of biological substances such as surface coating with a phospholipid bilayer or monolayer, surface decoration with proteins, carbohydrates, peptides or antibodies are an attractive way for addressing the issue of biological barriers inside the body.<sup>83</sup> This approach has been widely applied to nanosystems but less for microdevices. A model for the application of this technology is the one proposed by *Parodi et al* in which the discoidal silicon micro particles are covered with proteo-lipid patches obtained from fresh leukocytes cellular membranes.<sup>84</sup> These anionic patches are bound to the cationic surface by electrostatic and hydrophobic interactions. Interestingly, the protein content was analyzed and more than 300 leukocytes membrane proteins were found on the patches, notably proteins involved in endothelial adhesion and transendothelial migration, which could enhance the interaction with the inflamed endothelium like the leukocytes do.<sup>85</sup> To assess the overcoming of the cellular membrane a transwell chamber assay was carried out in presence of tumor necrosis factor (TNF- $\alpha$ ) to simulate an inflammatory environment the results showed that the proteo-lipid coated microparticles cross the endothelium considerably more than non-coated particles. For the *in vivo* studies two different coating were prepared one derived from syngenic murine leukocyte membrane and the other from xenogenic human. The biodistribution profile differs in that the syngenic showed a delay in liver accumulation and consequentially a longer circulation time.<sup>86</sup>

### **3.3.4 Immunotherapy**

Cancer and immune system are closely interrelated to one side release of antigens from tumor and subsequent presentation of these antigens by antigen-presenting cells (APCs) to native T cells which after activation migrate into the tumor and kill cancerous cells as effector T cells and on the other side tumours suppress immune responses by activating negative regulatory pathways (checkpoints). Therefore dendritic cell-based vaccines and immune checkpoint inhibitors have harvested interest in the field of cancer research in recent past. Most important achievement in cancer immunology led to Sipuleucel-T (Provenge®) the first FDA

---

<sup>83</sup> Gong, Y. K., & Winnik, F. M. (2012). Strategies in biomimetic surface engineering of nanoparticles for biomedical applications. *Nanoscale*, 4(2), 360-368.

<sup>84</sup> Parodi, A., Quattrocchi, N., van de Ven, A. L., Chiappini, C., Evangelopoulos, M., Martinez, J. O., et al. (2013). Synthetic nanoparticles functionalized with biomimetic leukocyte membranes possess cell-like functions. *Nat Nanotechnol*, 8(1), 61-68.

<sup>85</sup> Corbo, C., Parodi, A., Evangelopoulos, M., Engler, D. A., Matsunami, R. K., Engler, A. C., et al. (2015). Proteomic Profiling of a Biomimetic Drug Delivery Platform. *Curr Drug Targets*, 16(13), 1540-1547.

<sup>86</sup> Evangelopoulos, M., Parodi, A., Martinez, J. O., Yazdi, I. K., Cevenini, A., van de Ven, A. L., et al. (2016). Cell source determines the immunological impact of biomimetic nanoparticles. *Biomaterials*, 82, 168-177.

approved immune cell based vaccine that showed an increased overall survival in prostate cancer patients.<sup>87</sup> This treatment is based on the incubation *ex vivo* of antigen protein and patient's APCs that only later are injected again. New strategies need to be developed to stimulate the APCs cells *in vivo* and in that nano- and micro-carrier could be helpful.<sup>88,89</sup> Porous silicon particles were recently exploited as adjuvants for cancer vaccine.<sup>90</sup> Human epidermal growth factor (HER2) peptide antigen containing liposomes were loaded into the pores of the microparticles. The peptide was used to stimulate an antigen specific immune response against cancer cells that overexpress this receptor. APCs such as dendritic cells (DC) or B cells display antigen complexed with major histocompatibility complexes (MHCs) on their surfaces; this process is known as antigen presentation. T cells recognize these complexes using T cell receptors (TCRs) and this leads to the activation of effector T cells that at this point are able to recognize and kill the cancer cells. The porous particles generated a strong anti-tumor immunity in mice tumor model by inducing efficient antigen cross-presentation and also by activated simultaneously a type I interferons (IFN-I) response. These findings highlight the advantage of particulate vaccine and the IFN-I signaling for successful immunotherapy.

### **3.3.5 Injectable nanoparticle generator (INPG)**

An innovative approach consists in the injectable nanoparticle generator. The microdevice is used to deliver a chemotherapeutic agent covalently linked to poly(L-glutamic acid), the exposure to aqueous media triggered the formation of polymeric nanoparticles sized by the pore of the silicon vector and released as the silicon degraded. Triple negative breast cancer (TNBC) mouse model was used to evaluate the platform. Unlike other types of breast cancer TNBC does not express receptors such as estrogen receptor (ER), progesterone receptor (PR), or HER-2. This makes chemotherapy, hormone therapies, and targeted therapies inefficient. Also TNBC is often associated to the development of liver and lungs metastases. The MSV is able to accumulate preferentially into the metastasized organs and release therapeutic agent only in acidic environment. This result as very promising approach in the treatment of TNBC. In the work of *Xu et al* the median survival is evaluated into TNBC mouse model by comparing

---

<sup>87</sup> Cheever, M. A., & Higano, C. S. (2011). PROVENGE (Sipuleucel-T) in prostate cancer: the first FDA-approved therapeutic cancer vaccine. *Clin Cancer Res*, 17(11), 3520-3526.

<sup>88</sup> Goldberg, M. S. (2015). Immunoengineering: how nanotechnology can enhance cancer immunotherapy. *Cell*, 161(2), 201-204.

<sup>89</sup> Moon, J. J., Huang, B., & Irvine, D. J. (2012). Engineering nano- and microparticles to tune immunity. *Adv Mater*, 24(28), 3724-3746.

<sup>90</sup> Xia, X., Mai, J., Xu, R., Perez, J. E., Guevara, M. L., Shen, Q., et al. (2015). Porous silicon microparticle potentiates anti-tumor immunity by enhancing cross-presentation and inducing type I interferon response. *Cell Rep*, 11(6), 957-966.

the treatment between free doxorubicin, Doxil® and the nanoparticles generator. It was observed that the survival rate increases in the group treated with the microparticles despite the groups treated with free doxorubicin and Doxil.<sup>91</sup>

#### **4 Brain therapy**

Despite this wide range of application, this versatile platform has not yet been used to treat brain disease. This is because brain represents a major challenge in drug delivery. The development of innovative therapeutic strategies for the treatment of the brain diseases constitutes a great challenge and the major hindrance is the overcoming of the Blood Brain Barrier (BBB). Although the knowledge of the BBB continues to evolve in the years, a structure has been delineated characterized by the presence of closely associated areas named tight junctions (TJ) and from the lack of fenestrature.<sup>92</sup> Such anatomical features determine the formation of a continuous barrier among the blood stream and the interstitial fluid that restricts permeability of most substances from blood to brain. However the BBB, in the cerebral microvessels, constitutes the principal site of exchange between the whole organism and the central nervous system (CNS) because it serves to exclude the xenobiotic substances and at the same time to regulate brain homeostasis. Therefore some transport mechanisms are located at BBB level including i) simple diffusion for transport of water, gases and lipophilic substances, ii) carrier-mediated transport involved in the carriage of nutrients as the glucose transporter 1 (GLUT-1), ions transport, monocarboxylic acid and neutral amino acids transports, iii) two transcytosis systems, one receptor-mediated (insulin and transferrin) and the other based on electrostatic interactions.<sup>93</sup> Further, biological barriers at BBB including cytochrome P450 (CYPs) systems and more the presence of efflux transporter that can actively transport a huge variety of drugs out of the cell. These transporters are belonging to the family of the gene ABC (ATP-binding cassettes)/MDR1 as the Glycoprotein P (P-gp) that has a key role in the transport of drugs through the BBB. Brain metastases commonly arise from lung, breast and skin (melanoma) cancers and the approaches to the treatment of the patients with this metastases include whole brain radiotherapy (WBRT), surgery and stereotactic radiosurgery (SRS). Chemotherapy is used only in association to the radiotherapy or to the surgery to maintain under

---

<sup>91</sup> Xu, R., Zhang, G., Mai, J., Deng, X., Segura-Ibarra, V., Wu, S., et al. (2016). An injectable nanoparticle generator enhances delivery of cancer therapeutics. *Nat Biotechnol*, 34(4), 414-418.

<sup>92</sup> Cardoso, F. L., Brites, D., & Brito, M. A. (2010). Looking at the blood-brain barrier: molecular anatomy and possible investigation approaches. *Brain Res Rev*, 64(2), 328-363.

<sup>93</sup> Pardridge, W. M. (2012). Drug transport across the blood-brain barrier. *J Cereb Blood Flow Metab*, 32(11), 1959-1972.

control the systemic disease because the presence of the BBB prevents the 98% of the chemotherapeutic to access the SNC.

### ***5 Aim of the work***

In this context, our overall aim was to develop different strategies for the delivery of conventional chemotherapeutics in the field of cancer therapies.

The first mark was to develop a rationally-designed Dox-dextran conjugate with appropriate MW based on estimated EPR effect in established liver metastases mice model to overcome the limited clinical efficacy of pegylated liposomes and Dox.

In the field of physically entrapped drug into polymeric NPs we develop novel folate-targeted polymeric NPs made of PEG-PCL diblock by the solvent displacement method. Notably the fabrication method can affect the amount of PEG on the particles surface therefore the interaction with plasma protein and the exposition of the folate moieties. The aim was to test different length of PEG chains (short 1.0 kDa, long 2.0 kDa) to maximize the surface exposition of folate and how this could change the interaction with human cells and biological fluids.

A third aim of the project is the development of novel approaches based on the combination of micro- and nano-delivery systems to treat brain metastases arise from primary tumors as melanoma and breast cancer. The basic concept is to functionalize the micro-vector surface with a Polysorbate 80 (Tween 80) coating to have a preferential accumulation at the brain microvasculature. Overcoating with these materials seems to lead to the adsorption of apolipoprotein E from blood plasma onto the nanoparticle surface. The particles then seem to mimic low density lipoprotein (LDL) particles and could interact with the LDL receptor leading to their uptake by the endothelial cell. Alternatively molecules able to bind receptors highly expressed at the BBB such as transferrin (Tf) will be covalently linked to the silicon surface to obtain the same preferential accumulation. Thereafter, the capacity of transporting simultaneously more than one active component in the porous micro particle will be exploited. Especially will be developed targeted NPs capable to overcome the BBB by taking advantage of receptors such as GLUT-1. These nanoparticles will be loaded in the pore of the microparticle together with an efflux pump inhibitor to increase the efficiency of drug delivery. A proof-of-concept will be provided by in vitro and in vivo models.

The research activity has been summarized in three chapters and two annexes:

- Synthesis and characterization of rationally-designed Dextran-Doxorubicin conjugate: a novel strategy to improve the antitumor efficacy of doxorubicin in multiple breast cancer liver metastases (Chapter 2)
- Shedding light on surface exposition of poly(ethylene glycol) and folate targeting units on nanoparticles of poly( $\epsilon$ -caprolactone) diblock copolymers: beyond a paradigm (Chapter 3)
- Strategies to overcome the Blood Brain Barrier (BBB) (Chapter 4)

In Annex I the development of a novel antibacterial polymeric film of poly(lactic-co-glycolic acid) (PLGA) for the release of nitric oxide (NO) under visible light is reported. In Annex II a study of the growth of the drug delivery literature published during 1974-2015 was discussed.

The work has been carried in collaboration with the Institute of Polymers, Composites and Biomaterials (Italian National Research Council, Pozzuoli, Napoli, Italy) Department of Biology (University of Padua, Italy), Department of Drug Science (University of Catania, Italy) and Department of Nanomedicine (Houston Methodist Research Institute, Houston, Texas).

## **Chapter 2**

**Synthesis and characterization of rationally-designed  
Dextran-Doxorubicin conjugate: a novel strategy to  
improve the antitumor efficacy of doxorubicin in multiple  
breast cancer liver metastases.**

Megumi Kai, Alessandro Venuta, Elvin Blanco, Kenji Yokoi and Mauro Ferrari

## ***1 Introduction***

Metastatic breast cancer (MBC) is the common cause of cancer death in women and generally is considered incurable (Redig & McAllister, 2013). The choice of the treatment depend on several consideration such as the characteristics of the cancer cells, where the cancer has spread and previous therapy. In the case that cancer is hormone receptor-positive or HER2-positive, the first line treatment is hormone therapy or targeted therapy respectively (Abdulkareem & Zurmi, 2012; Fabi, Malaguti, Vari, & Cognetti, 2016). Chemotherapy has a fundamental role in the treatment of this disease, in that it can be used to reduce the growth of tumors or to ease symptoms of the cancer itself. Amongst the chemotherapeutics anthracyclines have a central role in the treatment of MBC (Rivera, 2003). However, these therapeutics are often associated to severe systemic side effects such as the case of Doxorubicin (Dox) that causes myelosuppression, alopecia, gastrointestinal toxicity, and cardiotoxicity and furthermore does not achieve expected drug concentration inside tumors (Kaminskas et al., 2012; McGowan et al., 2017). This is due to the spreading of the drug from blood stream to various organs through blood vessels caused by its small molecular size. Moreover, size affects the exposition of tumor cells to drugs, because of small molecules are rapidly cleared up from the body. Taken together, the non-specific accumulation and limited pharmacokinetic (PK) profile of this compound both in systemic circulation and tumors has been considered a major reason for insufficient therapeutic index (Speth, van Hoesel, & Haanen, 1988). The development of a carrier able to avoid the rapid clearance and the non-specific accumulation is a crucial needing for MBC treatment. For this purpose nanoparticles (NPs) have been developed as novel drug carriers that due to the largest size, as compared to conventional drugs, are able to overcome these limits. The preferential accumulation of NPs into the tumor site is based on the enhanced permeability and retention (EPR) effect (Bazak, Hourri, Achy, Hussein, & Refaat, 2014; Ngoune, Peters, von Elverfeldt, Winkler, & Pütz, 2016). Indeed, solid tumor show vascular abnormalities that increase the accumulation of macromolecules in tumor tissues and moreover prolong their retention for long periods (Carmeliet & Jain, 2000). This delivery strategy has the potential to lead to superior therapeutic indices. Despite this, only a limited number of NPs exploiting EPR effect have been approved for clinical use (Ragelle, Danhier, Préat, Langer, & Anderson, 2017). The first-approved formulation for the delivery of chemotherapeutics was a pegylated liposome able to reduced systemic side effects compared to the free drugs but not to significantly improve the anti tumor effects into the metastatic diseases (O'Brien et al., 2004). This clinical evidence suggests that further delivery approaches needs to

be developed and there is a need for an in depth study of the anatomical knowledge of the EPR. Another strategy to improve the systemic PK profile of Dox in circulation is the use of polysaccharides such as Dextrane that have been widely used in polymer-drug conjugates (Varshosaz, 2012). Advantages of polysaccharides as a drug carrier include a repetitive and well-defined chemical structure, reactive groups useful for drug conjugation, high stability, biodegradability and water solubility. Preclinical studies using primary tumor models have shown less systemic side effects and superior anti-tumor effects in primary tumors compared to conventional drug formulations. Dox-dextran 70 kDa was tested in a phase I clinical trial, but clinical efficacy was comparable with Dox (Danhauser-Riedl et al., 1993). One of the key factors in the development and successful utilization of therapeutic agents is the understanding of the mechanisms regulating their delivery to the tissue. Using real-time live imaging in tumor-bearing animals such as Intravital Microscopy (IVM) an enhanced understanding of several pathological and physiological dynamic processes at a subcellular resolution have been elucidated such as: (i) local PK in tumors/organs (using fluorescently labeled antibody, chemotherapy or liposomes); (ii) vascular pathology (vascular density/architecture); (iii) vascular physiology (flow rate and vascular permeability using fluorescence tracers/labeled blood cells); and (iv) local pharmacodynamics (PD) (tumor size, proliferation, apoptosis using labeled cancer cells) (Beerling, Ritsma, Vriskoop, Derksen, & van Rheenen, 2011). The application of IVM, however, is limited by the accessibility of the tumors and by the survival of the animals following surgical procedures. Recently, imaging window chambers have been developed for animals to allow optical access to large target areas without repeated surgical exposure of organs or tumors, allowing both local PK and PD analysis in the targeted area.

The final aim of this work was to select the ideal molecular weight dextran as a Dox carrier for liver metastases using IVM imaging. To evaluate the EPR effect in MBC, a mouse model with multiple liver metastases by injecting 4T1 or MDA-MB-231 murine breast cancer cells into the spleen was developed. Once multiple liver metastases were well established, a window chamber was implanted above the liver. To estimate the relative EPR effect in metastatic liver tumors the diffusion of systemically injected fluorescently labeled dextran tracer with different molecular weight 10 kDa 70 kDa inside/outside tumors in liver using IVM through window chamber was evaluated.

## ***2 Experimental section***

### ***2.1 Materials***

Aldehyde functionalized dextrans (Dex-CHO) with average molecular weight of 10 kDa and 70 kDa were obtained from Nanocs Inc, Doxorubicin hydrochloride (DOX-HCl) and Dimethyl Sulfoxide (DMSO) were bought from Fisher Scientific Co L.L.C. Triethylamine (TEA) ( $\geq 99\%$ ), Acetone and Dimethyl sulfoxide-d<sub>6</sub> were bought from Sigma-Aldrich, Phosphate Buffered Saline (PBS), ethylenediaminetetraacetic acid (EDTA). Roswell Park Memorial Institute (RPMI) 1640 Medium (Life Technologies, Inc., Grand Island, NY), and a penicillin–streptomycin mixture (Flow Laboratories, Rockville, MD)

## ***2.2 Synthesis of Dextran<sub>10k</sub>-Doxorubicin (Dex-Dox)***

Dex<sub>10k</sub>-CHO and DOX-HCl were coupled to give Dex<sub>10k</sub>-DOX through Schiff base reaction between aldehyde groups of Dex<sub>10k</sub>-CHO and amino groups of DOX-HCl. The molar ratio between Dex<sub>10k</sub>-CHO, DOX-HCl and TEA was 1:1:1.2. Briefly, Dex<sub>10k</sub>-CHO was dissolved in 0.5 mL of DMSO and after TEA was added to the solution. Then DOX-HCl was dissolved in 0.5 mL of DMSO, slowly dropped into the Dex<sub>10k</sub>-CHO/TEA solution and stirred for 1.5 h at RT in the dark. The final product was precipitated in acetone and the unbound Dox was removed by centrifugation at 4700 rpm x 10 mins. Finally, the purified Dex<sub>10k</sub>-DOX was dried under vacuum. Ultraviolet-visible (UV-vis) spectrophotometry was conducted to determine the Dox content in Dex<sub>10k</sub>-DOX by a standard curve method ( $\lambda_{\text{abs}} = 480\text{nm}$ , DU 730 Beckman Coulter). Proton Nuclear Magnetic Resonance (<sup>1</sup>H NMR) spectroscopy was employed for determining the percentage of the bond in the purified product (Bruker 400 MHz NMR) in 1 mL of DMSO-d<sub>6</sub>.

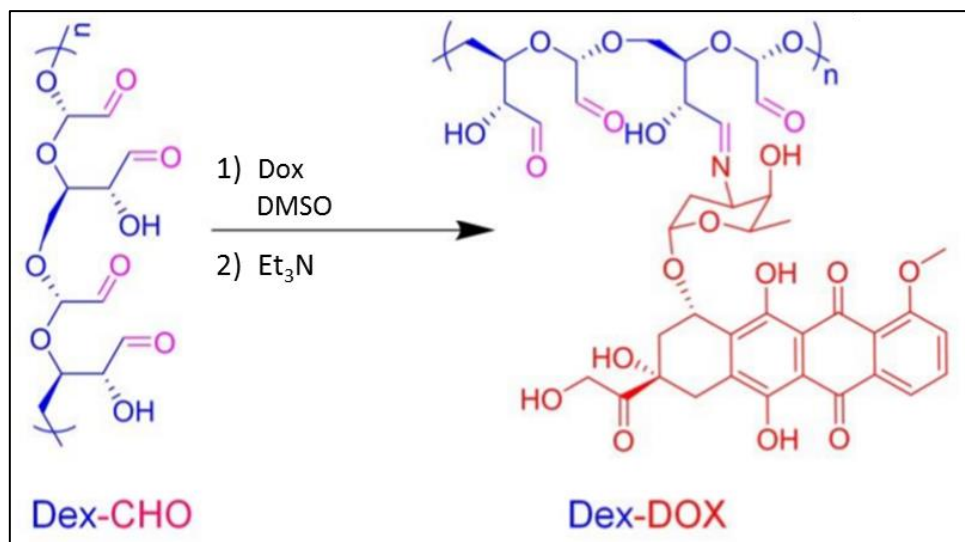


**Figure 1.** Synthetic strategy for synthesis of Dex-DOX conjugate.

### 2.3 Cancer cell preparation

4T1 mouse breast cancer cells were kindly provided by Dr. Isaiah J. Fidler (UT MD Anderson Cancer Center). The cells were cultured in RPMI 1640 medium, completed by adding 10% fetal bovine serum and 1% penicillin streptomycin solution (Cellgro, MA), at 37 °C in a humidified incubator in 5% CO<sub>2</sub>. Cells were grown to 80% confluency, trypsinized with 3 ml of 0.25% trypsin 0.53 mM EDTA solution for 5 min at 37 °C until cells started to detach. Trypsin was quenched with 9 ml of medium, and cells were then washed with 9 mL of PBS containing 1 mM EDTA. Final 4T1 cell concentration was  $\sim 5 \times 10^5$  cells/mL. Human cancer cell line MDA-MB-231 from ATCC (Manassas, VA) was cultured in Dulbecco's modified Eagle medium (DMEM)/F-12 base medium (Lonza, Walkersville, MD) supplemented with 10% FBS and 1% penicillin streptomycin solution. Cell culture was maintained in humidified environment with 5% CO<sub>2</sub> at 37 °C. At 80% confluence, cells were harvested by incubation with trypsin solution (PromoCell, Heidelberg, Germany).

### 2.4 Cell cytotoxicity

MTT (3-[4,5- dimethylthiazol-2-yl]-2,5 diphenyl tetrazolium bromide) (Sigma, USA) assay was performed according to the manufacturer's protocols to assess viability of 4T1 cells. Cancer cells were seeded into 96-well plates at concentrations  $1 \times 10^3$  cells/well and fed with new medium (negative control) or medium containing increasing concentrations of Dex-Dox and free Dox. After 72h of incubation cell viability was assessed at 570 nm. Localization of Dox-dextran conjugates inside cells was determined using confocal microscope.

### ***2.5 In Vivo Model of Breast Cancer Liver Metastasis***

Animal studies were performed in accordance with approved protocols by Houston Methodist Research Institute Institutional Animal Care and Use Committee (AUP-1214-0066). Balb/c mice and immunodeficient SCID mice were purchased from Charles Rivers Laboratories (Wilmington, MA) and mouse breast cancer liver metastases xenograft were generated by splenic injection of  $1 \times 10^5$  4T1 tumor cells/200  $\mu$ L PBS or MDA-MB-231  $1 \times 10^6$  tumor cells/200  $\mu$ L respectively.

### ***2.6 Models of breast and lung cancer liver metastasis and primary breast tumor***

Female Balb/c mice, 10 to 12 weeks old were maintained in animal facilities at Houston Methodist Research Institute approved by the American Association for Accreditation of Laboratory Animal Care and in accordance with current regulations and standards of the United States Department of Agriculture, Department of Health and Human Services, and NIH (Bethesda, MD).

To establish experimental liver metastasis, breast cancer 4T1 cells ( $1 \times 10^5$ /200  $\mu$ L) or MDA-MB-231 cells ( $1 \times 10^6$  cells/200  $\mu$ L) were injected into the spleen of female Balb/c or immunodeficient SCID mice respectively. The cells injected in the spleen disseminate to the liver through portal vein, producing experimental liver metastasis. The spleen was removed 10 min after the injection to prevent tumor growth in this organ. Six days after the injection, mice have been anesthetized and window chamber was implanted into the abdominal wall above the liver.

All the surgical procedures were approved by the Institutional Animal Care and Use Committee (IACUC) of Houston Methodist Research Institute.

### ***2.7 Intravital microscopy analysis***

Seven days after tumor inoculation, tumor-bearing mice were injected with fluorescently-labeled dextran tracer or Dex-Dox conjugates of different MW (10 [red], 70 [green] kDa of Dextran) intravenously into the retro-orbital space of the mice immediately before intravital microscopy (IVM). IVM imaging through window chamber was performed, 3 min, 3 h, 24 h after injection, to determine local PK of these drugs in tumors. Mice were anesthetized with isoflurane and mounted on heated microscope stage during IVM imaging under Nikon A1R

multiphoton microscope (Nikon Inc.). The images were processed for evaluation of fluorescent intensities of the tracers inside and outside the lesions at different times using NIS-Elements Image Processing Software (Nikon). The recorded fluorescent intensities in the site of interest were then normalized to the fluorescent intensity in the unaffected liver.

### ***3 Results and discussion***

#### ***3.1 Molecular weight dependent tumors accumulation of dextrans***

To estimate the relative EPR effect in metastatic liver tumors we evaluated the diffusion of systemically injected fluorescently labeled dextran tracer with different molecular weights (10 kDa [red] and 70 kDa [green]) inside and outside tumors in liver using IVM through abdominal window chamber (Fig 2). Live imaging of multiple tumors at different time points after injection of both tracers revealed a MW-dependent difference in accumulation in tumors. While fluorescence intensity of both tracers outside of tumors decreased over time, 10k but not 70k tracers accumulated in tumors as a function of time.

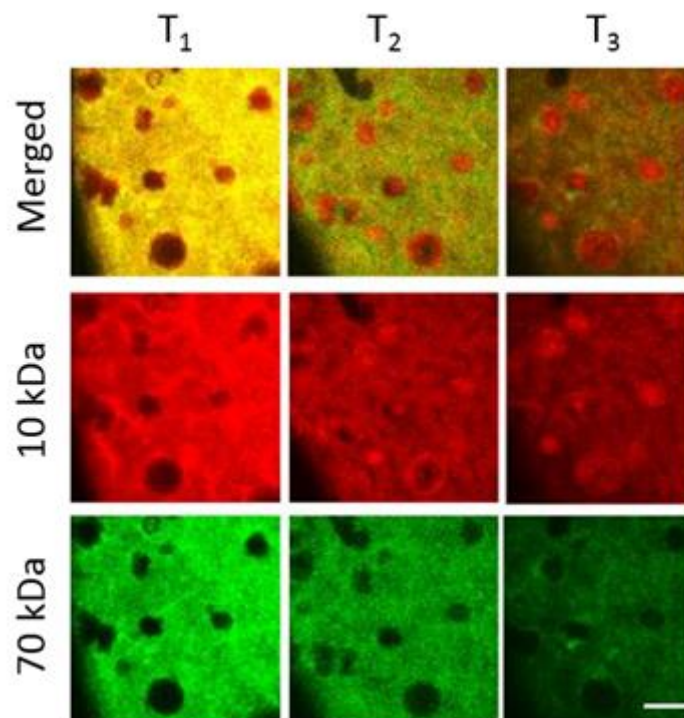


**Figure 2.** Perfusion and accumulation of fluorescently-labeled dextran tracers with molecular weight of 10 kDa and 70 kDa into mice liver metastases at different time points (T<sub>1</sub>- 3 min, T<sub>2</sub>- 3h and T<sub>3</sub>- 24 h). Scale bar 500  $\mu$ m.

### ***3.2 Synthetic strategy***

Based on the evidence of IVM images a Dex10<sub>kDa</sub>-Dox conjugate was successfully synthesized through a Schiff base formation between the aldehyde group of the Dextran and the amino group of Dox. The purification of the final product was carried out by several washes exploiting the different solubility of the conjugate and the free drug, since the conjugated polysaccharide precipitates in acetone. Finally, the purified Dex10<sub>kDa</sub>-Dox was dried overnight under vacuum. The amount of Dox linked to the polysaccharide was quantified by UV-vis spectroscopy (78 µg/mg), using Dox standard solutions in water to construct calibration curves. Reaction was confirmed by <sup>1</sup>H NMR; the absence of azide band in the spectrum of Dex10<sub>kDa</sub>-Dox accounts for a 100% conversion (Fig. 3). <sup>1</sup>H NMR analysis, spectra were recorded with Bruker 400 MHz NMR spectrometer. The NMR spectrum of the Dex10<sub>kDa</sub>-Dox conjugate exhibits an evident decrease (dark blue inset) in aldehyde group associated with the Dex10<sub>kDa</sub>-CHO (light blue inset) and as well the presence of aromatic protons associated with Dox (orange inset). The absence of unbound Dox was also confirmed by filtration through Sephadex G-10 columns that allow separation on the basis of different molecular weights.

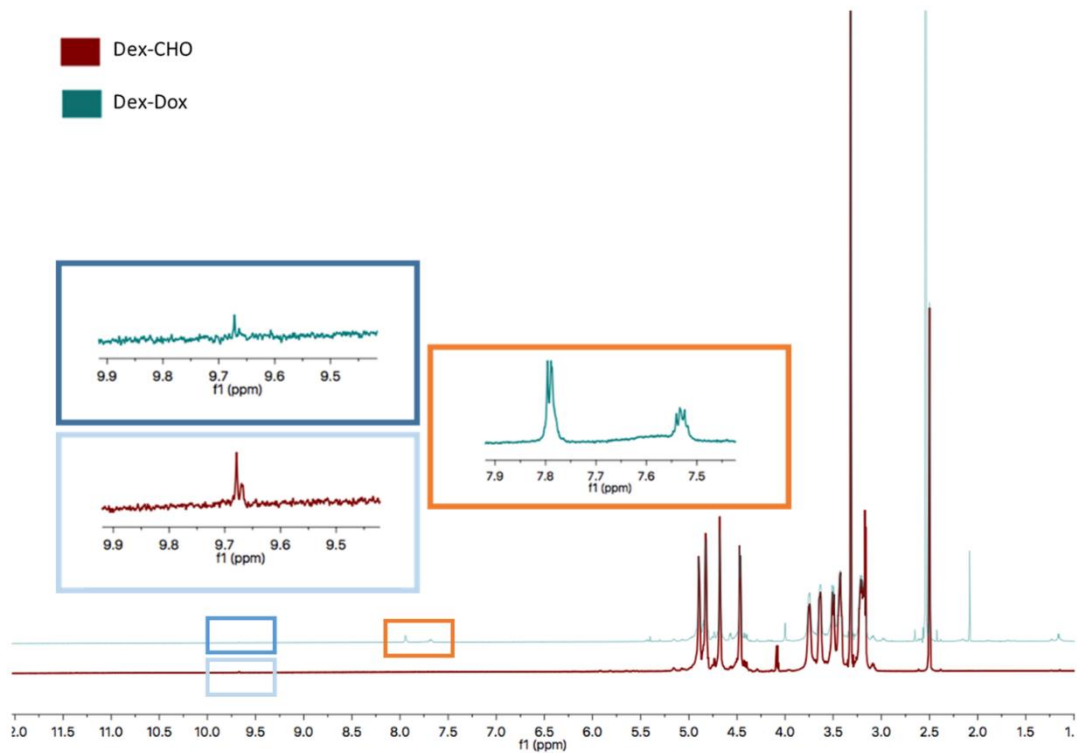


**Figure 3.** Comparison of <sup>1</sup>H-NMR spectra of Dex<sub>10kDa</sub>-Dox conjugate and Dox in DMSO-d<sub>6</sub>. Dark blue inset showed the decrease of the aldehyde group associated with the Dex<sub>10kDa</sub>-CHO, orange inset represents Dox aromatic protons.

### 3.3 Cell proliferation assay

The conjugate and the free drug showed similar effects on 4T1 cell viability *in vitro* (Fig.4A). Upon application of Dox-dextran conjugate or free Dox to culture media of 4T1 cells, the conjugate was found localized in the nucleus at 3 h in a manner similar to free Dox (Fig. 4B).

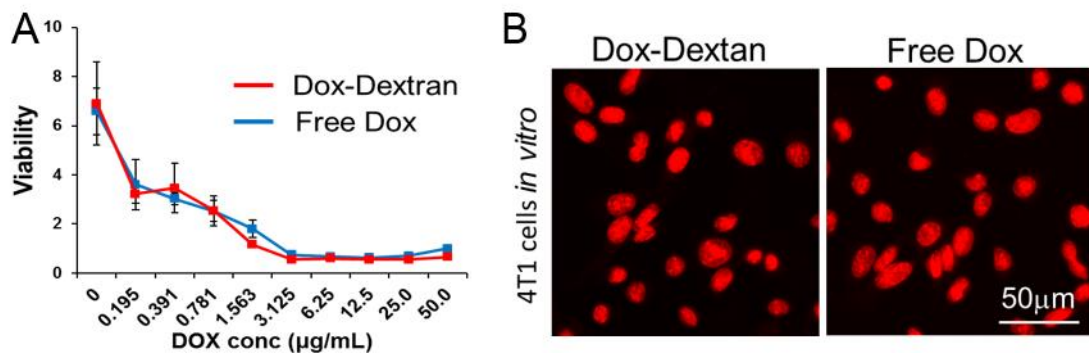


**Figure 4** A) Effect of Dox-dextran conjugate and free Dox on 4T1 cell viability B) nuclear localization of drugs imaged *in vitro*.

Upon IV administration in mice bearing 4T1 liver metastases, the Dox<sub>10kDa</sub>-dextran conjugate accumulated in tumors at 24 h after the injection (Fig. 5). This result was in contrast to the imaging data previously acquired (data not showed) in which almost no accumulation was found of Dox or pegylated liposomes inside tumors.

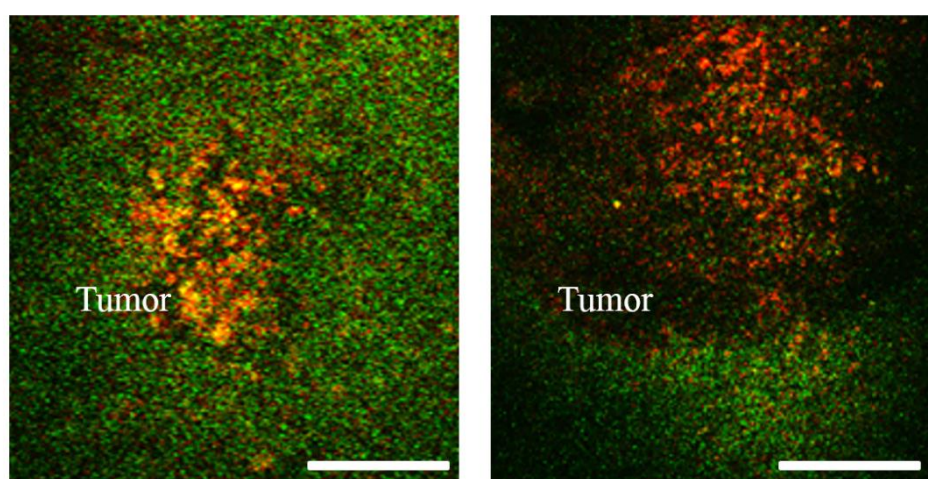


**Figure 5.** Accumulation of Dox-dextran in 4T1 metastatic tumors in liver. Scale bar 100  $\mu\text{m}$  (left) and 200  $\mu\text{m}$ .

#### **4 Conclusions**

These preliminary data suggest that rationally-designed Dox-dextran conjugates may result in improved accumulation as compared with pegylated liposomes and free Dox. Live imaging of multiple tumors at different time points after injection of both tracers revealed a molecular weight-dependent difference in accumulation in tumors. These data suggest that the drug delivery and the EPR effect in metastatic liver tumors is different from that in primary tumors: i) EPR effect inside 4T1 liver metastatic tumor is limited to allow only 10 kDa Dextran to accumulate; and ii) 10 kDa Dextran can be used as drug carrier of Dox for 4T1 liver metastases. Finally, we have successfully developed a rationally-designed Dox-dextran conjugate with appropriate MW based on estimated EPR effect in established liver metastases to overcome the limited clinical efficacy of pegylated liposomes and Dox.

Antitumor efficacy and safety of Dox-dextran conjugates as compared with those of free Dox and pegylated liposomes is ongoing on already established multiple liver metastases using 4T1 murine and MDA-MB-231 human breast cancer cells xenografts. Kinetic profiles of systemically injected Dox-dextran in circulation (blood), major organs (heart, lungs and

kidneys) and liver tumors will be determined using high performance liquid chromatography (HPLC), confocal microscopy imaging, or tissue MSI. Statistical analysis will be performed to correlate kinetic profiling data of fluorescently-labeled dextran and Dox-Dex conjugates. There is the possibility for heterogeneity in accumulation of tracers among multiple metastases due to difference in tumor size. We will evaluate this heterogeneity and correlate tumor size and accumulation of tracers among multiple tumors. Possible personalization of metastasis therapy using Dox-dextran conjugates with appropriate MW, selected by dextran-based clinically-relevant imaging analysis (*e.g.*, PET scan), could possibly translate in rapid clinical application.

## References

1. Redig AJ, McAllister SS. Breast cancer as a systemic disease: a view of metastasis. *J Intern Med.* 2013;274(2):113-26.
2. Fabi A, Malaguti P, Vari S, Cognetti F. First-line therapy in HER2 positive metastatic breast cancer: is the mosaic fully completed or are we missing additional pieces? *J Exp Clin Cancer Res.* 2016;35:104.
3. Abdulkareem IH, Zurmi IB. Review of hormonal treatment of breast cancer. *Niger J Clin Pract.* 2012;15(1):9-14.
4. Rivera E. Liposomal anthracyclines in metastatic breast cancer: clinical update. *Oncologist.* 2003;8 Suppl 2:3-9.
5. McGowan JV, Chung R, Maulik A, Piotrowska I, Walker JM, Yellon DM. Anthracycline Chemotherapy and Cardiotoxicity. *Cardiovasc Drugs Ther.* 2017;31(1):63-75.
6. Kaminskas LM, McLeod VM, Kelly BD, Sberna G, Boyd BJ, Williamson M, et al. A comparison of changes to doxorubicin pharmacokinetics, antitumor activity, and toxicity mediated by PEGylated dendrimer and PEGylated liposome drug delivery systems. *Nanomedicine.* 2012;8(1):103-11.
7. Speth PA, van Hoesel QG, Haanen C. Clinical pharmacokinetics of doxorubicin. *Clin Pharmacokinet.* 1988;15(1):15-31.
8. Ngoune R, Peters A, von Elverfeldt D, Winkler K, Pütz G. Accumulating nanoparticles by EPR: A route of no return. *Journal of Controlled Release.* 2016;238(Supplement C):58-70.
9. Bazak R, Hourri M, Achy SE, Hussein W, Refaat T. Passive targeting of nanoparticles to cancer: A comprehensive review of the literature. *Mol Clin Oncol.* 2014;2(6):904-8.
10. Carmeliet P, Jain RK. Angiogenesis in cancer and other diseases. *Nature.* 2000;407(6801):249-57.

11. Ragelle H, Danhier F, Pr at V, Langer R, Anderson DG. Nanoparticle-based drug delivery systems: a commercial and regulatory outlook as the field matures. *Expert Opin Drug Deliv.* 2017;14(7):851-64.
12. O'Brien ME, Wigler N, Inbar M, Rosso R, Grischke E, Santoro A, et al. Reduced cardiotoxicity and comparable efficacy in a phase III trial of pegylated liposomal doxorubicin HCl (CAELYX/Doxil) versus conventional doxorubicin for first-line treatment of metastatic breast cancer. *Ann Oncol.* 2004;15(3):440-9.
13. Varshosaz J. Dextran conjugates in drug delivery. *Expert Opin Drug Deliv.* 2012;9(5):509-23.
14. Danhauser-Riedl S, Hausmann E, Schick HD, Bender R, Dietzfelbinger H, Rastetter J, et al. Phase I clinical and pharmacokinetic trial of dextran conjugated doxorubicin (AD-70, DOX-OXD). *Invest New Drugs.* 1993;11(2-3):187-95.
15. Beerling E, Ritsma L, Vrisekoop N, Derksen PWB, van Rheenen J. Intravital microscopy: new insights into metastasis of tumors. *Journal of Cell Science.* 2011;124(3):299.

## **Chapter 3**

# **Shedding light on surface exposition of poly(ethylene glycol) and folate targeting units on nanoparticles of poly( $\epsilon$ -caprolactone) diblock copolymers: beyond a paradigm**

Published as:

Alessandro Venuta, Francesca Moret, Giovanni Dal Poggetto, Diletta Esposito, Aurore Fraix, Concetta Avitabile, Francesca Ungaro, Mario Malinconico, Salvatore Sortino, Alessandra Romanelli, Paola Laurienzo, Elena Reddi, and Fabiana Quaglia

## Abstract

Polymeric nanoparticles (NPs) of poly( $\epsilon$ -caprolactone) (PCL) covered with a hydrophilic poly(ethylene glycol) (PEG) shell are usually prepared from diblock PEG-PCL copolymers through different techniques. Furthermore PEG, NPs can be decorated with targeting ligands to accumulate in specific cell lines. However, the density and conformation of PEG on the surface and its impact on the exposition of small targeting ligands has been poorly considered so far although this has a huge impact on biological behavior. Here, we focus on PEG-PCL NPs and their folate-targeted version to encourage accumulation in cancer cells overexpressing folate receptor  $\alpha$ . NPs were prepared from copolymer mixtures with different PEG length by the widely employed solvent displacement method. An in depth characterization of NPs surface by  $^1\text{H}$  NMR, fluorescence and photon correlation spectroscopy was carried out in the attempt to evaluate PEG/Folate spatial organization in the shell and its impact on the interaction with proteins as well as uptake in human macrophages/cancer cells. Overall, the present results demonstrate that PEG length critically affects protein interaction and folate exposition with a logical impact on receptor-mediated cell uptake. Our study highlights that the too simplistic view suggesting that PEG-PCL gives NPs with a brush shell needs to be reconsidered in the light of actual surface properties, which should always be considered case-by-case.

## ***1. Introduction***

Polymeric nanoparticles (NPs) are in the limelight in cancer nanotechnology due to the advantages of prompt manipulation of the overall features (size, surface hydrophilicity/charge, release rate, biodegradability) through appropriate tailoring of the chemistry of building blocks (Grossen, Witzigmann, Sieber, & Huwyler, 2017). Amid the huge amount of biomaterials developed so far, poly( $\epsilon$ -caprolactone)-poly(ethylene glycol) PEG-PCL copolymers with different hydrophilic/lipophilic balance and architectures have been synthesized resulting in a wide arsenal for drug delivery application (Z. Li & Tan, 2014). In the context of cancer therapies, NPs of PEG-PCL block copolymers have gained attention in preclinical studies and in clinical settings with the promise to ameliorate chemotherapy outcome and decrease treatment toxicity. As far as PEG-PCL NPs for intravenous injection are concerned, a PEGylated surface can help to escape mononuclear phagocyte system (MPS), to attain long-circulation and to promote extravasation in inflamed tissues with a typical dysfunctional capillary bed such as in tumors (3). While demonstrating excellent stability in PBS, PEG-PCL NPs were even found to aggregate in the presence of serum (4).

Surface modification of PEGylated NPs with covalently-linked small ligands is a further strategy followed to increase drug level in cancer cells. To this purpose, the design of folate-decorated NPs carrying a chemotherapeutic and internalizing in cancer cells through FR $\alpha$ -mediated endocytosis has become a hot topic (5). FR $\alpha$  expression level is a marker of tumor aggressiveness, plays a role in the low response rate to chemotherapeutics resistance and is insensitive to chemotherapy regimen (5), thus strengthening the potential utility of FR-mediated delivery. Folate decoration of PEG-PCL NPs has been attempted by us and other authors by synthesizing all-in-one amphiphilic block copolymers bearing folate at PEG hydroxyl-end group and able to form core-shell NPs (1). When the amphiphilic diblock polymers self-assemble into NPs in an aqueous phase, the PEG segments are expected to form the outer corona allowing the conjugated folic acid to become fully accessible on the surface. In contrast to this paradigm, we observed that for highly PEGylated micelle-like NPs, folate exposition in the presence of serum is highly dependent by the formation of a protein corona (6).

Another aspect to consider when fabricating PEG-PCL NPs refers to the mode of copolymer assembly. While dialysis has been largely employed to prepare PEG-PCL micelles/NPs, scale-up of production as well as in-process sterilization is feasible with microfluidics which takes after solvent displacement (nanoprecipitation) techniques. Importantly, mode of assembly of

PEG-PCL copolymers can highly affect the amount of PEG on the surface (7) while its impact on protein adsorption and targeting features has been poorly considered.

On this basis, it is evident that PEG coverage plays a crucial role in controlling the biological fate of PEGylated NPs with an huge impact on the processes driven by protein interactions (immune system recognition, biodistribution), transport through biological matrices (tumor extracellular matrix, mucus, bacteria biofilm), and target recognition and docking (cell uptake) (8). Despite the extensive use of PEG, there is no consensus on the target product profile in term of PEG density, molecular weight and conformation when developing PEGylated NPs intended for a specific application, in cancer as well (9). Thus, surface of NPs should be characterized in depth through complimentary techniques in view of a full optimization of the nanocarrier and following clinical application (8).

In this study, we try to focus on the surface exposition of PEG and folate targeting units on NPs of PEG-PCL diblock copolymers prepared by solvent displacement technique and to relate shell features to uptake in human cells. To this purpose, we synthesized PEG-PCL copolymers with either 1 kDa or 2 kDa PEG chains and a Fol-PEG-PCL copolymers with 1.5 kDa PEG segment. Shell properties of untargeted and folate-targeted NPs were fully characterized through complementary techniques, such as  $^1\text{H}$  NMR, fluorescence, photon correlation spectroscopy and  $\xi$  potential. The impact of shell features on NPs interaction with human serum albumin, stability in biologically-relevant media as well as internalization in human macrophages and cancer cells overexpressing folate receptor were investigated.

## ***2 Experimental section***

### ***2.1 Materials***

Poly(ethylene glycol) (PEG) with Mn 1.5 kDa (PEG1.5k, Sigma-Aldrich, Milan, Italy), monomethoxy-poly(ethylene glycol) with Mn 2.0 kDa (mPEG<sub>L</sub>, Sigma-Aldrich, Italy) and monomethoxy-poly(ethylene glycol) with Mn 1.0 kDa (mPEG<sub>S</sub>, Nanocs Inc., USA) were dehydrated by azeotropic distillation with dry toluene in a Dean-Stark trap.  $\epsilon$ -Caprolactone (CL, Sigma-Aldrich, Italy) was distilled over CaH<sub>2</sub> under vacuum. Stannous-(2-ethylhexanoate)<sub>2</sub> (Sn(oct)<sub>2</sub>), N-hydroxysuccinimide (NHS), N,N'-dicyclohexylcarbodiimide (DCC), triethylamine (TEA), dimethylaminopyridine (DMAP), tosyl chloride (TsCl), folic acid (Fol), propargylamine, triphenylphosphine (PPh<sub>3</sub>), silver(I) oxide, potassium iodide and sodium azide were used without further purification. Copper wires (Carlo Erba, Italy) were treated with H<sub>2</sub>SO<sub>4</sub>

for 3 min, washed with water and methanol, and finally dried under vacuum in an oven for 30 minutes at 60°C. 1,4-butanediol, 1-hexanol, N,N-dimethylformamide (DMF) and dichloromethane (DCM) were dried before use according to standard procedures. All the other solvents (analytical grade) were purchased from Sigma-Aldrich and used as received. (2-Hydroxypropyl)- $\beta$ -cyclodextrin (HP $\beta$ CD, DS 0.9), Nile Red (NR) and Human Serum Albumin (HSA) were from Sigma (Italy).

## ***2.2 Copolymer characterization***

FTIR analysis was performed with a Perkin-Elmer spectrometer (Paragon 500) equipped with a ZnSe attenuated total reflectance (ATR) crystal accessory. Samples were placed in direct contact with the ATR crystal and pressed with a pressure clamp positioned over the crystal/sample area to allow intimate contact between the material and the crystal. Spectra were acquired in the 4000-400  $\text{cm}^{-1}$  range, at a resolution of 2  $\text{cm}^{-1}$  (average of 20 scans).  $^1\text{H}$  NMR analysis, spectra were recorded with a Bruker Avance DPX400 apparatus operating at 400 MHz. For GPC analysis, samples were dissolved in THF and passed through a 0.22  $\mu\text{m}$  PTFE membrane filter. Measurements were performed on an injected volume of 100  $\mu\text{L}$  by using a Malvern-Viscotek GPC MAX/TDA 305 quadruple detector array equipped with a precolumn and two Phenogel columns (Phenomenex) with exclusion limits  $10^6$  and  $10^3$  respectively. The GPC instrument was used at a flow rate of 0.8 mL/min and at columns and system temperature of 35 °C. Triple detectors calibration was based on a standard of polystyrene with molecular weight 104,959 Da. Residual copper content was estimated by Microwave Plasma-Atomic Emission Spectrometry (MP-AES) with a Agilent 4100 spectrometer. A microwave digestion system Milestone Ethos Touch Control was used for digestion of sample. The finely ground sample (0.1 g) was transferred in a teflon microwave digestion vessel and treated with 6 mL of  $\text{HNO}_3$ , 3 mL of  $\text{HCl}$  and 1 mL of  $\text{H}_2\text{O}_2$  (Ultrapure Reagents, trace metal grade < 1  $\mu\text{g/L}$ ). The samples were processed by microwave digestion as follows: ramp to 200 °C over 10 min, then hold at 200 °C for 20 min. After digestion, the samples were cooled to room temperature, filtered, transferred in a 50 mL volumetric flask and adjusted to 50 mL with distilled water for spectrometric analysis. The amount of Fol linked to the copolymer was quantified by UV-vis spectroscopy on DMSO polymer solutions (0.2-2 mg/mL), using Fol standard solutions in DMSO to construct calibration curves. The absorbance of the sample was evaluated at 360 nm on a Shimadzu 1800 spectrophotometer.

## ***2.3 Synthesis of MPEG<sub>S</sub>-PCL and MPEG<sub>L</sub>-PCL***

Linear diblock copolymers were prepared by ring-opening polymerization (ROP) of CL at 120 °C for 24 h using mPEG<sub>L</sub> or mPEG<sub>S</sub> as initiator and Sn(Oct)<sub>2</sub> as catalyst (20%). CL/initiator molar ratio = 36. <sup>1</sup>H NMR (CDCl<sub>3</sub>, δ in ppm), PCL block: 1.29–1.78 (m), 2.19–2.43 (t) 3.20 (m); 3.92–4.21 (t), 4.31(t); PEG block: 4.10 (t), 3.64 (s), 3.38, (t).

## ***2.4 Synthesis of Fol-PEG-PCL***

### ***2.4.1 Synthesis of PCL-PEG-azido copolymer (N<sub>3</sub>-PEG-PCL)***

Step 1. Synthesis of monotosyl-PEG (Ts-PEG-OH). PEG (5.00 g, 3.34 mmol) was dissolved in 50 mL of dry toluene. Ag<sub>2</sub>O (1.161 g, 5.01 mmol) and KI (110 mg, 0.668 mmol) were finely dispersed in the solution by stirring, then TsCl (2.76 g, 14.5 mmol) was added. The reaction mixture was kept at room temperature under stirring and nitrogen atmosphere for 12 h. The solution was filtered and solvent removed by rotary evaporation. The polymer was dissolved in 10 mL of DCM and precipitated in cold diethyl ether (yield 95%). <sup>1</sup>H NMR (d<sub>6</sub>-DMSO, δ in ppm): 7.79 (2H, d), 7.49 (2H, d), 4.56 (1H, t), 4.11 (2H, t), 3.49 (128H, s), 2.43 (3H, s). Step 2. Synthesis of monoazido-PEG (N<sub>3</sub>-PEG-OH). Ts-PEG-OH (1.00 g, 0.66 mmol) was dissolved in 15 mL of dry DMF, then NaN<sub>3</sub> (214 mg, 3.3 mmol) was added and the mixture was stirred at 90 °C overnight under nitrogen atmosphere. The reaction mixture was cooled to room temperature, filtered, and DMF removed under vacuum. The product was dissolved in 10 mL of DCM and the solution was extracted twice with brine and twice with water in a separating funnel. The organic phase was dried over anhydrous Na<sub>2</sub>SO<sub>4</sub>, concentrated and poured in cold diethyl ether. Polymer was collected by filtration (yield 81%). <sup>1</sup>H NMR (d<sub>6</sub>-DMSO, δ in ppm): 4.56 (1H, t), 3.6 (2H, t), 3.5 (127H, s, PEG backbone), 3.4 (2H, t). FTIR diagnostic band: 2107cm<sup>-1</sup> (N<sub>3</sub> stretching). Step 3. Synthesis of N<sub>3</sub>-PEG-PCL copolymer. N<sub>3</sub>-PEG-OH (600 mg, 0.393 mmol), CL (1.572 g, 13.77 mmol) and Sn(Oct)<sub>2</sub> (31 mg, 0.078 mmol) were charged in a flask under dry nitrogen. The polymerization was carried out at 120°C for 24 h under stirring. The copolymer was dissolved in 10 mL of DCM, precipitated in cold hexane, recovered by filtration and finally dried (yield 91%). <sup>1</sup>H NMR (CDCl<sub>3</sub>, δ in ppm): 3.6 (2H, t), 3.5 (127H, s, PEG backbone), 3.4 (2H, t), 1.29–1.78 (139H, m); 2.19–2.43 (82H, m), 3.92–4.21 (82H, t), 4.31 (2H, t); Mn of PCL evaluated by <sup>1</sup>H NMR = 4,6 kDa.

### ***2.4.2 Synthesis of propargylfolate***

Fol (500 mg, 1.13 mmol) was charged in a flask under dry nitrogen and dissolved by stirring in 20 mL of DMSO over mild heating, then DCC (446 mg, 2.16 mmol) and NHS (260 mg, 2.26

mmol) were added. Reaction was carried out in the dark at room temperature for 17 h, the solution was filtered to remove the side product (dicyclohexylurea, DCU), then propargylamine (124 mg, 2.25 mmol) and TEA (228 mg, 2.25 mmol) were added. The reaction was left overnight. The product was precipitated with a diethylether/acetone 80/20 mixture, repeatedly washed first with acetone and then with diethylether, and finally dried under vacuum overnight. A yellow powder was obtained and analyzed by LC-MS (Agilent Technologies, 6230 ESI-TOF) on a Phenomenex Jupiter column (C18, 3 $\mu$ m, 150x2.0 mm) with a gradient of acetonitrile (0.1% TFA) in water (0.1% TFA), from 5 to 50% in 15 minutes at a flow rate of 0.2 mL/min.

#### ***2.4.3 Click conjugation of propargylfolate with N<sub>3</sub>-PEG-PCL (Fol-PEG-PCL )***

N<sub>3</sub>-PEG-PCL (800 mg, 0.12 mmol) dissolved in 15 mL of DMSO was charged in a flask under dry nitrogen, then propargylfolate (86 mg, corresponding to a propargyl/N<sub>3</sub> molar ratio of 1.1) and copper wires (120 mg) were added; the reaction was carried out under stirring at room temperature overnight. The solution was filtered to remove copper and then dialyzed against DMSO with a 2000 cut-off dialysis tube for 4 days, in order to eliminate free propargylfolate and other side products. Finally, DMSO was evaporated under nitrogen stream. The occurrence of reaction was confirmed by FTIR through the complete disappearance of 2097 cm<sup>-1</sup> N<sub>3</sub> stretching band (yield 95%). Fol content =6.5% by wt, functionalization degree=90%.

#### ***2.5 Preparation and characterization of nanoparticles***

Non-targeted NPs were prepared from mPEG<sub>S</sub>-PCL and mPEG<sub>L</sub>-PCL while folate-decorated NPs were prepared from a mixture of mPEG<sub>S</sub>-PCL or mPEG<sub>L</sub>-PCL with Fol-PEG-PCL. NPs were formed by solvent diffusion of an organic phase (10 mg of copolymer in 1 mL of acetone) added dropwise in water (2 mL) under magnetic stirring (500 rpm). After solvent evaporation, NPs were filtered through 0,45  $\mu$ m Phenex® filters (Phenomenex, USA). NPs could be freeze-dried after the addition of HP $\beta$ CD as cryoprotectant (polymer: HP $\beta$ CD 1:10 wt. ratio) and stored at 4 °C. Recovery yield of the production process was evaluated on an aliquot of NPs without cryoprotectant by weighing the solid residue after freeze-drying. To evaluate cell uptake, the lipophilic dye NR was physically entrapped (0.2% of copolymer weight). The hydrodynamic diameter (D<sub>H</sub>), polydispersity index (PI) and zeta potential ( $\xi$ ) of NPs were determined on a Zetasizer Nano Z (Malvern Instruments Ltd).

Fixed aqueous layer thickness (FALT) of NPs was measured by monitoring the influence of ionic strength on  $\xi$ . Different amounts of NaCl stock solutions were added to NPs dispersed in

water (5 mg/mL, 100  $\mu$ l) and zeta potential of the samples measured. A plot of  $\ln \xi$  against  $3.33[\text{NaCl}]^{0.5}$  gives a straight line where the slope represents the thickness of the shell in nm. (10)  $^1\text{H}$  NMR was carried out on NPs dispersions to evaluate the amount of PEG on the surface. Spectra were recorded for either NPs prepared in  $\text{D}_2\text{O}$  or NPs freeze-dried without cryoprotectant (5 mg) dissolved in  $d_6$ -DMSO. Steady state fluorescence spectra were carried out with a RF6000 spectrofluorimeter (Shimadzu, Japan). Fluorescence lifetimes were recorded with Fluorolog-2 spectrofluorimeter (Model F111, Horiba) equipped with a TCSPC Triple Illuminator. The samples were irradiated by pulsed diode excitation source Nanoled at 370 nm. The kinetics were monitored at 450 nm and each solution was used to register the prompt at the excitation wavelength. The system allowed measurement of fluorescence lifetimes from 200 ps. The multiexponential fit of the fluorescence decay was obtained using the following equations:

$$I(t) = \alpha_1 \exp(-t/\tau_1) + \alpha_2 \exp(-t/\tau_2).$$

All measurements were performed in a thermostated quartz cell (1 cm path length, 3 mL capacity).

Stability of NPs in the presence of HSA (1-500  $\mu\text{M}$ ) was evaluated by placing a NPs sample (0.05 mg/mL) in the HSA water solution and monitoring immediately the size distribution by PCS.

## ***2.6 Intracellular uptake of NPs in cancer cells***

KB carcinoma cells (American Type Culture Collection, ATCC, Rockville, USA) over-expressing FR ( $\text{FR}\alpha$ ) were selected to study the specific internalization of Fol-decorated NPs vs. non-targeted NPs. The cells were grown in Eagle's medium (MEM) (Life Technologies) supplemented with 10% fetal bovine serum (FBS) (Gibco), 100 U/mL Penicillin G and 100  $\mu\text{g}/\text{mL}$  Streptomycin and maintained at 37  $^\circ\text{C}$  in a humidified atmosphere containing 5%  $\text{CO}_2$ . Flow cytometry measurements of the uptake of  $\text{DBL}_s$ ,  $\text{DBL}_s/\text{DBL-Fol}$ ,  $\text{DBL}_L$ ,  $\text{DBL}_L/\text{DBL-Fol}$  were performed using fluorescent NR-loaded NPs. For all the experiments mentioned above, cells were seeded in 24 wells/plate (40000 cells/well) in folate-deficient RPMI medium (Life Technologies) supplemented with 10% FBS. After 24 h of growth at 37  $^\circ\text{C}$ , the cells were incubated for 1 h with 20  $\mu\text{g}/\text{mL}$  of NR-loaded NPs, freshly re-suspended in milliQ water and diluted in RPMI medium with or without 10% of FBS. After incubation with NPs, the cells were washed, detached from the plates with trypsin (Life Technologies), centrifuged and re-

suspended in Versene before measuring NR fluorescence using a BD FACSCanto™ II instrument (Becton Dickinson). The blue laser at 488 nm was used as excitation source and the PerCP channel (670–735 nm) and the PE channel (564–606 nm) were selected for the detection of NR fluorescence, respectively.  $10^4$  events/sample were acquired and analyzed with the FACSDiva Software. Competition experiments with 1 mM free Fol (Sigma Aldrich) were carried out incubating the cells for 1 h prior to the addition of NPs in order to saturate FRs present on cell surface. The internalization of NPs in cells pre-incubated or not with 1 mM free Fol was assessed also by confocal microscopy using a SP5 laser scanning microscope (Leica Microsystems).  $6 \times 10^4$  cells were seeded in special tissue culture dishes for fluorescence microscopy ( $\mu$ -Dish 35 mm, high, Ibidi GmbH), were allowed to growth for 24 h and then incubated for 1 h with 20  $\mu\text{g}/\text{mL}$  NPs in medium added with 10% FBS. After incubation, the cells were washed twice with PBS with  $\text{Ca}^{2+}$  and  $\text{Mg}^{2+}$  and immediately visualized under the microscope.

### ***2.7 Capture of NPs by human macrophages***

The capture by human macrophage of NPs decorated or not with Fol and pre-incubated in human serum (HS) was measured in order to assess their stealth properties. A positive control of non-PEGylated NPs (PCL) was tested too. Macrophages were derived from monocytes isolated from buffy coats of healthy donors by centrifugation over a Ficoll-Hypaque step gradient and subsequent Percoll gradient (Sigma-Aldrich).  $2 \times 10^6$  isolated monocytes/well were seeded in 24 wells/plate and cultured for 7 days in RPMI 1640 medium (Life Technologies) supplemented with 20% FBS and 100 ng/mL of human macrophage colony-stimulating factor (Peprotech) to promote macrophage differentiation. On day 4 from the seed, the macrophage colony-stimulating factor was added again. For the uptake experiment, macrophages were incubated for 3 h in RPMI added with 10% FBS and 20  $\mu\text{g}/\text{mL}$  fluorescent NPs previously incubated at 37 °C in human serum type AB (Sigma-Aldrich) for 0, 10 or 30 min. Macrophages were then washed and detached from the plates using PBS with 5 mM EDTA, centrifuged, re-suspended in PBS + 1% BSA and analyzed by flow cytometry for fluorescence as described previously. Propidium Iodide (1  $\mu\text{g}/\text{mL}$ ) staining of the samples during flow cytometry acquisition was used to measure the macrophage viability, which was higher than 95%.

## **2.8 Statistical analysis:**

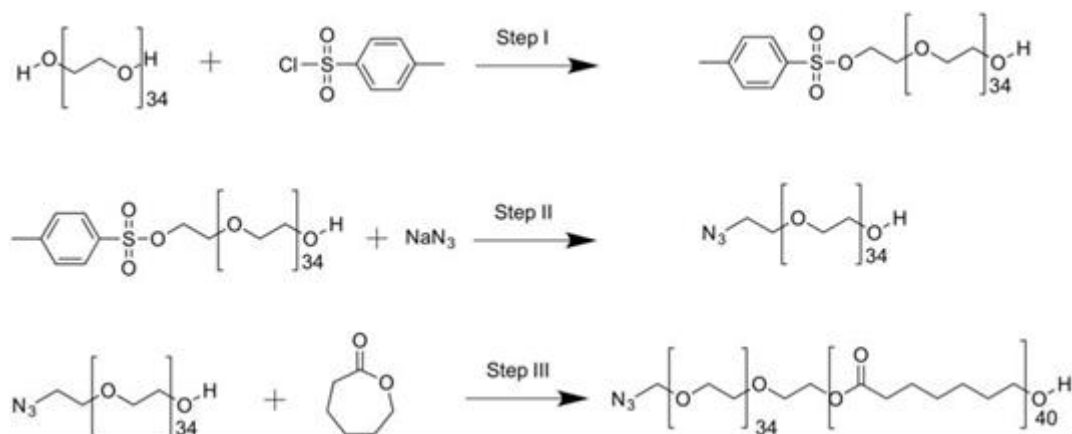
The Primer software for biostatistics (McGraw-Hill, Columbus, USA) was used for statistical analysis of the data. The data are expressed as means  $\pm$  SD of at least 3 independent experiments. The difference between groups was evaluated using the Student's t-test considered significant for  $p < 0.05$ .

## **3 Results and discussion**

### **3.1 Synthetic strategy**

The following PEG-PCL diblock copolymers with different PEG lengths were synthesized: i) Fol-PEG-PCL copolymer (PEG MW= 1.5 kDa); ii) MPEG-PCL with a PEG MW= 1.0 kDa (PCL-mPEG<sub>S</sub>); iii) MPEG-PCL with a PEG MW= 2.0 kDa (PCL-mPEG<sub>L</sub>). Copolymers were synthesized by typical ROP polymerization of  $\epsilon$ -caprolactone using a mono-hydroxyl PEG as initiator. The molecular weight of PCL block was controlled by the CL/initiator molar ratio in the feed. A value of around 4.0 kDa was fixed for PCL on the basis of previous works (6,11-12).

To prepare Fol-PEG-PCL copolymer, Cu(I)-catalyzed 1,3-Huisgen cycloaddition ("click" reaction) was chosen to conjugate folate to PEG-PCL (13). 1,3-Huisgen cycloaddition is the addition of alkynes to azides, with formation of highly stable 1,2,3-triazoles. The reaction is high yielding, stereospecific, does not create any byproduct, and can be conducted in mild conditions. PEG was first modified by introduction of an azide on one terminal group (Scheme 1). Synthetic strategies aimed to asymmetrically modify PEG are largely explored in the literature. In general, the reported methods suffers from a complex chemistry and/or low purity of the final product (14,15). The most common way to synthesize heterot-telechelic PEG remains polymerization of ethylene oxide from different initiators (16,17,18,19,20). To achieve mono-functionalization, the use of a large excess of PEG has been reported too (21) although separation of non-modified from modified polymer requires tedious chromatography and yields are generally low. In the present paper, we used a method recently reported (22) to achieve asymmetric activation of low molecular weight alcohols to low molecular weight PEG, so that it becomes possible to selectively link a biomolecule of interest to one end of PEG, and use the residual —OH for copolymerization.



**Scheme 1.** Synthetic pathway for synthesis of N<sub>3</sub>-PEG-PCL diblock copolymer. Monofunctionalization of PEG was checked by <sup>1</sup>H NMR analysis through the ratios between the intensities of —OH (4.56 δ) and —CH<sub>2</sub>—O—Ts (4.11 δ) protons of PEG, and aromatic (7.79, 7.49 δ) and —CH<sub>3</sub> (2.43 δ) protons of tosyl group (step 1).

N<sub>3</sub>-PEG-OH is used as initiator for ring-opening polymerization of CL, leading to a PEG-azido functionalized copolymer. Azide is stable at the temperature required by ROP (120°C), as confirmed through FTIR analysis, where no change of diagnostic band of azide at 2097 cm<sup>-1</sup> is detected in the copolymer spectrum. Mn of PCL block in the copolymers was calculated by the ratio between intensities of the resonance associated to —CH<sub>2</sub>—OH methylene protons at 3.64 δ and —CH<sub>2</sub>—CO— units in the PCL chain at 2.31 δ of <sup>1</sup>H NMR spectrum. A good agreement between theoretical and experimental values is found (Table 1). In order to introduce an alkyne group, folic acid was first conjugated with propargylamine through carbodiimide chemistry. It is known from the literature that only γ-folate conjugates retain affinity towards the receptor (Chen et al., 2013) Remarkably, γ-conjugates are intrinsically obtained as the major product in reactions with carbodimide ((Viola-Villegas, Rabideau, Cesnavicious, Zubieta, & Doyle, 2008); nevertheless, a clean product is hard to obtain, as separation of γ-conjugate from α- and bis-conjugates and unreacted folic acid is troublesome. For this reason, it is critical to find reaction conditions under which formation of “clickable” α- and bis-conjugates is negligible. In this case, the crude product can be used as such for coupling with N<sub>3</sub>-PEG-PCL, then final Fol-PEG-PCL copolymer will be easily separated from non-conjugated folic acid and other byproducts (i.e., activated folic acid, Fol-NHS) by dialysis ((Liu, Zheng, Renette, & Kissel, 2012). For purposes of optimization, a screening at different reaction conditions (type and amount of catalyst and propargylamine/catalyst molar ratio) was preliminary carried out, and products were characterized by LC-MS (Table S1 and Fig. S1, supplementary material). Identification of α- and γ-conjugate peaks was made according to literature ((Trindade et al.,

2014). Conditions in which no  $\alpha$ - and bis-conjugate are forming, were adopted for  $\gamma$ -propargylfolate synthesis.

**Table 1.** Theoretical and experimental molecular weights of copolymers.

Sample	Mn (Da) <sup>a</sup>	Mn (Da) <sup>b</sup>	Mn (Da) <sup>c</sup>	Mw (Da) <sup>c</sup>	PDI <sub>d</sub> (Mw/Mn)
N <sub>3</sub> -PEG-PCL	5547	6203	5943	8049	1.36
PCLmPEGs-	5047	5446	5059	6737	1.33
PCLmPEG-	6047	6579	6594	8720	1.35

- a Theoretical number-average molecular weight.  
 b Number-average molecular weight evaluated by <sup>1</sup>H NMR.  
 c Molecular weight obtained by GPC.  
 d Molecular weight polydispersity index obtained by GPC.

In the click reaction, copper in form of wires was preferred as catalyst, since concentration of Cu(I) ions in solution is very low with respect to other catalysts type (Nahrwold et al., 2013), avoiding long purification steps. The total amount of crude propargylfolate used was such as to have a propargyl/N<sub>3</sub> molar ratio = 1.1. The copolymer is easily purified by extensive dialysis to remove non-conjugated molecules. Reaction was followed by FTIR; the absence of azide band in the spectrum of Fol-PEG-PCL accounts for a 100% conversion (Fig. S2, supplementary material). For sake of accuracy, Fol-PEG-PCL was analyzed by GPC-UV. The chromatogram shows a single peak at a retention time corresponding to that of pristine N<sub>3</sub>-PEG-PCL copolymer, confirming the absence of free folic acid and/or derivatives (Fig. S3, supplementary material). Finally, MP-AES analysis of Fol-PEG-PCL gives an amount of copper as low as 12 ppm, which allows to exclude any possible cytotoxic effect (Cao et al., 2012).

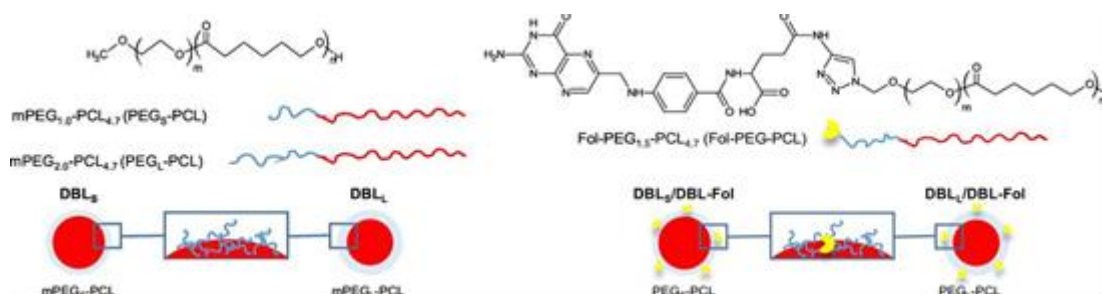


**Figure 1.** Design of untargeted and targeted NPs prepared from PEG-PCL diblock copolymers with different PEG length.

### ***3.2 Influence of PEG length on nanoparticle shell***

We aimed at studying the effect of PEG length on the shell properties of folate-decorated NPs. To this purpose, NPs based on mixtures of Fol-PEG-PCL with either mPEG<sub>L</sub>-PCL (DBL<sub>L</sub>/DBL-Fol), where PEG is 2.0 kDa, or mPEG<sub>S</sub>-PCL (DBL<sub>S</sub>/DBL-Fol), where PEG is 1.0 kDa (Fig. 1) were prepared. We fixed Fol-PEG-PCL amount in the composition at 20% by wt based on the results obtained in a previous paper (Conte et al., 2016). Corresponding non-targeted NPs were prepared from mPEG<sub>L</sub>-PCL (DBL<sub>L</sub>) and mPEG<sub>S</sub>-PCL (DBL<sub>S</sub>). Solvent diffusion method, currently indicated as nanoprecipitation, was selected since it is very popular for preparing biodegradable NPs. Furthermore, solvent diffusion is a working principle in microfluidics, a process useful to increase the scale of NP production.

As can be seen in Table 2, monodispersed NPs spontaneously form in high yield without the help of any surfactant. DBL<sub>L</sub> are smaller than DBL<sub>S</sub> likely due to higher hydrophilicity of PCL-mPEG<sub>L</sub>. A size lower than 100 nm as determined by dynamic light scattering and comprised in a narrow size range (PI<0.22) makes this formulation suitable for intravenous injection.  $\xi$  is slightly negative as commonly found for PEGylated NPs and unaffected by the incorporation of folate-modified copolymer. NPs exhibit spherical morphology and preserve their shape once freeze-dried in the presence of HP $\beta$ CD (Fig. S4, supplementary material).

The amount of PEG on NPs surface was evaluated by <sup>1</sup>H NMR and the packing extent of PEG on the surface calculated (Auguste et al., 2006; Q. Xu et al., 2015). Results are reported in Table 2. For all the samples, the experimental amount of PEG on the surface is much lower than the theoretical value, suggesting that, in the conditions adopted to produce non-targeted and folate-targeted NPs, PEG is located inside NP core and partly confined to the surface. The amount of PEG on the surface decreases for DBL<sub>L</sub> (despite their low size) and more in general upon addition of folate copolymer. Furthermore,  $[\Gamma]/[\Gamma^*]$  values well below the cut-off value of 1 indicate that PEG chains are in the mushroom-like conformation. These data demonstrate that, although NPs are prepared from PEGylated copolymers, the amount of PEG on the surface is below 7% in line with our previous results on triblock and star-shaped PEG-PCL copolymers (Ungaro et al., 2012). Similar degree of PEG coverage has been found preparing NPs by emulsion-solvent evaporation from mixtures of non-PEGylated and PEGylated copolymers (Q. Xu et al., 2015).

**Table 2.** Properties of NPs prepared from short (DBL<sub>S</sub>) and long (DBL<sub>L</sub>) MPEG-PCL copolymers without and with Fol-PEG-PCL (DBL-Fol).

Formulation	D <sub>H</sub> <sup>a</sup> (nm)	PI	ξ (mV)	Surface PEG <sub>b</sub> (wt%)	[Γ] <sub>c</sub> (chains/100 nm <sup>2</sup> )	[Γ]/[Γ*] <sup>d</sup>
DBL <sub>S</sub>	78 ± 1	0.12	- 13 ± 2	7.1	2.3	0.10
DBL <sub>S</sub> /DBL-Fol 20	82 ± 4	0.11	- 18 ± 2	4.2	1.4	0.07
DBL <sub>L</sub>	34 ± 2	0.16	- 15 ± 1	3.5	0.6	0.06
DBL <sub>L</sub> /DBL-Fol 20	59 ± 5	0.22	- 17 ± 3	2.0	0.6	0.05

The thickness of the external shell of NPs was evaluated by FALT, measuring the values of NPs ξ in NaCl solutions at different concentrations and fitting the data to a regression line ( $r > 0.980$ ) (Fig. 2A). The slope of these lines in absolute value represents FALT in nm. FALT is lower for NPs prepared from DBL<sub>S</sub> with short PEG ( $2.51 \pm 0.20$  nm) and higher for NPs prepared from DBL<sub>L</sub> with long PEG ( $3.84 \pm 0.15$  nm). In folate-decorated NPs, however, FALT increases for DBL<sub>S</sub>/DBL-Fol ( $2.72 \pm 0.11$  nm) and decreases for DBL<sub>L</sub>/DBL-Fol ( $3.58 \pm 0.29$  nm) suggesting a different arrangement of folate in the shell. Folate folding in PEG chains on the surface is likely occurring for DBL<sub>L</sub>/DBL-Fol, which could hide targeting ligand on the surface and prevent receptor recognition.

To gain insights into the environment experienced by folate moieties in the NPs, the emission behaviour of DBL<sub>S</sub>/DBL-Fol and DBL<sub>L</sub>/DBL-Fol was investigated by steady-state and time-resolved fluorescence spectroscopy. In fact, folate is a fluorescent molecule emitting in the visible range with an emission maximum at 450 nm. Fig. 2B shows the typical fluorescence emission of the folic acid, which is slightly more intense for DBL<sub>L</sub>/DBL-Fol. Inasmuch the two samples contain the same number of fluorogenic units, these slight but reproducible differences account for a larger fluorescence quantum yield for DBL<sub>L</sub>/DBL-Fol. In principle, this can be the result of i) self-quenching effects occurring in DBL<sub>S</sub>/DBL-Fol, ii) the different polarity experienced by the folate groups, or both. The dynamic behavior of the fluorescence is in line with the former hypothesis. As shown in Table 3, the fluorescence decay was bi-exponential in both cases.

**Table 3.** Lifetimes (in ns) and amplitudes ( $\Sigma\alpha = 1$ ) obtained by the biexponential fitting of the fluorescence decay for the different samples ( $\lambda_{ex} = 370$  nm  $\lambda_{em} = 450$  nm).

Sample	$T_1$	$\alpha_1$	$T_2$	$\alpha_2$
DBL <sub>S</sub> /DBL-Fol 20	0.50	0.30	7.71	0.70
DBL <sub>L</sub> /DBL-Fol 20	0.63	0.22	8.00	0.78

However, we observed a more pronounced contribution of the longer component in the case of DBL<sub>L</sub>/DBL-Fol. These findings are in fairly good agreement with a picture involving the folate group of DBL<sub>S</sub>/DBL-Fol more exposed to water pool instead of being extended in the PEG shell.

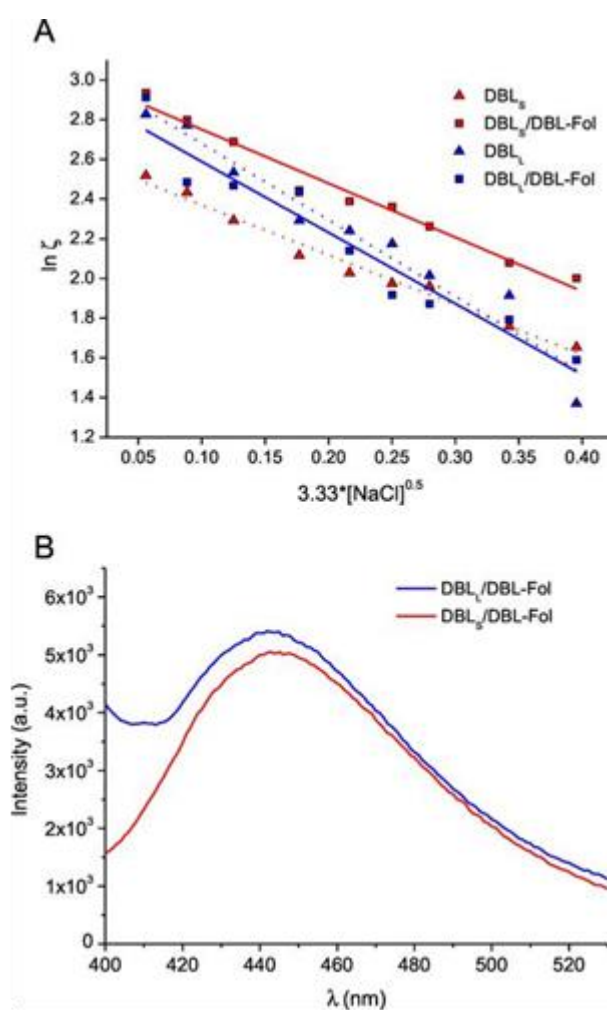


**Figure 2.** Properties of the NPs shell. A) Thickness of the outer shell of non-targeted NPs (DBL<sub>S</sub> and DBL<sub>L</sub>) and targeted NPs (DBL<sub>S</sub>/DBL-Fol and DBL<sub>L</sub>/DBL-Fol). Shell thickness (in nm) can be derived from the absolute value of the slope in the regression lines. For clarity purpose, results of a single experiment are reported. B) Emission spectra of folate-decorated NPs (5 mg/mL) in water ( $\lambda_{ex} = 370$ ).

### ***3.3 Interaction of nanoparticles with HSA***

Conformation of PEG on NPs surface can drive interactions with proteins. Here we focused on HSA, the most abundant protein in the blood pool. Interaction of NPs with HSA was clearly demonstrated by fluorescence spectroscopy. Fig. 3A shows the fluorescence spectra of HSA in the absence and in the presence of NPs upon excitation at 278 nm. This wavelength allows the selective excitation of HSA over folate. The black spectrum shows the typical dual band fluorescence spectrum of HSA, which reflects the contribution of the tyrosine ( $\lambda_{em}$  ca 310 nm) and tryptophan ( $\lambda_{em}$  ca 340 nm) fluorogenic centres. This strong emission is quenched by more than one order of magnitude upon addition of NPs. In contrast, the fluorescence of folate is basically unaffected in the presence of HSA (data not shown).

Since the emission of HSA fluorescent aminoacids well overlaps with the absorption spectrum of the folate, one could explain the quenching observed as a result of a photoinduced energy transfer via FRET mechanism. However, this is not the case since no emission of the folate was in fact observed concurrently to the quenching. Rather, the fluorescence behaviour might be simply due to static quenching effects arising by the massive aggregation of HSA on the NPs.

Formation of a HSA corona was evidenced also by evaluating size distribution curves of NPs at increasing HSA concentration (Fig. 3B). As compared to water, addition of HSA up to 5  $\mu$ M does not change greatly the shape of the size curves, while at physiologically relevant HSA concentrations (500  $\mu$ M) NPs mean size is increased for NPs of DBL<sub>L</sub> series and is unaltered for DBL<sub>S</sub>. The appearance of the peaks at 3 and 11 nm corresponding to free HSA monomers/tetramers/hexamers, indicate that in this adopted conditions, the surface of NPs is fully occupied by HSA. Remarkably, these results highlight that despite the low PEGylation extent, NPs developed here adsorb HSA forming a soft corona without inducing their aggregation.

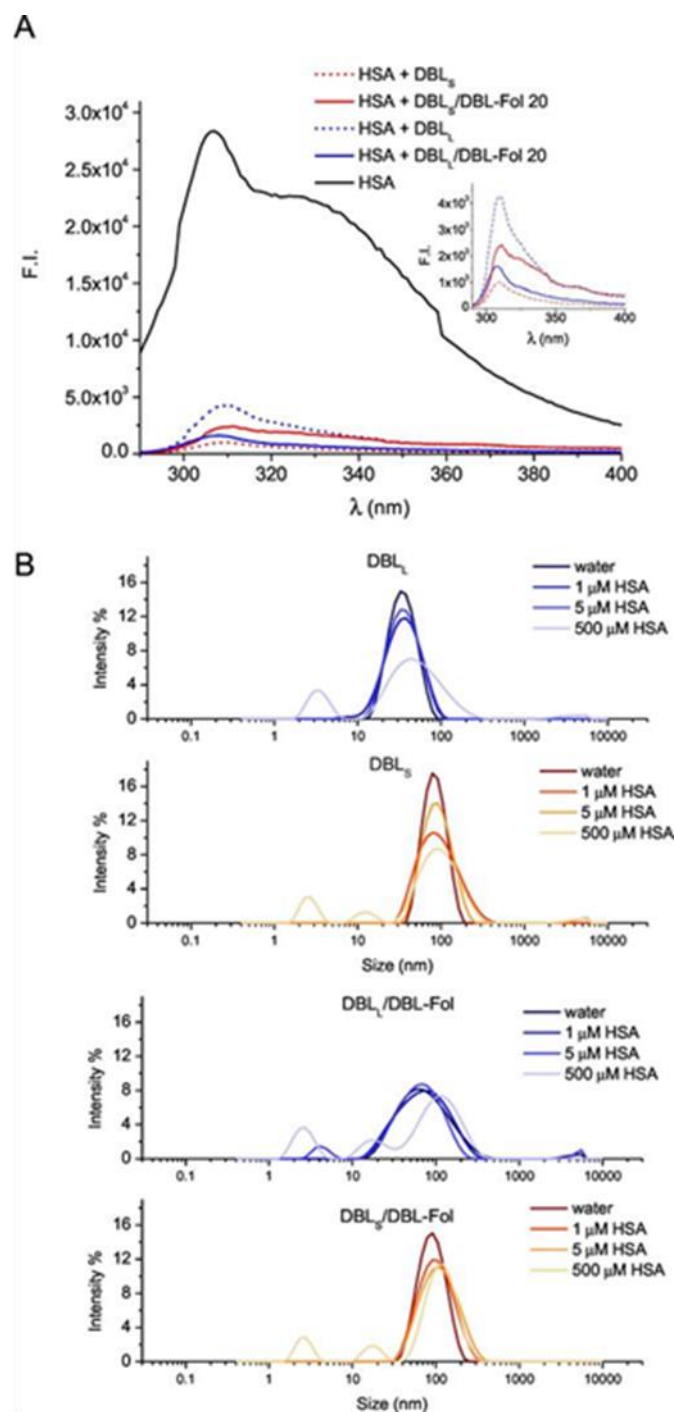


**Figure 3.** Behaviour of NPs in the presence of HSA. A) Emission spectra of folate-deco-rated NPs (5 mg/mL) in the presence of HSA (3  $\mu$ M). A reference curve of a HSA solution(0.3  $\mu$ M) is reported for comparison. Excitation wavelength was 278 nm. B) Size distribu-tion curves of NPs (0.05 mg/mL) in the presence of HSA (1–500  $\mu$ M).

### 3.4 Interaction of nanoparticles with human macrophages

To predict NPs *in vivo* capture by mononuclear phagocyte system (MPS) once NPs are intravenously injected, we studied *in vitro* their uptake in human macrophages differentiated from monocytes and isolated from human buffy coats. Untargeted and folate-targeted NPs were

pre-incubated with human serum for 10 or 30 min at 37 °C before a 3 h incubation with macrophages. A positive control of PCL NPs (non-PEGylated) was employed. Pre-incubation of NPs with human serum significantly increases the time-dependent uptake by macrophages for non-PEGylated NPs only (Fig. 4), while the uptake of all the PEGylated NPs is unaffected or shows the opposite trend. Confirming a general paradigm, non-PEGylated NPs demonstrate the highest capture level by macrophages. The uptake of untargeted NPs increases when shortening the PEG length from 2.0 kDa to 1.0 kDa. In any case, the presence of folate on the surface does not affect significantly NPs phagocytosis. This results are in line with the general observation that the presence of a PEG shell on NPs surface limits the adsorption of serum proteins largely preventing NPs capture by phagocytes as macrophages ((Walkey, Olsen, Guo, Emili, & Chan, 2012).

### ***3.5 Cellular uptake of nanoparticles in KB cancer cells***

To assess if the exposition of folate over the PEGylated surface increased the specific uptake of NPs in cells over-expressing FRs, we measured the uptake of targeted and non-targeted NPs in KB cells by flow cytometry. The uptake was measured in the absence and in the presence of 10% serum in the cell incubation medium to highlight the impact of NPs interaction with serum proteins. As reported in Fig. 5A, the uptake of DBL<sub>S</sub>/DBL-Fol occurs at least in part through FR-mediated endocytosis. In fact, pre-incubation of cells with 1 mM free Fol for 1 h to saturate FRs prior to NPs addition significantly decreases internalization. The extent of FR-mediated endocytosis of DBL<sub>S</sub>/DBL-Fol is higher without serum in the medium, probably due to partial ‘masking effect’ exerted by protein association to NPs shell (Conte et al., 2016). On the contrary, although PEGylation degree is low and PEG is in a mushroom conformation for both DBL<sub>S</sub>/DBL-Fol and DBL<sub>L</sub>/DBL-Fol, only DBL<sub>S</sub>/DBL-Fol allows the recognition of folate moieties by FR in the presence of serum. For DBL<sub>L</sub>/DBL-Fol, folate amount is lower than expected on the basis of fluorescence lifetimes, and is probably unable to extend over the NPs surface because of the presence of a serum proteins corona. Flow cytometry (Fig. 5A) and confocal microscopy analysis (Fig. 5B,C) confirm the capability of DBL<sub>S</sub>/DBL-Fol to be taken up by KB cells with some selectivity. Microscopy images highlight a cytoplasmic and more in particular a perinuclear localization of DBL<sub>S</sub>/DBL-Fol with a clear decrease of fluorescence signal in the case of cells pre-incubated with free folate.

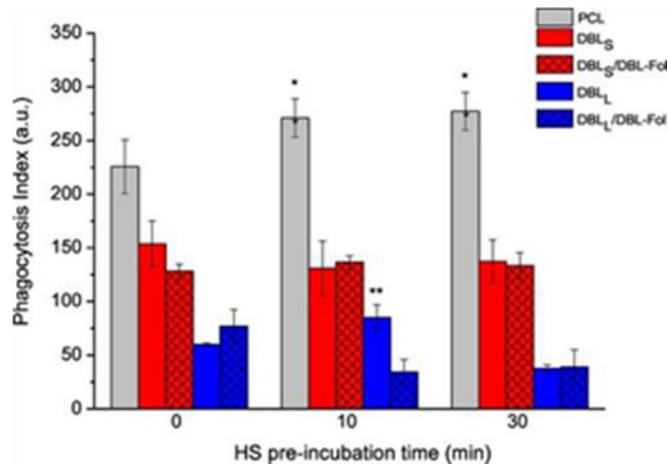


**Figure 4.** NPs capture by macrophages. NPs were pre-incubated in human serum (HS) for 10 or 30 min before a 3 h incubation with macrophages at 37 °C. Phagocytosis Index represents the median total fluorescence intensity measured per macrophage by FACS. \* $p < 0.005$ , \*\* $p < 0.001$ , with respect to NPs not pre-incubated with human serum (Student's  $t$ -test).

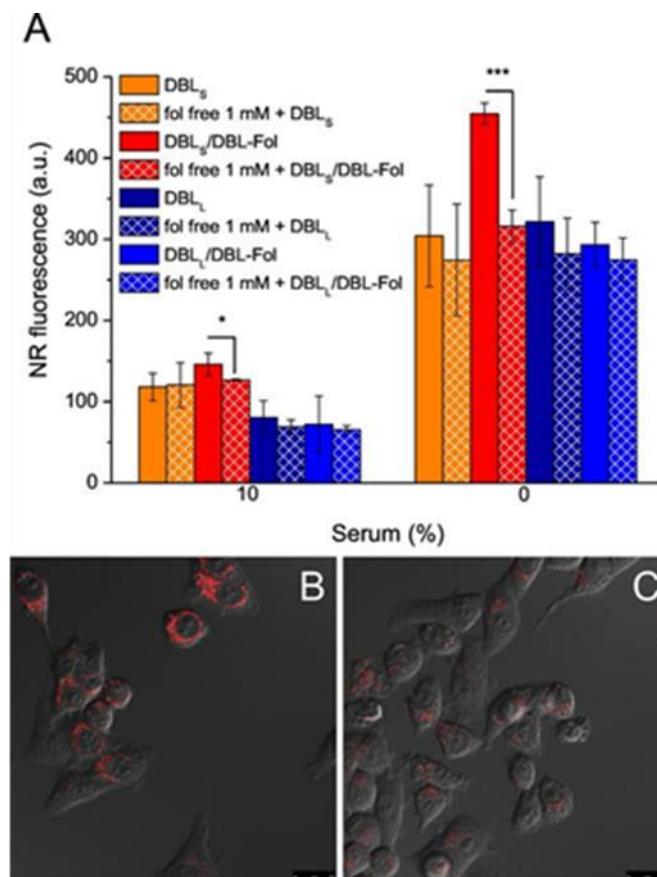


**Figure 5.** Intracellular uptake of NPs in KB cells over-expressing FRs. Flow cytometry measurements of the uptake of 20  $\mu\text{g}/\text{mL}$  of Nile Red-loaded NPs (A). Cells were incubated with NPs for 1 h with or without 10% serum in the medium and in the absence or the presence of 1 mM free folate (competition experiment). Significant different for \* $p < 0.05$ , \*\*\* $p < 0.001$ , Student's  $t$ -test. Confocal images of cells incubated with DBL<sub>S</sub>/DBL-Fol in the absence (B) or in the presence (C) of 1 mM free folate. (For interpretation of the references to color in this figure legend, the reader is referred to the web version of this article).

### ***3.6 Modulating degree of valency in folate-decorated nanoparticles based on PCL-mPEG<sub>s</sub>***

As a final experiment, we prepared DBL<sub>s</sub>/DBL-Fol at different folate copolymer percentage (0-50% by wt of total copolymer) to understand if the amount of folate copolymer affected uptake in KB cells. Size distribution curves indicate that all the formulations are monodispersed (Fig. 6A) with a size below 100 nm up to 30% of folate copolymer. A trend toward an increase of mean size and PI is observed for NPs at 50% Fol-PEG-PCL. All the NPs show a negative surface ( $\zeta$  potential from -13 to -18 mV) as generally found for PEGylated NPs. As it can be seen in Fig. 6B, emission intensity of NPs is increased when increasing folate content whereas NPs of PEG<sub>s</sub>-PCL (without folic acid) do not exhibit any fluorescence signal. Furthermore, increase of Fol-PEG-PCL to 50% does not increase significantly NPs fluorescence, confirming that a fluorescence quenching is observed when the surface is more populated by folate moieties. Uptake studies in KB cells incubated with DBL<sub>s</sub>/DBL-Fol containing 10%, 20% or 30% DBL-Fol polymers (Fig. 6C) demonstrated that, even in the presence of serum all the folate targeted formulations are taken up by cells via FR $\alpha$ -mediated endocytosis. Nevertheless, the extent of NPs accumulation through FR $\alpha$ -mediated endocytosis was comparable for all the formulations suggesting that an increase of folate amount in the NPs does not improve the extent of NPs intracellular accumulation.

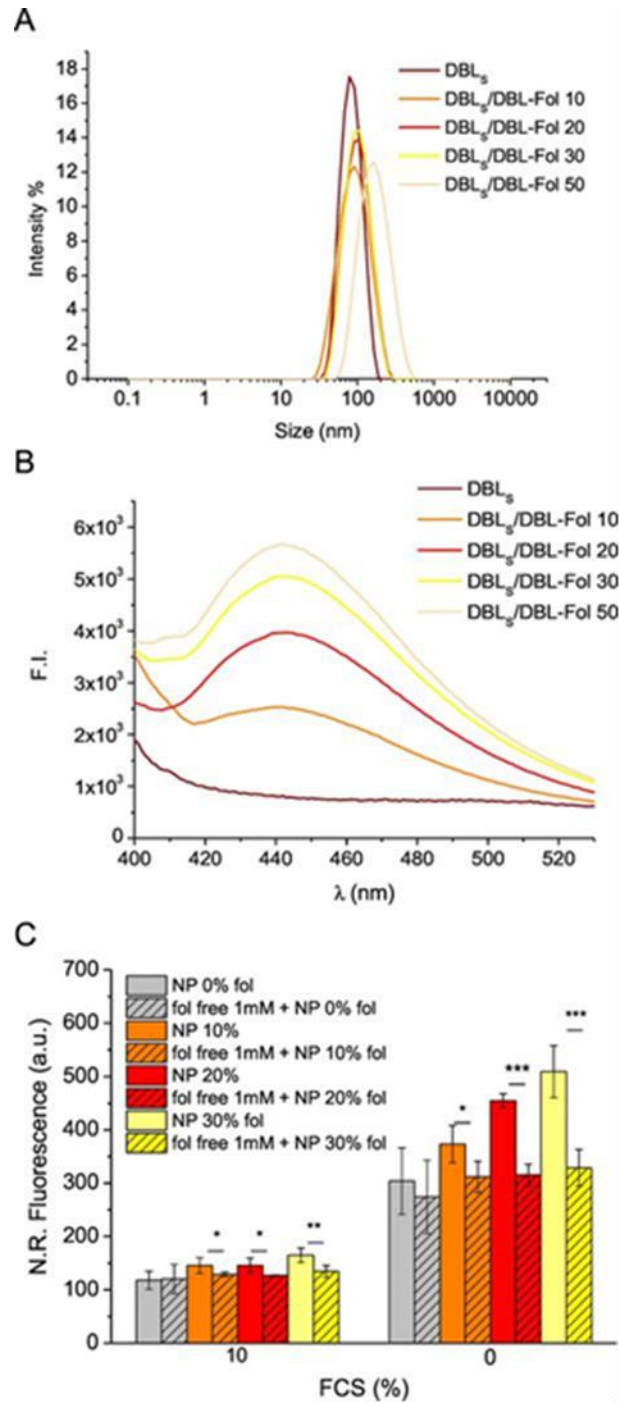


**Figure 6.** Properties of DBLS /DBL-Fol NPs with different percentages of Fol-PEG-PCL. A) Size distribution curves. B) Emission spectra at  $\lambda_{ex}$  278 nm (NPs concentration was 5 mg/mL). C) Uptake of NR-loaded NPs (20  $\mu$ g/mL) in KB cells after 1 h incubation in the presence and absence of FCS.

#### ***4 Conclusions***

Our study highlights that the too simplistic view of PEGylated NPs, both untargeted and targeted, is out to be close to the actual situation and needs to be elucidated if one wishes to correlate appropriately NPs properties to biological behaviour. We demonstrate that NPs prepared from diblock PEG-PCL copolymers by the widely employed solvent displacement method show a degree of PEGylation much lower than expected which depends on the length of PEG block. PEG acquires a mushroom conformation on NPs surface and its length affects the thickness of the hydrophilic shell as well as folate amount and exposition. HSA interacts with all NPs forming a protein corona which is not detrimental for stability. While all NPs show limited uptake in human macrophages, only the presence of short PEG (1.0 kDa) in the copolymer ensures that folate-bearing NPs are accumulated in KB cancer cells via FR $\alpha$ -mediated endocytosis.

This study offers a proof on how complimentary and simple techniques such as light scattering, fluorescence and NMR, can be employed to finely characterize the shell of targeted NPs with a PEGylated surface in the attempt to drive downstream effect such as NPs internalization in sub-set cell populations.

#### ***5 Acknowledgments***

This work was supported by Italian Association for Cancer Research (IG2014 #15764). The authors thank Mrs. D. Melck (NMR Service of Institute of Biomolecular Chemistry, CNR, Pozzuoli, Italy) for technical assistance. The authors are indebted to Prof. M. Trifuoggi (ACE Laboratory, University of Naples Federico II, Italy) for MP-AES analysis.

## References

1. Grossen, P., Witzigmann, D., Sieber, S., Huwyler, J., 2017. PEG-PCL-based nanomedicines: a biodegradable drug delivery system and its application. *J. Control. Release* 260, 46–60.
2. Li, Z., Tan, B.H., 2014. Towards the development of polycaprolactone based amphiphilic block copolymers: molecular design, self-assembly and biomedical applications. *Mater. Sci. Eng. C* 45, 620–634.
3. Bertrand, N., Leroux, J.C., 2012. The journey of a drug-carrier in the body: an anatomo-physiological perspective. *J. Control. Release* 161, 152–163.
4. Gao, H., Yang, Z., Zhang, S., Pang, Z., Jiang, X., 2014. Internalization and subcellular fate of aptamer and peptide dual-functioned nanoparticles. *J. Drug Target.* 22, 450–459.
5. Cheung, A., Bax, H.J., Josephs, D.H., Ilieva, K.M., Pellizzari, G., Opzoomer, J., Bloomfield, J., Fittall, M., Grigoriadis, A., Figini, M., Canevari, S., Spicer, J.F., Tutt, A.N., Kara-giannis, S.N., 2016. Targeting folate receptor alpha for cancer treatment. *Oncotarget*
6. Conte, C., Fotticchia, I., Tirino, P., Moret, F., Pagano, B., Gref, R., Ungaro, F., Reddi, E., Giancola, C., Quaglia, F., 2016. Cyclodextrin-assisted assembly of PEGylated polyester nanoparticles decorated with folate. *Colloids Surf. B: Biointerfaces* 141, 148–157.
7. Quaglia, F., Ostacolo, L., De Rosa, G., La Rotonda, M.I., Ammendola, M., Nese, G., Maglio, G., Palumbo, R., Vauthier, C., 2006. Nanoscopic core-shell drug carriers made of am-phiphilic triblock and star-diblock copolymers. *Int. J. Pharm.* 324, 56–66.
8. Rabanel, J.M., Hildgen, P., Banquy, X., 2014. Assessment of PEG on polymeric particles surface, a key step in drug carrier translation. *J. Control. Release* 185, 71–87.
9. Owens 3rd, D.E., Peppas, N.A., 2006. Opsonization, biodistribution, and pharmacokinetics of polymeric nanoparticles. *Int. J. Pharm.* 307, 93–102.
10. Endres, T.K., Beck-Broichsitter, M., Samsonova, O., Renette, T., Kissel, T.H., 2011. Self-assembled biodegradable amphiphilic PEG–PCL–IPEI triblock copolymers at the border-line between micelles and nanoparticles designed for drug and gene delivery. *Biomaterials* 32, 7721–7731.

11. Tirino, P., Conte, C., Ordegno, M., Palumbo, R., Ungaro, F., Quaglia, F., Maglio, G., 2014. Y- and H-shaped amphiphilic PEG-PCL block copolymers synthesized combining ring-opening polymerization and click chemistry: characterization and self-assembly behavior. *Macromol. Chem. Phys.* 215, 1218–1229.
12. Ungaro, F., Conte, C., Ostacolo, L., Maglio, G., Barbieri, A., Arra, C., Misso, G., Abbruzzese, A., Caraglia, M., Quaglia, F., 2012. Core-shell biodegradable nanoassemblies for the passive targeting of docetaxel: features, antiproliferative activity and in vivo toxicity. *Nanomedicine* 8, 637–646.
13. Himo, F., Lovell, T., Hilgraf, R., Rostovtsev, V.V., Noodleman, L., Sharpless, K.B., Fokin, V.V., 2005. Copper(I)-catalyzed synthesis of azoles. DFT study predicts unprecedented reactivity and intermediates. *J. Am. Chem. Soc.* 127, 210–216.
14. Li, Z., Chau, Y., 2010. Synthesis of heterobifunctional poly(ethylene glycol)s by an acetal protection method. *Polym. Chem.* 1, 1599–1601.
15. Szekely, G., Schaepertoens, M., Gaffney, P.R.J., Livingston, A.G., 2014. Iterative synthesis of monodisperse PEG homostars and linear heterobifunctional PEG. *Polym. Chem.* 5, 694–697.
16. Cammas, S., Nagasaki, Y., Kataoka, K., 1995. Heterobifunctional poly(ethylene oxide): synthesis of alpha-methoxy-omega-amino and alpha-hydroxy-omega-amino PEOs with the same molecular weights. *Bioconjug. Chem.* 6, 226–230.
17. Hiki, S., Kataoka, K., 2007. A facile synthesis of azido-terminated heterobifunctional poly(ethylene glycol)s for “Click” conjugation. *Bioconjug. Chem.* 18, 2191–2196.
18. Ishii, T., Yamada, M., Hirase, T., Nagasaki, Y., 2005. New synthesis of heterobifunctional poly(ethylene glycol) possessing a pyridyl disulfide at one end and a carboxylic acid at the other end. *Polym. J.* 37, 221–228.
19. Raynaud, J., Absalon, C., Gnanou, Y., Taton, D., 2009. N-Heterocyclic carbene-induced zwitterionic ring-opening polymerization of ethylene oxide and direct synthesis of  $\alpha,\omega$ -difunctionalized poly(ethylene oxide)s and poly(ethylene oxide)-b-poly( $\epsilon$ -caprolactone) block copolymers. *J. Am. Chem. Soc.* 131, 3201–3209.

20. Thompson, M.S., Vadala, T.P., Vadala, M.L., Lin, Y., Riffle, J.S., 2008. Synthesis and applications of heterobifunctional poly(ethylene oxide) oligomers. *Polymer* 49, 345–373.
21. El-Gogary, R.I., Rubio, N., Wang, J.T.-W., Al-Jamal, W.T., Bourgoignon, M., Kafa, H., Naeem, M., Klippstein, R., Abbate, V., Leroux, F., Bals, S., Van Tendeloo, G., Kamel, A.O., Awad, G.A.S., Mortada, N.D., Al-Jamal, K.T., 2014. Polyethylene glycol conjugated polymeric nanocapsules for targeted delivery of quercetin to folate-expressing cancer cells in vitro and in vivo. *ACS Nano* 8, 1384–1401.
22. Mahou, R., Wandrey, C., 2012. Versatile route to synthesize heterobifunctional poly(ethylene glycol) of variable functionality for subsequent pegylation. *Polymer* 4, 561.
23. Chen, C., Ke, J., Zhou, X.E., Yi, W., Brunzelle, J.S., Li, J., Yong, E.-L., Xu, H.E., Melcher, K., 2013. Structural basis for molecular recognition of folic acid by folate receptors. *Nature* 500, 486–489.
24. Viola-Villegas, N., Rabideau, A.E., Cesnavicious, J., Zubieta, J., Doyle, R.P., 2008. Targeting the folate receptor (FR): imaging and cytotoxicity of ReI conjugates in FR-overexpressing cancer cells. *ChemMedChem* 3, 1387–1394.
25. Liu, L., Zheng, M., Renette, T., Kissel, T., 2012. Modular synthesis of folate conjugated ternary copolymers: polyethylenimine-graft-polycaprolactone-block-poly(ethylene glycol)-folate for targeted gene delivery. *Bioconjug. Chem.* 23, 1211–1220.
26. Trindade, A.F., Frade, R.F.M., Macoas, E.M.S., Graca, C., Rodrigues, C.A.B., Martinho, J.M.G., Afonso, C.A.M., 2014. “Click and go”: simple and fast folic acid conjugation. *Org. Biomol. Chem.* 12, 3181–3190.
27. Nahrwold, M., Weiß, C., Bogner, T., Mertink, F., Conradi, J., Sammet, B., Palmisano, R., Royo Gracia, S., Preuße, T., Sewald, N., 2013. Conjugates of modified cryptophycins and RGD-peptides enter target cells by endocytosis. *J. Med. Chem.* 56, 1853–1864.
28. Cao, B., Zheng, Y., Xi, T., Zhang, C., Song, W., Burugapalli, K., Yang, H., Ma, Y., 2012. Concentration-dependent cytotoxicity of copper ions on mouse fibroblasts in vitro: effects of copper ion release from TCu380A vs TCu220C intra-uterine devices. *Biomed. Microdevices* 14, 709–720.

29. Auguste, D.T., Armes, S.P., Brzezinska, K.R., Deming, T.J., Kohn, J., Prud'homme, R.K., 2006. pH triggered release of protective poly(ethylene glycol)-b-polycation copolymers from liposomes. *Biomaterials* 27, 2599–2608
- 30 Xu, Q., Ensign, L.M., Boylan, N.J., Schon, A., Gong, X., Yang, J.C., Lamb, N.W., Cai, S., Yu, T., Freire, E., Hanes, J., 2015. Impact of surface polyethylene glycol (PEG) density on biodegradable nanoparticle transport in mucus ex vivo and distribution in vivo. *ACS Nano* 9, 9217–9227.
- 31 Walkey, C.D., Olsen, J.B., Guo, H., Emili, A., Chan, W.C., 2012. Nanoparticle size and surface chemistry determine serum protein adsorption and macrophage uptake. *J. Am. Chem. Soc.* 134, 2139–2147.

## **Chapter 4**

### **Strategies to overcome the Blood Brain Barrier (BBB)**

Alessandro Venuta, Carlotta Borsoi, Elvin Blanco and Mauro Ferrari

## ***1 Introduction***

The development of therapeutic strategy to treat brain diseases drew major attention in the last decades. This is because, especially for diseases such as cancer, when the disease affects the brain region, life expectancy drastically reduces. Cancers that usually lead to brain metastases are lung cancer, that commonly is divided in non small cell lung cancer (NSCLC) causing the majority of brain metastases in lung cancer patient, as well breast cancer, particularly HER2/neu type and triple negative (TNBC). Melanoma skin cancer, colon cancer and kidney cancer are also related to the development of brain metastases (1). Presently, the most effective therapy is surgery (2) coupled with several approaches based on radiation such as intensity modulated radiation therapy (IMRT) (3), image guided radiation therapy (IGRT) (4), whole brain radiation therapy (WBRT) (which is associated to the highest success rate) (5), stereotactic radiosurgery (SRS) (6). No systemic drug therapy (chemotherapy, targeted or immune-based therapy) has received FDA approval for the treatment of brain metastases from solid tumor. This occurs because most chemotherapeutic agents are not able to cross the blood brain barrier (BBB).

The idea of a brain barrier was first highlighted by Ehrlich and Goldman who observed that water soluble dyes injected through systemic injection did not stain the brain or the cerebrospinal fluid (CSF). Additional experiments showed that these same dyes injected directly into the brain colored the brain and CSF, but not other organs. The observations drawn from these dye studies brought about the concept of a barrier between blood and brain, known as BBB. The anatomical structural knowledge of the BBB is still growing although a basic architecture of the cerebral vascular endothelium has been outlined. It consists of highly specialized vascular endothelial cells (EC) associated with astrocytic and pericytes that maintain BBB properties such as tight junction (TJ) and regulation of vesicular trafficking (7). Also at endothelial level there is a system of P450 cytochrome and enzymes. Further, the presence of efflux transporter transporters belonging to the family of the gene ABC (ATP-binding cassettes) /MDR1 as the Glycoprotein P (P-gp) that can actively transport a huge variety of drugs out of the cell plays a key role in the transport of drugs through the BBB (8). These anatomical features establish a continuous barrier between blood and brain interstitial fluid (ISF) with reduces permeability. Nonetheless, BBB represents the principal site of exchange between the whole organism and the central nervous system (CNS) because it serves to exclude the xenobiotic substances and at the same time to regulate brain homeostasis. Several mechanisms of membrane transport such as simple diffusion for transport of water, gases and

lipophilic substances, carrier-mediated transport is involved in the carriage of nutrient as glucose (GLUT-1), ions, monocarboxylic acid and neutral amino acids, while other two transcytosis systems, one receptor-mediated (insulin and transferrin) and the other based on electrostatic interactions, drive exchanges with blood. (9). Against this background, it is clear why systemic drug therapy fails since BBB prevents the passage of 98% of chemotherapeutics (10).

In the development of novel approaches for brain tumors, nanotechnology seems very hopeful. Indeed, the possibility to design a carrier that protects the payload from the degradation in the blood stream, avoids the opsonization improving circulation time and biodistribution profile, circumvents the efflux pumps and even more drives therapeutic agents directly to the target site is a fascinating option. In brain cancer research, different types of nanoparticles (NPs) have been employed as imaging and delivery agents, including inorganic metal based NPs (magnetic Fe<sub>3</sub>O<sub>4</sub> NPs (11), gadolinium NPs (12), gold NPs [AuNPs] (13) and quantum dots [QDs] (14)) and organic polymer based NPs (dendrimer (15), hydrogel (16) and polymer (17)). Metallic NPs have gained major attention, owing to the fact that they can be used also in magnetic resonance imaging (MRI) as contrast agents for monitoring of brain tumors. Organic NPs on the other side give the opportunity to simply modify their surface properties, which is important in that one of the most popular method used to cross the BBB involves the conjugation of peptides, antibodies or small molecules directly to the drug of interest or to its delivery vehicle, to overcome the BBB through specific interaction with receptors that are expressed on endothelial cells. An example is the low-density lipoprotein receptor proteins (LRPs). LRPs are expressed on neurons and astrocytes, but are also overexpressed in malignant astrocytomas such as glioblastomas, which are the most common and aggressive forms of brain cancer. However, BBB still constitutes a hindrance and this technology has not achieved the expected results due to low accumulation to the cancerous areas.

An innovative approach in this field could be the development of a platform able to protect these nanosized carrier into the circulatory system facilitating the transport directly into the cells. One possibility is combine micro- and nano-technology designing a carrier that can effort in a sequentially manner the various biological barriers such as Multi Stage Vectors (MSV) (18,19).

In order to obtain preferential accumulation of a drug at the brain microvasculature, a functionalized MSV-based system was developed. The micro-vector surface was coated with

the surfactant Polysorbate 80 (Tween® 80) that seems to lead to the adsorption of apolipoprotein E from blood plasma onto the nanoparticle surface and to mimic low density lipoprotein (LDL) particles by interacting with the LDL receptor or with molecules such as transferrin (Tf) to exploit overexpressed receptors at the BBB for transport. After obtaining accumulation, near the endothelial wall, the capacity of transporting simultaneously more than one active component in the porous micro particle has been exploited in vitro and in vivo.

## ***2 Experimental section***

### ***2.1 Materials***

3 -aminopropyltriethoxysilane (APTES), 3-(Triethoxysilyl)propyl isocyanate 95%, holo-Transferrin human  $\geq 98\%$ , sulfuric acid (99.999% w/v), triethanolamine, 98+% (TEA) N,N-dicyclohexylcarbodiimide (DCC) and N-hydroxysuccinimide (NHS) were bought from Sigma-Aldrich, Invitrogen Alexa Fluor 647 dye from ThermoFisher scientific , Phosphate Buffered Saline (PBS), Dimethyl Sulfoxide (DMSO), 30% hydrogen peroxide (30% w/v), polysorbate 80 (Tween® 80) and 2-Propanol (Certified ACS) were bought from Fisher Scientific Co L.L.C.

### ***2.2 Oxidation and APTES modification of MSV***

The porous silicon particles were oxidized and chemically modified with 3 -aminopropyltriethoxysilane (APTES). Piranha solution (9 mL) was prepared with 70% sulfuric acid (99.999% w/v) and 30% hydrogen peroxide (30% w/v) by first pouring the peroxide solution into a glass flask containing the MSV, which was positioned in an oil bath ( $\sim 95^{\circ}\text{C}$ ) to control the temperature. Then, the acid was slowly poured into the flask under stirring for 2 h. The reaction mixture was let overnight at room temperature and the oxidized-particles (OX-MSV) were washed three times with 2-propanol (IPA). The OX-MSV were put in a 2% APTES IPA solution for 48 h at  $65^{\circ}\text{C}$  under stirring. The particles were washed twice with water by centrifugation (10000 rpm x 30 min) and stored in IPA at  $4^{\circ}\text{C}$ .

### ***2.3 Polysorbate 80 (Tween 80) coating***

For the overcoating with polysorbate 80, in two different glass vials respectively one and two percent (m/v) of polysorbate 80 was added to the microparticles suspensions under gentle stirring for 30 min (Tween80-MSV). The coating was evaluated by Scanning Electron Microscopy (SEM) and Energy Dispersive X-ray Analysis (EDAX).

### ***2.4 Conjugation of holo-Transferrin human (hTf) to MSV***

The conjugation procedure was carried out by the surface activation method. Briefly, 5 billion of oxidized MSV were put overnight in 2% IPA solution of 3-isocyanatopropyltriethoxysilane under stirring at RT to conjugate isocyanate groups to the surface of MSV (MSV-NCO). MSV-NCO were collected by centrifugation at 10000 rpm x 30 min and the solvent was removed under vacuum. The silicon surface was activated with an organic solution of N,N-dicyclohexylcarbodiimide (DCC) and N-hydroxysuccinimide (NHS) using dimethylsulfoxide (DMSO) as a solvent. NHS concentration was 0.1 M and that of DCC was 0.2 M in DMSO. The final product was washed 3 times with IPA. Human transferrin (hTf) was chemically grafted to the functionalized porous particles (hTf-MSV) using an aqueous solutions containing particles and hTF under magnetic stirring (100 rpm) at room temperature overnight. The protein concentration was determined using the BCA Protein Assay Kit (Pierce Biotechnology, Rockford, IL). Microplate assays were performed according to manufacturer's recommendations and absorbance was measured on microplate reader (Synergy H4 hybrid reader, BioTek Instruments Inc., Winooski, VT). The final product was washed with IPA and stored at 4° C after concentration (Vacufuge®).

### ***2.5 Fluorescent particles***

In order to track the accumulation of MSV inside brain microcirculation, fluorescent MSV covalently grafted with Alexa Fluor™ 647 were produced. For loading of Alexa Fluor™ 647 (Invitrogen), approximately 1 billion of MSV-OX were suspended in 400 µL of DMSO. Afterwards, 67 µL of a 1 mg/mL solution of Alexa Fluor™ 647 in DMSO and 40 µL of a 100 mM triethanolamine, 98+% (TEA) in DMSO were added. The microparticles were then shaken for 2 h at room temperature and washed five times with sterile water. After sample concentration (Cacufuge®) overnight, the samples were stored at 4° C.

### ***3 In Vivo Studies***

The animal studies were performed in accordance with the guidelines of the Animal Welfare Act and the Guide for the Care and Use of Laboratory Animals and The Houston Methodist Institutional Animal Care and Use Committee based on approved protocols (AUP-1214-0066). Healthy 4- to 8-week-old female BALB/c were injected via retro orbital venous sinus with labeled MSV dispersed in 100 µL saline.

### ***3.1 Inductively coupled plasma mass spectroscopy (ICP-MS)***

Si contents released from the particles during the degradation process were measured using a Inductively coupled plasma mass spectroscopy (ICP-MS). Si was detected at 250.69, 251.43, 251.61, and 288.158 nm. Yttrium (1 ppm) was added to both standards and samples to correct for instrumental drift during the run. A calibration run including the internal control was made before each group of samples. The detection limit of Si was 15 ppb. The results are expressed as a percentage of the silicic acid released into the medium. At 2 h after the injection, the groups of animals (n = 4) were sacrificed and the major organs (liver, spleen, heart, lungs, and kidneys) were harvested, weighed, and processed for elemental analysis. Briefly, the organs were homogenized in 20% EtOH in 1 N NaOH and left for 72 h at room temperature for extraction of Si. Then the extracts were centrifuged at 5,000 rpm for 30 minutes and 0.5 mL of the supernatant was picked up, diluted with 2.5 mL of deionized water, and analyzed for Si contents. Si content was measured by ICP-MS as described earlier. Further, all results were recalculated considering the dilutions performed and were normalized to individual organ weight.

### ***3.2 Immunohistochemistry (IHC)***

To confirm that the MSV accumulated at the BBB, the animals (n = 4) were sacrificed 2 h after the injection, and the brains were harvested, weighed, and frozen in optimal cutting temperature compound (OCT) at -80° C. The frozen block was cut into slices and fixed on glass to perform immunohistochemical analysis. Briefly, sections were incubated with a 4% paraformaldehyde solution in phosphate buffered saline (PBS) pH 7.4 and washed twice for 30 sec with PBS. Serial longitudinal sections (n=6, thickness 8 µm) were then incubated for 20 min at RT in a blocking solution containing 1% normal goat serum (NGS) and 5% normal horse serum (NHS) in PBS and overnight at 4°C with primary anti-mouse CD31 rat polyclonal antibody (Abcam) (Cambridge, MA, USA) appropriately diluted in blocking buffer (1:100). Control sections were incubated in the absence of primary antibody (data not shown). The following day, sections were rinsed in PBS (3 x 5 min) and incubated for 5 min at RT in blocking buffer, followed by 1 h incubation at RT in the dark with diluted rhodamine (TRITC) AffiniPure F(ab')<sub>2</sub> Fragment Donkey Anti-Rat IgG (H+L) (Jackson immunoresearch). Sections were washed twice for 1 min with PBS and then incubated for 3 min with 4',6-Diamidino-2-Phenylindole, Dihydrochloride (DAPI) (Fisherscientific). Immunofluorescence was imaged by confocal microscopy (Nikon, Tokyo, Japan) and the fluorescent images were analyzed using NISElements software (Nikon).

### ***3.3 Intravital Microscopy (IVM)***

Fluorescent MSV were functionalized as described above and the accumulation of the fluorescent hTf-MSV in the brain microcirculation was evaluated by intravital microscopy (IVM) in BALB/c mice. The animals were anesthetized by inhalation of isoflurane (4-5% + 0.8-1 L/min) and then put on a polycarbonate plate with the head immobilized. Briefly, the animals were anesthetized and a longitudinal incision of the skin was made. The periosteum was scraped off and a 6-mm circle over the frontal and parietal regions of the skull was made by using a high-speed dental drill. The glass window was applied with the aid of glue. The plate was placed on the heated stage of an intravital fluorescence microscope. Under the microscope AlexaFluor647-labeled particles (1 billion/ 23 g body weight) and the tracer fluorescein isothiocyanate-conjugated dextran (FITClabeled 70 kDa dextran, see chapter 2 for details) (0.1 ml/25 g body weight) were administered via retro-orbital injection. Tracer was used to delineate the vasculature. Video and images of blood flow were acquired using an upright Nikon A1R laser scanning confocal microscope equipped with a resonance scanner and heated stage at different time points (T<sub>1</sub>- 15 min, T<sub>2</sub>- 20 min, T<sub>3</sub> – 90 min and T<sub>4</sub> – 120 min). All settings including laser power, gain, offset, and pinhole diameter were maintained throughout each acquisition. All images were analyzed with NIS-Elements software to quantify the amount of particles in different tissues at different time points. Data were obtained by averaging results on at least three images from three mice

### ***3.4 In Vivo Imaging Systems (IVIS)***

Animals were sedated with isoflurane and imaged on an IVIS Lumina (Xenogen; Caliper Life Sciences, Hopkinton, MA) after intravenous administration of fluorescent-MSV decorated with hTf (1 billion/ 23 g body weight). Animals were imaged using Alexa Fluor 647™ excitation (650 nm) and emission (665 nm) filters. At 2 h groups of animals (n = 4) were sacrificed and their organs were excised and imaged under the same conditions as live animals to determine the organ distribution of fluorescent hTf-MSV. Images and data were analyzed using Living Image 4.0 software (Caliper Life Sciences).

## 4 Result and discussion

### 4.1 Particles characterization

#### 4.1.1 MSV coated with polysorbate 80

The formation of a polysorbate 80 coating was evaluated by Scanning Electron Microscopy (SEM) (Figure 1) and Energy Dispersive X-ray Analysis (EDAX) (Figure 2). The images revealed that the particles were successfully coated and element mapping performed with X-ray spectrometer coupled to the microscope confirmed the parallel presence of elements such as Carbon and Oxygen together with Silicon presence.

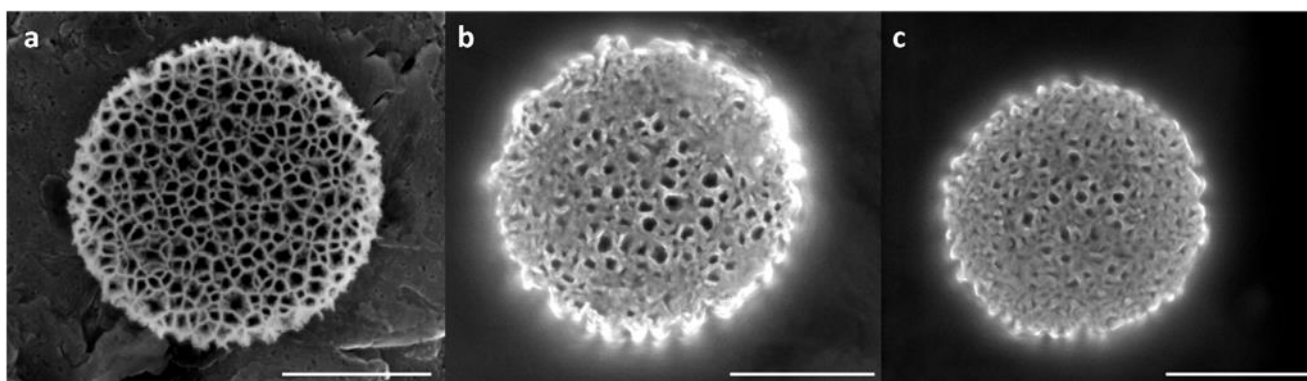


**Fig 1.** SEM images of uncoated and coated MSV. a) Uncoated discoidal porous silicon particles. Scale bar, 500 nm; b) Particle coated with a 1 % solution of polysorbate 80. Scale bar, 400 nm; c) Particles coated with 2 w/v% solution of polysorbate 80. Scale bar, 400 nm.

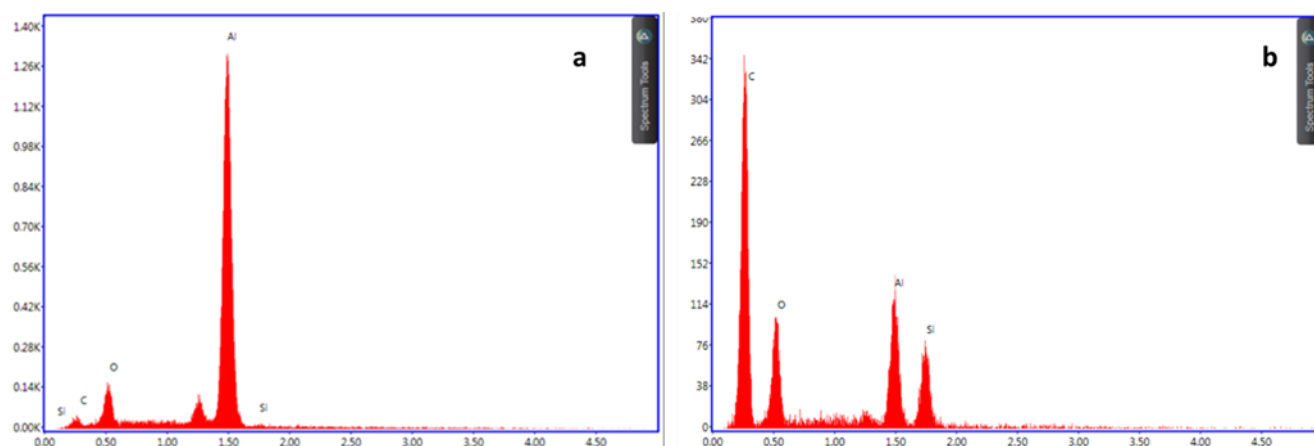


**Fig 2.** Elements mapping performed with EDAX. The resulting spectra reveal that in absence of Si, the main element in the composition of MSV, there is no evidence of C and O. a) Spectrum of an area without MSV, b) spectrum of a coated MSV.

#### 4.1.2 MSV coated with hTf

The quantification of the total amounts of hTf on the surface of MSV was performed with an indirect BCA assay. Briefly, for the BCA assay, protein reduces  $\text{Cu}^{2+}$  to  $\text{Cu}^{+}$  under alkaline conditions, and this ion binds 2 molecules of BCA dye, which absorbs at 562 nm and is sensitive in the range 20–2000  $\mu\text{g}/\text{mL}$  protein. Standard curves were prepared using BSA in  $\text{H}_2\text{O}$ . The assay showed that hTf was successfully conjugated to the microparticles surface, being the amount of protein on particles surface 2.83 mg/billion. Particles were also imaged by SEM (Fig.3).

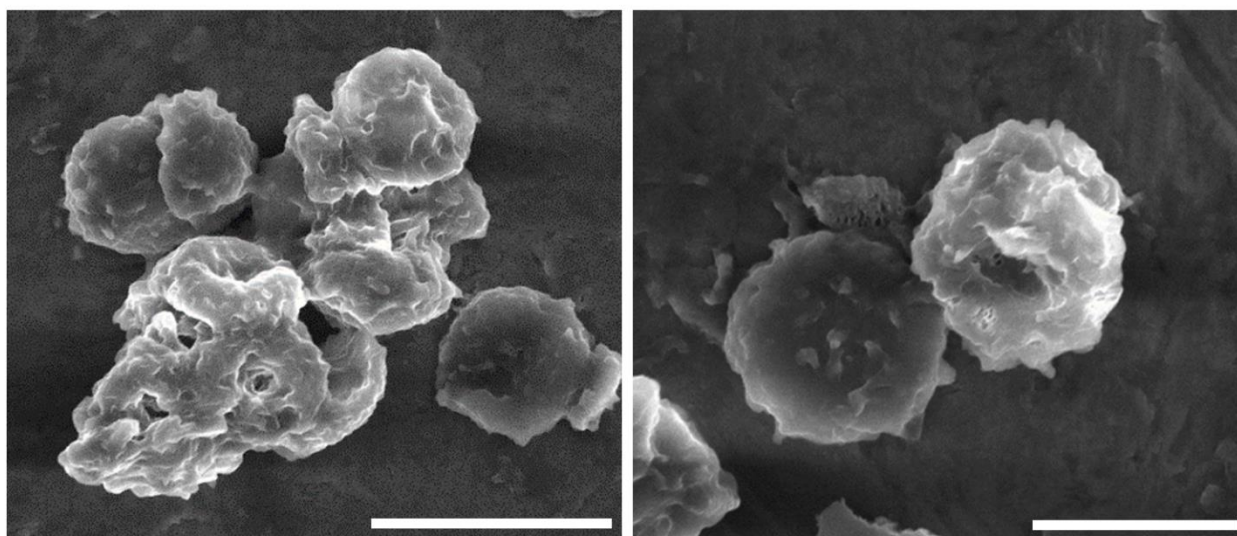


**Figure 3.** SEM images of hTf coated MSV. Scale bar, 5  $\mu\text{m}$  (left); Scale bar, 3  $\mu\text{m}$  (right).

The reaction was followed also by monitoring the change of particle surface charge through the measurement of zeta potential ( $\zeta$ ). The conjugation of hTf resulted in a radical change of the surface charge from negative to positive values due to its covalent anchoring (Table 1).

**Table 1.** Surface charge of MSV before and after hTf decoration.

	<b>Zeta potential (<math>\zeta</math>) (mV)</b>
<b>MSV-OH</b>	-40
<b>MSV-NCO</b>	-45
<b>MSV-hTf</b>	+2.5

## ***4.2 Brain accumulation***

To evaluate the accumulation of the functionalized vectors at BBB various techniques have been employed.

### ***4.2.1 Immunohistochemical analysis of frozen brain section***

Immunohistochemical analysis coupled with confocal microscopy allowed to observe the presence of fluorescence in brain sections in proximity of the nucleus (Figure 4). To clarify where the particles accumulated, CD31 was used to highlight if the hTF-MSV reached the endothelial cells in histological tissue. In contrast with the previous analysis no fluorescence was detected in the new sections (Figure5) thus led to further investigation on the ability of targeted particles to accumulate at the BBB.

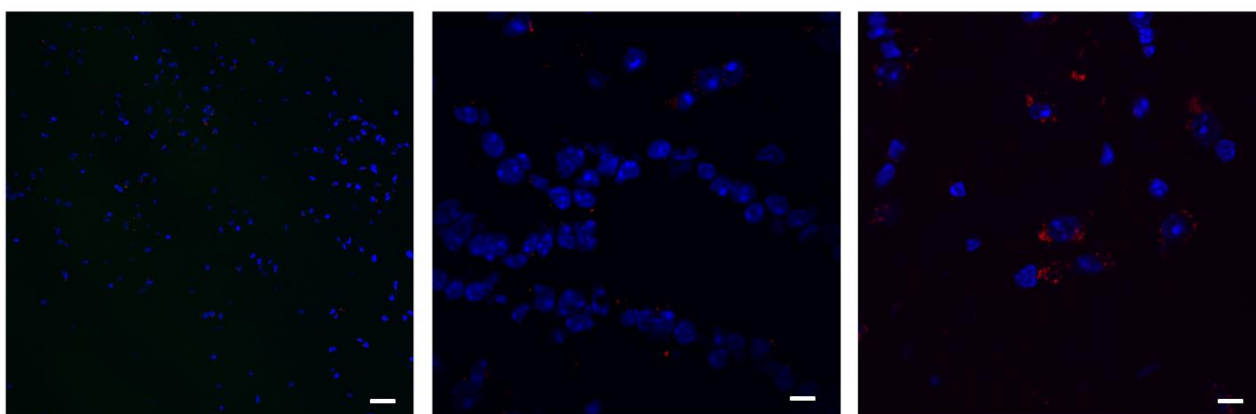


**Figure 4** Immunohistochemical analysis of fluorescent hTF-MSV in brain sections from mice.

Scale bar 5 $\mu$ m

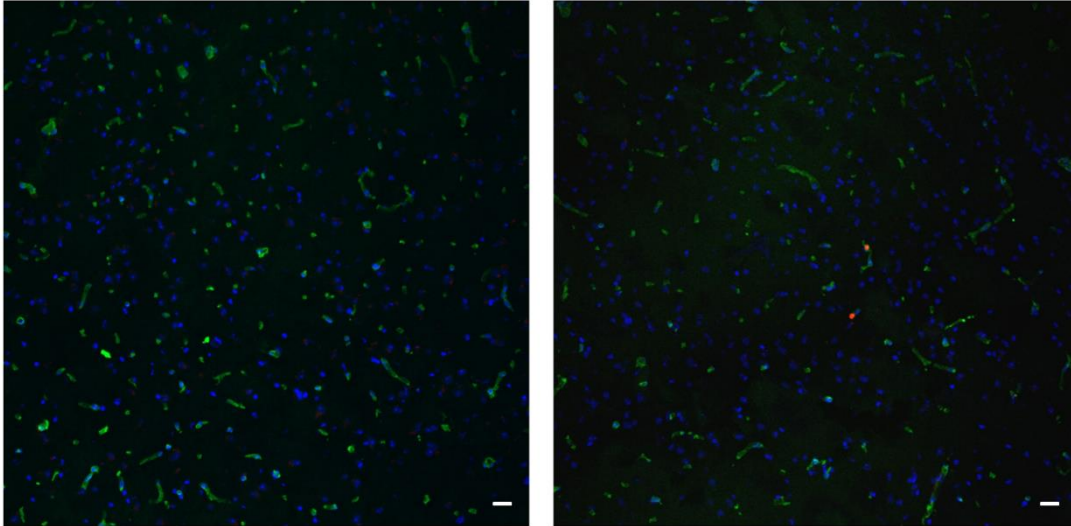


**Figure 5.** Frozen section of mouse brain mouse injected with hTF-MSV. Sections were stained with primary anti-mouse CD31 rat polyclonal antibody followed by a secondary antibody and DAPI. Scale bar

#### ***4.2.2 In vivo accumulation of functionalized particles***

Intravital imaging was performed at three time points ( $T_1$ -15 min,  $T_2$ -30 min and  $T_3$ -2h) to monitor the behaviour of Tween 80 coated MSV and hTf-MSV in the brain environment. Particles were administrated via retro orbital injection and their circulation was monitored for 2 h. In both cases, at  $T_1$  particles were detected in the bloodstream but after 30 min dissapeared from circulation showing no accumulation at the site of interest.

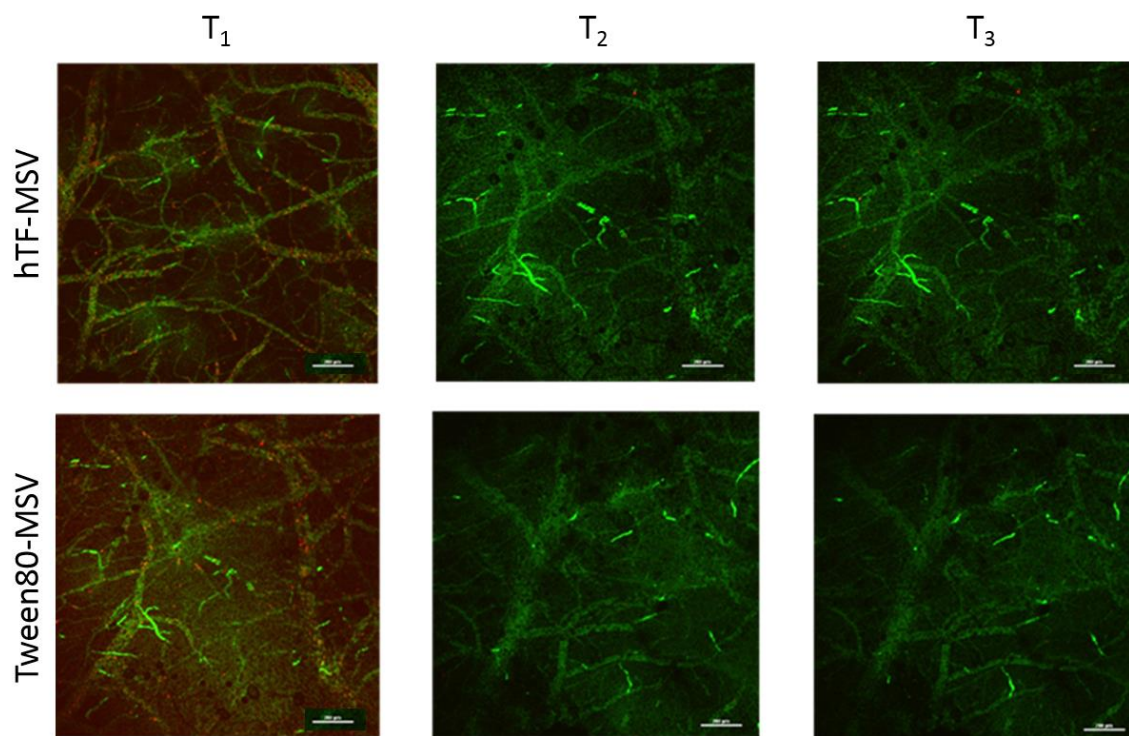


**Figure 6** Brain microcirculation of BALB/c monitored in real time via intravital microscopy. Images were recorded at different time points (T<sub>1</sub>- 15 min, T<sub>2</sub>- 30 min and T<sub>3</sub>- 2 h) after injection of hTf-MSV (upper row) and Tween 80-MSV (lower row). Vessels were highlighted before MSV administration through injection of fluorescein isothiocyanate–dextran average MW 70k. No particle accumulation at BBB was detected after 2 h. Scale bar

#### ***4.2.3 Evaluation of in vivo biodistribution***

To evaluate organ biodistribution after systemic injection, an in vitro optical imaging system based on NIR fluorescence detection was employed. After 2 h, corresponding to observation time T<sub>3</sub> in the intravital microscopy of brain, the animals were sacrificed and the major organ were harvested and weighted (Figure 7). At this time point, a prominent accumulation of the fluorescent signal was observed in the liver and in the lungs while in the case of hTf-MSV, particles accumulated also in the kidneys and in the spleen. No signal was detected from the brain.

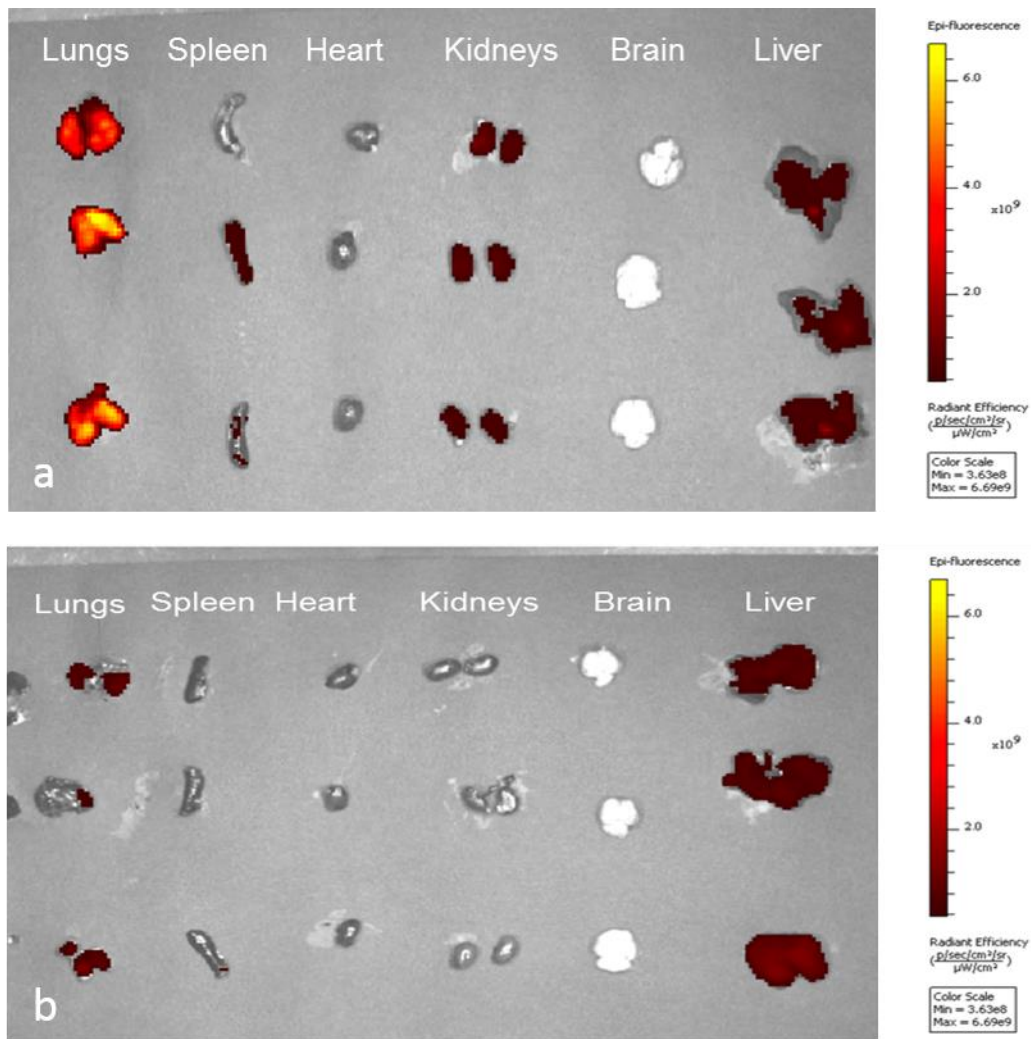


**Figure 7.** In vivo NIR imaging following intravenous administration of hTf-MSV (a) and Tween 80-coated MSV (b) tagged with Alexa Fluor 647. Organs collected after sacrificing the animal (time point 2 hours) for ex vivo evaluation of the accumulation of the fluorescence signal in the different organs and tissues.

#### 4.2.4 Quantification of Si

To further validate results obtained with IVIS, the amount of Si in different organs after MSV and hTf-MSV injection was quantified using ICP (Figure 8). The data were normalized to the weight of the corresponding organ. Among the tested tissues, significant amounts of MSV were found in the spleen, liver, and lungs. The presence of targeted particles in the heart, kidney and brain tissues was relatively low or undetectable. These data correlate well with the in vivo NIR imaging, supporting that no accumulation was detected at the BBB using functionalized particles. Nevertheless, it seems evident that targeting ability of MSV is changing upon hTf decoration increasing the accumulation in lung. This effect could be highly relevant to decrease accumulation of MSV in MPS organs and target lung metastasis.

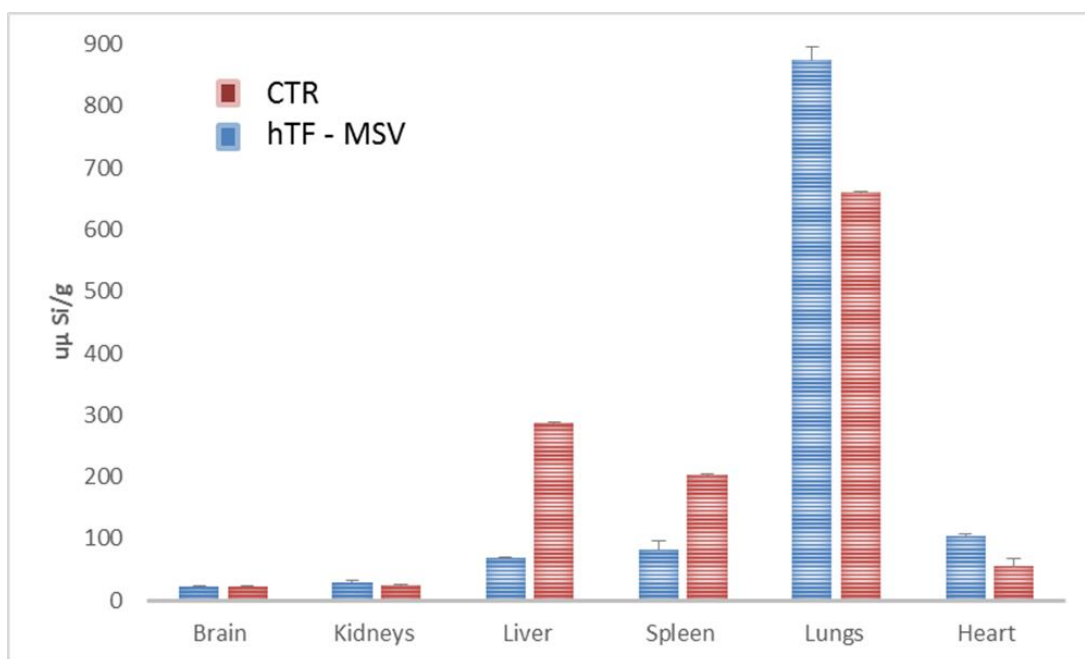


**Figure 8.** Biodistribution of Si (Si/organ) ( $\mu\text{g/g}$ ) in mice organs after i.v injection of hTf-MSV. Significant amounts of MSV were found in the spleen, liver, and lungs. The presence of targeted particles in the heart, kidney and brain tissues was relatively low or undetectable.

### 5 Conclusion

This study showed that for the delivery of micro- particles to the brain site a surface functionalization is not enough. The MSV platform is well-suited to chemical modification that not affect the biodistribution of the disc shaped porous silicon particles. However further in-depth studies should be made to achieve the intended result. Possibly, a shape and size modification might be a promising approach to exploit the anatomical features of the BBB in the disease.

## References

- Abd Ellah, N. H., & Abouelmagd, S. A. (2017). Surface functionalization of polymeric nanoparticles for tumor drug delivery: approaches and challenges. *Expert Opin Drug Deliv*, 14(2), 201-214.
- Abdulkareem, I. H., & Zurmi, I. B. (2012). Review of hormonal treatment of breast cancer. *Niger J Clin Pract*, 15(1), 9-14.
- Akbarzadeh, A., Rezaei-Sadabady, R., Davaran, S., Joo, S. W., Zarghami, N., Hanifehpour, Y., et al. (2013). Liposome: classification, preparation, and applications. *Nanoscale Res Lett*, 8(1), 102.
- Akhtar, M. J., Ahamed, M., Alhadlaq, H. A., Alrokayan, S. A., & Kumar, S. (2014). Targeted anticancer therapy: overexpressed receptors and nanotechnology. *Clin Chim Acta*, 436, 78-92.
- Ali, A., Zafar, H., Zia, M., Ul Haq, I., Phull, A. R., Ali, J. S., et al. (2016). Synthesis, characterization, applications, and challenges of iron oxide nanoparticles. *Nanotechnol Sci Appl*, 9, 49-67.
- Anglin, E. J., Cheng, L., Freeman, W. R., & Sailor, M. J. (2008). Porous silicon in drug delivery devices and materials. *Adv Drug Deliv Rev*, 60(11), 1266-1277.
- Arvizo, R., Bhattacharya, R., & Mukherjee, P. (2010). Gold nanoparticles: opportunities and challenges in nanomedicine. *Expert Opin Drug Deliv*, 7(6), 753-763.
- Ascierto, P. A., Kirkwood, J. M., Grob, J. J., Simeone, E., Grimaldi, A. M., Maio, M., et al. (2012). The role of BRAF V600 mutation in melanoma. *J Transl Med*, 10, 85.
- Auguste, D. T., Armes, S. P., Brzezinska, K. R., Deming, T. J., Kohn, J., & Prud'homme, R. K. (2006). pH triggered release of protective poly(ethylene glycol)-b-polycation copolymers from liposomes. *Biomaterials*, 27(12), 2599-2608.
- Banerjee, S. S., Aher, N., Patil, R., & Khandare, J. (2012). Poly(ethylene glycol)-Prodrug Conjugates: Concept, Design, and Applications. *Journal of Drug Delivery*, 2012, 17.
- Banik, B. L., Fattahi, P., & Brown, J. L. (2016). Polymeric nanoparticles: the future of nanomedicine. *Wiley Interdiscip Rev Nanomed Nanobiotechnol*, 8(2), 271-299.
- Barenholz, Y. (2012). Doxil®--the first FDA-approved nano-drug: lessons learned. *J Control Release*, 160(2), 117-134.
- Bayat Mokhtari, R., Homayouni, T. S., Baluch, N., Morgatskaya, E., Kumar, S., Das, B., et al. (2017). Combination therapy in combating cancer. *Oncotarget*, 8(23), 38022-38043.
- Bazak, R., Hourri, M., Achy, S. E., Hussein, W., & Refaat, T. (2014). Passive targeting of nanoparticles to cancer: A comprehensive review of the literature. *Mol Clin Oncol*, 2(6), 904-908.
- Beerling, E., Ritsma, L., Vriskoop, N., Derksen, P. W. B., & van Rheenen, J. (2011). Intravital microscopy: new insights into metastasis of tumors. [10.1242/jcs.072728]. *Journal of Cell Science*, 124(3), 299.
- Bisht, S., Feldmann, G., Koorstra, J. B., Mullendore, M., Alvarez, H., Karikari, C., et al. (2008). In vivo characterization of a polymeric nanoparticle platform with potential oral drug delivery capabilities. *Mol Cancer Ther*, 7(12), 3878-3888.
- Bisht, S., Feldmann, G., Soni, S., Ravi, R., Karikar, C., & Maitra, A. (2007). Polymeric nanoparticle-encapsulated curcumin ("nanocurcumin"): a novel strategy for human cancer therapy. *J Nanobiotechnology*, 5, 3.
- Bissett, D., Cassidy, J., de Bono, J. S., Muirhead, F., Main, M., Robson, L., et al. (2004). Phase I and pharmacokinetic (PK) study of MAG-CPT (PNU 166148): a polymeric derivative of camptothecin (CPT). *Br J Cancer*, 91(1), 50-55.

- Blanco, E., Sangai, T., Hsiao, A., Ferrati, S., Bai, L., Liu, X., et al. (2013). Multistage delivery of chemotherapeutic nanoparticles for breast cancer treatment. *Cancer Lett*, 334(2), 245-252.
- Blanco, E., Shen, H., & Ferrari, M. (2015). Principles of nanoparticle design for overcoming biological barriers to drug delivery. *Nat Biotechnol*, 33(9), 941-951.
- Cao, B., Zheng, Y., Xi, T., Zhang, C., Song, W., Burugapalli, K., et al. (2012). Concentration-dependent cytotoxicity of copper ions on mouse fibroblasts in vitro: effects of copper ion release from TCu380A vs TCu220C intra-uterine devices. *Biomedical Microdevices*, 14(4), 709-720.
- Cardoso, F. L., Brites, D., & Brito, M. A. (2010). Looking at the blood-brain barrier: molecular anatomy and possible investigation approaches. *Brain Res Rev*, 64(2), 328-363.
- Carmeliet, P., & Jain, R. K. (2000). Angiogenesis in cancer and other diseases. *Nature*, 407(6801), 249-257.
- Cheever, M. A., & Higano, C. S. (2011). PROVENGE (Sipuleucel-T) in prostate cancer: the first FDA-approved therapeutic cancer vaccine. *Clin Cancer Res*, 17(11), 3520-3526.
- Chen, C., Ke, J., Zhou, X. E., Yi, W., Brunzelle, J. S., Li, J., et al. (2013). Structural basis for molecular recognition of folic acid by folate receptors. [Letter]. *Nature*, 500(7463), 486-489.
- Cheng, C. J., Tietjen, G. T., Saucier-Sawyer, J. K., & Saltzman, W. M. (2015). A holistic approach to targeting disease with polymeric nanoparticles. *Nat Rev Drug Discov*, 14(4), 239-247.
- Choi, H. S., Liu, W., Misra, P., Tanaka, E., Zimmer, J. P., Itty Ipe, B., et al. (2007). Renal clearance of quantum dots. *Nat Biotechnol*, 25(10), 1165-1170.
- Coffer, J. L., Whitehead, M. A., Nagesha, D. K., Mukherjee, P., Akkaraju, G., Totolici, M., et al. (2005). Porous silicon-based scaffolds for tissue engineering and other biomedical applications. *physica status solidi (a)*, 202(8), 1451-1455.
- Conte, C., Fotticchia, I., Tirino, P., Moret, F., Pagano, B., Gref, R., et al. (2016). Cyclodextrin-assisted assembly of PEGylated polyester nanoparticles decorated with folate. *Colloids Surf B Biointerfaces*, 141, 148-157.
- Corbo, C., Parodi, A., Evangelopoulos, M., Engler, D. A., Matsunami, R. K., Engler, A. C., et al. (2015). Proteomic Profiling of a Biomimetic Drug Delivery Platform. *Curr Drug Targets*, 16(13), 1540-1547.
- Croy, S. R., & Kwon, G. S. (2006). Polymeric micelles for drug delivery. *Curr Pharm Des*, 12(36), 4669-4684.
- D'Souza, A. J., Schowen, R. L., & Topp, E. M. (2004). Polyvinylpyrrolidone-drug conjugate: synthesis and release mechanism. *J Control Release*, 94(1), 91-100.
- Danhauser-Riedl, S., Hausmann, E., Schick, H. D., Bender, R., Dietzfelbinger, H., Rastetter, J., et al. (1993). Phase I clinical and pharmacokinetic trial of dextran conjugated doxorubicin (AD-70, DOX-OXD). *Invest New Drugs*, 11(2-3), 187-195.
- De Jong, W. H., & Borm, P. J. (2008). Drug delivery and nanoparticles: applications and hazards. *Int J Nanomedicine*, 3(2), 133-149.
- Dunne, M., Corrigan, I., & Ramtoola, Z. (2000). Influence of particle size and dissolution conditions on the degradation properties of polylactide-co-glycolide particles. *Biomaterials*, 21(16), 1659-1668.
- Evangelopoulos, M., Parodi, A., Martinez, J. O., Yazdi, I. K., Cevenini, A., van de Ven, A. L., et al. (2016). Cell source determines the immunological impact of biomimetic nanoparticles. *Biomaterials*, 82, 168-177.

- Fabi, A., Malaguti, P., Vari, S., & Cognetti, F. (2016). First-line therapy in HER2 positive metastatic breast cancer: is the mosaic fully completed or are we missing additional pieces? *J Exp Clin Cancer Res*, *35*, 104.
- Fitzmaurice, C., Dicker, D., Pain, A., Hamavid, H., Moradi-Lakeh, M., MacIntyre, M. F., et al. (2015). The Global Burden of Cancer 2013. *JAMA Oncol*, *1*(4), 505-527.
- Florence, A. T. (2012). Reductionism and complexity in nanoparticle-vectored drug targeting. *J Control Release*, *161*(2), 399-402.
- Fossati, R., Confalonieri, C., Torri, V., Ghislandi, E., Penna, A., Pistotti, V., et al. (1998). Cytotoxic and hormonal treatment for metastatic breast cancer: a systematic review of published randomized trials involving 31,510 women. *J Clin Oncol*, *16*(10), 3439-3460.
- Gentile, F., Chiappini, C., Fine, D., Bhavane, R. C., Peluccio, M. S., Cheng, M. M., et al. (2008). The effect of shape on the margination dynamics of non-neutrally buoyant particles in two-dimensional shear flows. *J Biomech*, *41*(10), 2312-2318.
- Godin, B., Gu, J., Serda, R. E., Bhavane, R., Tasciotti, E., Chiappini, C., et al. (2010). Tailoring the degradation kinetics of mesoporous silicon structures through PEGylation. *J Biomed Mater Res A*, *94*(4), 1236-1243.
- Goldberg, M. S. (2015). Immunoengineering: how nanotechnology can enhance cancer immunotherapy. *Cell*, *161*(2), 201-204.
- Gong, Y. K., & Winnik, F. M. (2012). Strategies in biomimetic surface engineering of nanoparticles for biomedical applications. *Nanoscale*, *4*(2), 360-368.
- Gradishar, W. J. (2006). Albumin-bound paclitaxel: a next-generation taxane. *Expert Opin Pharmacother*, *7*(8), 1041-1053.
- Greenwald, R. B., Choe, Y. H., McGuire, J., & Conover, C. D. (2003). Effective drug delivery by PEGylated drug conjugates. *Adv Drug Deliv Rev*, *55*(2), 217-250.
- Grossen, P., Witzigmann, D., Sieber, S., & Huwyler, J. (2017). PEG-PCL-based nanomedicines: A biodegradable drug delivery system and its application. *Journal of Controlled Release*, *260*, 46-60.
- Grottkau, B. E., Cai, X., Wang, J., Yang, X., & Lin, Y. (2013). Polymeric nanoparticles for a drug delivery system. *Curr Drug Metab*, *14*(8), 840-846.
- Hansen, A. E., Petersen, A. L., Henriksen, J. R., Boerresen, B., Rasmussen, P., Elema, D. R., et al. (2015). Positron Emission Tomography Based Elucidation of the Enhanced Permeability and Retention Effect in Dogs with Cancer Using Copper-64 Liposomes. *ACS Nano*, *9*(7), 6985-6995.
- Hu, J., Fu, S., Peng, Q., Han, Y., Xie, J., Zan, N., et al. (2017). Paclitaxel-loaded polymeric nanoparticles combined with chronomodulated chemotherapy on lung cancer: In vitro and in vivo evaluation. *Int J Pharm*, *516*(1-2), 313-322.
- Jain, R. K., Martin, J. D., & Stylianopoulos, T. (2014). The role of mechanical forces in tumor growth and therapy. *Annu Rev Biomed Eng*, *16*, 321-346.
- Kakinoki, A., Kaneo, Y., Ikeda, Y., Tanaka, T., & Fujita, K. (2008). Synthesis of poly(vinyl alcohol)-doxorubicin conjugates containing cis-aconityl acid-cleavable bond and its isomer dependent doxorubicin release. *Biol Pharm Bull*, *31*(1), 103-110.
- Kaminskas, L. M., McLeod, V. M., Kelly, B. D., Sberna, G., Boyd, B. J., Williamson, M., et al. (2012). A comparison of changes to doxorubicin pharmacokinetics, antitumor activity, and toxicity mediated by PEGylated dendrimer and PEGylated liposome drug delivery systems. *Nanomedicine*, *8*(1), 103-111.
- Kopecek, J., Kopecková, P., Minko, T., & Lu, Z. (2000). HEMA copolymer-anticancer drug conjugates: design, activity, and mechanism of action. *Eur J Pharm Biopharm*, *50*(1), 61-81.

- Lee, S. H., Jeong, D., Han, Y. S., & Baek, M. J. (2015). Pivotal role of vascular endothelial growth factor pathway in tumor angiogenesis. *Ann Surg Treat Res*, 89(1), 1-8.
- Lee, T. R., Choi, M., Kopacz, A. M., Yun, S. H., Liu, W. K., & Decuzzi, P. (2013). On the near-wall accumulation of injectable particles in the microcirculation: smaller is not better. *Sci Rep*, 3, 2079.
- Li, C. (2002). Poly(L-glutamic acid)--anticancer drug conjugates. *Adv Drug Deliv Rev*, 54(5), 695-713.
- Li, Z., & Tan, B. H. (2014). Towards the development of polycaprolactone based amphiphilic block copolymers: molecular design, self-assembly and biomedical applications. *Materials Science and Engineering: C*, 45, 620-634.
- Liou, G. Y., & Storz, P. (2010). Reactive oxygen species in cancer. *Free Radic Res*, 44(5), 479-496.
- Liu, L., Zheng, M., Renette, T., & Kissel, T. (2012). Modular synthesis of folate conjugated ternary copolymers: polyethylenimine-graft-polycaprolactone-block-poly(ethylene glycol)-folate for targeted gene delivery. *Bioconjug Chem*, 23(6), 1211-1220.
- Mai, J., Huang, Y., Mu, C., Zhang, G., Xu, R., Guo, X., et al. (2014). Bone marrow endothelium-targeted therapeutics for metastatic breast cancer. *J Control Release*, 187, 22-29.
- Maiolino, S., Russo, A., Pagliara, V., Conte, C., Ungaro, F., Russo, G., et al. (2015). Biodegradable nanoparticles sequentially decorated with Polyethyleneimine and Hyaluronan for the targeted delivery of docetaxel to airway cancer cells. *J Nanobiotechnology*, 13, 29.
- Martinez, J. O., Evangelopoulos, M., Bhavane, R., Acciaro, S., Salvatore, F., Liu, X., et al. (2015). Multistage Nanovectors Enhance the Delivery of Free and Encapsulated Drugs. *Curr Drug Targets*, 16(14), 1582-1590.
- Matsumura, Y., & Maeda, H. (1986). A new concept for macromolecular therapeutics in cancer chemotherapy: mechanism of tumoritropic accumulation of proteins and the antitumor agent smancs. *Cancer Res*, 46(12 Pt 1), 6387-6392.
- McGowan, J. V., Chung, R., Maulik, A., Piotrowska, I., Walker, J. M., & Yellon, D. M. (2017). Anthracycline Chemotherapy and Cardiotoxicity. *Cardiovasc Drugs Ther*, 31(1), 63-75.
- Mehlen, P., & Puisieux, A. (2006). Metastasis: a question of life or death. *Nat Rev Cancer*, 6(6), 449-458.
- Mi, Y., Mu, C., Wolfram, J., Deng, Z., Hu, T. Y., Liu, X., et al. (2016). A Micro/Nano Composite for Combination Treatment of Melanoma Lung Metastasis. *Adv Healthc Mater*, 5(8), 936-946.
- Moon, J. J., Huang, B., & Irvine, D. J. (2012). Engineering nano- and microparticles to tune immunity. *Adv Mater*, 24(28), 3724-3746.
- Nahrwold, M., Weiß, C., Bogner, T., Mertink, F., Conradi, J., Sammet, B., et al. (2013). Conjugates of Modified Cryptophycins and RGD-Peptides Enter Target Cells by Endocytosis. *Journal of Medicinal Chemistry*, 56(5), 1853-1864.
- Ngoune, R., Peters, A., von Elverfeldt, D., Winkler, K., & Pütz, G. (2016). Accumulating nanoparticles by EPR: A route of no return. *Journal of Controlled Release*, 238(Supplement C), 58-70.
- O'Brien, M. E., Wigler, N., Inbar, M., Rosso, R., Grischke, E., Santoro, A., et al. (2004). Reduced cardiotoxicity and comparable efficacy in a phase III trial of pegylated liposomal doxorubicin HCl (CAELYX/Doxil) versus conventional doxorubicin for first-line treatment of metastatic breast cancer. *Ann Oncol*, 15(3), 440-449.
- Pardridge, W. M. (2012). Drug transport across the blood-brain barrier. *J Cereb Blood Flow Metab*, 32(11), 1959-1972.

- Park, J. H., Gu, L., von Maltzahn, G., Ruoslahti, E., Bhatia, S. N., & Sailor, M. J. (2009). Biodegradable luminescent porous silicon nanoparticles for in vivo applications. *Nat Mater*, 8(4), 331-336.
- Parker, N., Turk, M. J., Westrick, E., Lewis, J. D., Low, P. S., & Leamon, C. P. (2005). Folate receptor expression in carcinomas and normal tissues determined by a quantitative radioligand binding assay. *Anal Biochem*, 338(2), 284-293.
- Parodi, A., Quattrocchi, N., van de Ven, A. L., Chiappini, C., Evangelopoulos, M., Martinez, J. O., et al. (2013). Synthetic nanoparticles functionalized with biomimetic leukocyte membranes possess cell-like functions. *Nat Nanotechnol*, 8(1), 61-68.
- Queirolo, P., Picasso, V., & Spagnolo, F. (2015). Combined BRAF and MEK inhibition for the treatment of BRAF-mutated metastatic melanoma. *Cancer Treat Rev*, 41(6), 519-526.
- Ragelle, H., Danhier, F., Pr at, V., Langer, R., & Anderson, D. G. (2017). Nanoparticle-based drug delivery systems: a commercial and regulatory outlook as the field matures. *Expert Opin Drug Deliv*, 14(7), 851-864.
- Redig, A. J., & McAllister, S. S. (2013). Breast cancer as a systemic disease: a view of metastasis. *J Intern Med*, 274(2), 113-126.
- Rezaei Mokarram, A., Kebriaee Zadeh, A., Keshavarz, M., Ahmadi, A., & Mohtat, B. (2010). Preparation and in-vitro evaluation of indomethacin nanoparticles. *Daru*, 18(3), 185-192.
- Rivera, E. (2003). Liposomal anthracyclines in metastatic breast cancer: clinical update. *Oncologist*, 8 Suppl 2, 3-9.
- Santos, H. A., M kil , E., Airaksinen, A. J., Bimbo, L. M., & Hirvonen, J. (2014). Porous silicon nanoparticles for nanomedicine: preparation and biomedical applications. *Nanomedicine (Lond)*, 9(4), 535-554.
- Shen, H., Rodriguez-Aguayo, C., Xu, R., Gonzalez-Villasana, V., Mai, J., Huang, Y., et al. (2013). Enhancing chemotherapy response with sustained EphA2 silencing using multistage vector delivery. *Clin Cancer Res*, 19(7), 1806-1815.
- Shen, H., You, J., Zhang, G., Ziemys, A., Li, Q., Bai, L., et al. (2012). Cooperative, nanoparticle-enabled thermal therapy of breast cancer. *Adv Healthc Mater*, 1(1), 84-89.
- Shen, J., Wu, X., Lee, Y., Wolfram, J., Yang, Z., Mao, Z. W., et al. (2015). Porous silicon microparticles for delivery of siRNA therapeutics. *J Vis Exp*(95), 52075.
- Shen, J., Xu, R., Mai, J., Kim, H. C., Guo, X., Qin, G., et al. (2013). High capacity nanoporous silicon carrier for systemic delivery of gene silencing therapeutics. *ACS Nano*, 7(11), 9867-9880.
- Shen, Y., Tang, H., Radosz, M., Van Kirk, E., & Murdoch, W. J. (2008). pH-responsive nanoparticles for cancer drug delivery. *Methods Mol Biol*, 437, 183-216.
- Spagnolo, F., Ghiorzo, P., Orgiano, L., Pastorino, L., Picasso, V., Tornari, E., et al. (2015). BRAF-mutant melanoma: treatment approaches, resistance mechanisms, and diagnostic strategies. *Onco Targets Ther*, 8, 157-168.
- Speth, P. A., van Hoesel, Q. G., & Haanen, C. (1988). Clinical pharmacokinetics of doxorubicin. *Clin Pharmacokinet*, 15(1), 15-31.
- Tanaka, T., Godin, B., Bhavane, R., Nieves-Alicea, R., Gu, J., Liu, X., et al. (2010). In vivo evaluation of safety of nanoporous silicon carriers following single and multiple dose intravenous administrations in mice. *Int J Pharm*, 402(1-2), 190-197.
- Tanaka, T., Mangala, L. S., Vivas-Mejia, P. E., Nieves-Alicea, R., Mann, A. P., Mora, E., et al. (2010). Sustained small interfering RNA delivery by mesoporous silicon particles. *Cancer Res*, 70(9), 3687-3696.

- Tasciotti, E., Liu, X., Bhavane, R., Plant, K., Leonard, A. D., Price, B. K., et al. (2008). Mesoporous silicon particles as a multistage delivery system for imaging and therapeutic applications. *Nat Nanotechnol*, 3(3), 151-157.
- Thirumurugan, P., Matosiuk, D., & Jozwiak, K. (2013). Click Chemistry for Drug Development and Diverse Chemical–Biology Applications. *Chemical Reviews*, 113(7), 4905-4979.
- Torchilin, V. (2009). Multifunctional and stimuli-sensitive pharmaceutical nanocarriers. *Eur J Pharm Biopharm*, 71(3), 431-444.
- Trindade, A. F., Frade, R. F. M., Macoas, E. M. S., Graca, C., Rodrigues, C. A. B., Martinho, J. M. G., et al. (2014). "Click and go": simple and fast folic acid conjugation. [10.1039/C4OB00150H]. *Organic & Biomolecular Chemistry*, 12(20), 3181-3190.
- Udompornmongkol, P., & Chiang, B. H. (2015). Curcumin-loaded polymeric nanoparticles for enhanced anti-colorectal cancer applications. *J Biomater Appl*, 30(5), 537-546.
- Ulery, B. D., Nair, L. S., & Laurencin, C. T. (2011). Biomedical Applications of Biodegradable Polymers. *J Polym Sci B Polym Phys*, 49(12), 832-864.
- Ungaro, F., Conte, C., Ostacolo, L., Maglio, G., Barbieri, A., Arra, C., et al. (2012). Core-shell biodegradable nanoassemblies for the passive targeting of docetaxel: features, antiproliferative activity and in vivo toxicity. *Nanomedicine-Nanotechnology Biology and Medicine*, 8(5), 637-646.
- Varshosaz, J. (2012). Dextran conjugates in drug delivery. *Expert Opin Drug Deliv*, 9(5), 509-523.
- Vasey, P. A., Kaye, S. B., Morrison, R., Twelves, C., Wilson, P., Duncan, R., et al. (1999). Phase I clinical and pharmacokinetic study of PK1 [N-(2-hydroxypropyl)methacrylamide copolymer doxorubicin]: first member of a new class of chemotherapeutic agents-drug-polymer conjugates. Cancer Research Campaign Phase I/II Committee. *Clin Cancer Res*, 5(1), 83-94.
- Venuta, A., Wolfram, J., Shen, H., & Ferrari, M. (2017). Post-nano strategies for drug delivery: multistage porous silicon microvectors. [10.1039/C6TB01978A]. *Journal of Materials Chemistry B*, 5(2), 207-219.
- Viola-Villegas, N., Rabideau, A. E., Cesnavicious, J., Zubieta, J., & Doyle, R. P. (2008). Targeting the Folate Receptor (FR): Imaging and Cytotoxicity of ReI Conjugates in FR-Overexpressing Cancer Cells. *ChemMedChem*, 3(9), 1387-1394.
- Walkey, C. D., Olsen, J. B., Guo, H., Emili, A., & Chan, W. C. (2012). Nanoparticle size and surface chemistry determine serum protein adsorption and macrophage uptake. *J Am Chem Soc*, 134(4), 2139-2147.
- Wang, A. Z. (2015). EPR or no EPR? The billion-dollar question. [10.1126/scitranslmed.aac8108]. *Science Translational Medicine*, 7(294), 294ec112.
- Wang, C. F., Sarparanta, M. P., Mäkilä, E. M., Hyvönen, M. L., Laakkonen, P. M., Salonen, J. J., et al. (2015). Multifunctional porous silicon nanoparticles for cancer theranostics. *Biomaterials*, 48, 108-118.
- Wilhelm S. , T. A. J., Dai Q. , Ohta S. , Audet J. , Dvorak H.F. & Chan W. (2016). Analysis of nanoparticle delivery to tumors. *Nature Reviews Material*.
- Wilson, T. R., Longley, D. B., & Johnston, P. G. (2006). Chemoresistance in solid tumours. *Ann Oncol*, 17 Suppl 10, x315-324.
- Xia, X., Mai, J., Xu, R., Perez, J. E., Guevara, M. L., Shen, Q., et al. (2015). Porous silicon microparticle potentiates anti-tumor immunity by enhancing cross-presentation and inducing type I interferon response. *Cell Rep*, 11(6), 957-966.
- Xu, Q., Ensign, L. M., Boylan, N. J., Schon, A., Gong, X., Yang, J. C., et al. (2015). Impact of Surface Polyethylene Glycol (PEG) Density on Biodegradable Nanoparticle Transport in Mucus ex Vivo and Distribution in Vivo. *ACS Nano*, 9(9), 9217-9227.

- Xu, R., Huang, Y., Mai, J., Zhang, G., Guo, X., Xia, X., et al. (2013). Multistage vectored siRNA targeting ataxia-telangiectasia mutated for breast cancer therapy. *Small*, 9(9-10), 1799-1808.
- Xu, R., Zhang, G., Mai, J., Deng, X., Segura-Ibarra, V., Wu, S., et al. (2016). An injectable nanoparticle generator enhances delivery of cancer therapeutics. *Nat Biotechnol*, 34(4), 414-418.
- Y, M., C, M., J, W., Z, D., Y, H. T., X, L., et al. (2016). Enzyme-responsive multistage vector for drug delivery to tumor tissue.
- Zhang, L., He, Y., Yu, M., & Song, C. (2011). Paclitaxel-loaded polymeric nanoparticles based on PCL-PEG-PCL: preparation, in vitro and in vivo evaluation. *J Control Release*, 152 Suppl 1, e114-116.
- Zhang, M., Xu, R., Xia, X., Yang, Y., Gu, J., Qin, G., et al. (2014). Polycation-functionalized nanoporous silicon particles for gene silencing on breast cancer cells. *Biomaterials*, 35(1), 423-431.

## **General conclusions**

Overcoming biological barriers including rapid clearance from the bloodstream, opsonization and subsequent sequestration by MPS, nonspecific distribution, blood vessel flow limitations, pressure gradients, cellular membrane, escape from endosomal and lysosomal compartments, drug efflux pumps and the blood brain barrier is a key issue in the field of cancer therapy. The minimal therapeutic impact observed following the delivery of conventional chemotherapeutics is a direct consequence of their inability to overcome many of these barriers that basically prevents successful accumulation of therapeutic agent at the diseased sites. On this background the development of a single system able to drive the therapeutic agents through all the obstacles and applicable to all the different type of malignancies is a difficult aim. An efficient method consist in the use of different approaches to address all the challenges in drug delivery. The polymeric conjugate can serve to improve the pharmacokinetics profile, reduce the non-specific accumulation and therefore increase therapeutic effects of the conjugated drug. Chapter 2 “Synthesis and characterization of rationally-designed Dextran-Doxorubicin conjugate: a novel strategy to improve the antitumor efficacy of doxorubicin in multiple breast cancer liver metastases” showed how the conjugation of Doxorubicine with Dextran (10.000 kDa MW) has the potential to increase the accumulation of the anticancer drug into tumor metastases in a time dependent manner. Further, this work has highlighted an heterogeneity among the tumor masses in terms of permeation to the macromolecules.

Despite the proven benefits of the polymeric conjugate the most efficient way to drive molecules after the endothelial wall consist in entrapping and protecting the therapeutic into a nano based carrier such as polymeric NPs. This approach offers several advantages first of all the opportunity to obtain a controlled release of the cargo from the polymeric matrix. A big deal in the field of nanoparticles is the interaction with the proteins in the blood pool that activate the capture by the macrophages and consequent reduce the circulation time of the carriers. [PEG](#) exposed on the surface act as hindrance for the proteins absorption resulting in prolonged life for the NPs. On the other hand this hydrophilic shell could affect the behaviour of the particles and for this reason in Chapter 3 “Shedding light on surface exposition of poly(ethylene glycol) and folate targeting units on nanoparticles of poly( $\epsilon$ -caprolactone) diblock copolymers: beyond a paradigm” the role of PEG in interactions with human macrophages and in the internalization in tumor cell line has been investigated. Definitely the PEGylation degree depends on the length of PEG chain used to formulate the NPs and specifically a short PEG chain can [enhance](#) the degree of PEGylation, reduce the capture by the phagocytic cells and improve cellular uptake resulting in a excellent drug delivery system.

Another approaches to protect the NPs and their cargo from degradation and opsonization in the bloodstream is to combining different scales of delivery systems. A model is a discoidal porous silicon microparticles designed to navigate into the blood flow and showing preferential accumulation within the inflamed endothelium as in the case of tumors that can be used as a depot for a second nanostage that overcomes intact the endothelial wall and brings its cargo to the diseased cells. This system has been utilised for several application but not to treat brain metastases. At this purpose in Chapter 4 “Strategies to overcome the Blod Brain Barrier (BBB)” the accumulation at the brain microvasculature of a functionalised multistage delivery system has been evaluated *in vivo* and *ex vivo*. No accumulation was detected in the brain tissue and this leads to the need of further modification to use this promising approach for the delivery of chemotherapeutics beyond the BBB .

In conclusion the research work carried out during these three years of Ph.D. has demonstrated that only a multy-strategy approach razionalized on the basis of the application can result in an optimal drug delivery system.

## **ANNEX-I**

### **Photo-antimicrobial polymeric films releasing nitric oxide with fluorescence reporting under visible light**

Published as:

Nino Marino, Marta Perez-Lloret, Anna R. Blanco, Alessandro Venuta, Fabiana Quaglia and Salvatore Sortino

**Journal of Materials Chemistry B, 2016,4, 5138-5143**

## **Abstract**

A novel photoresponsive molecular hybrid has been embedded in poly(lactic-co-glycolic acid) (PLGA) to give an antibacterial polymeric film generating nitric oxide (NO) under visible light, with concomitant fluorescence reporting of NO release. The molecular hybrid integrates a nitroaniline NO photodonor and a coumarin latent fluorophore in the same molecular skeleton and results in quite homogeneous distribution in the polymer matrix where it preserves well the photobehavior exhibited in solution. The doped PLGA film shows an excellent optical transparency and can be excited by visible light leading to the production of NO and the parallel fluorescence revival of the coumarin fluorophore, which acts as an optical NO reporter. Photogenerated NO diffuses out of the polymer film, can be transferred to a biological milieu and induces remarkable antibacterial activity against *Escherichia coli*.

## 1.Introduction

The emergence of multi-drug resistance (MDR) bacteria (1,2-3) and the increase of opportunistic infections (4,5) associated with the alarmingly low turnover of new clinically approved antibiotic drugs (6) call for a shift of attention to other underappreciated or unexploited antibacterial treatment modalities. In this frame, one of the most promising approaches is based on the use of nitric oxide (NO) as a powerful antimicrobial agent (7,8). This small sized and uncharged radical does not suffer MDR problems (9) and represents a multitarget therapeutic species (10) with broad-spectrum antibacterial activity. Besides, as a result of its short half-life in blood (o1 s), NO diffuses into the cellular environ-ment over short distances (o200 nm) (11) confining the region of action and consequently avoiding systemic toxicity issues. Difficulties in the delivery of gaseous NO to selected targets have inspired the development of a range of molecular NO-donors (12,13) and their integration within a variety of materials where NO delivery is triggered by metabolic or light stimuli has been recently reported (14,15,16,17,18,19-20) Among these, photobactericidal film coatings are of particular relevance (21,22,23-24) not only due to the superb spatiotemporal control of NO that the light input offers (18) but also because they can be designed for a large use both inside and outside the human body. The therapeutic effects of NO are, however, strictly dictated by its concentration (25). This feature makes the quantification of the NO delivery a very important issue to be faced, especially when one is interested to reach a critical molecule concentration to induce a specific effect. A suitable way to address this quantification task is based on the use of a fluorescent reporter. This elegant strategy relies on the simultaneous photorelease of the desired bioactive species, i.e. NO, and a fluorescent component (the reporter) from the same nonfluorescent precursor (26,27-28). In such a way, the release process can be easily quantified by monitoring the fluorescence emission of the reporter, which acts exactly as an optical counter of the bioactive species. NO photoreleasers with fluorescence reporting function have only recently attracted attention (29,30,31-32), mainly limited to the solution phase. In the frame of our ongoing interest in NO photoreleasing constructs for therapeutic applications,(17,18,33-34) we report herein the first example of an NO photoreleasing antibacterial film with fluorescence reporting function.

## 2. Experimental section

### 2.1 Chemicals

All chemicals were from commercial sources at the highest possible purity and used as received. All solvents used were of spectrophotometric grade.

### 2.2 Synthesis

Compound 1 was synthesized according to the synthetic steps illustrated in figure 1 and described in the following. Syntheses were carried out at a low intensity level of visible light. Compounds 1a and 1b were synthesized according to literature procedures (35).

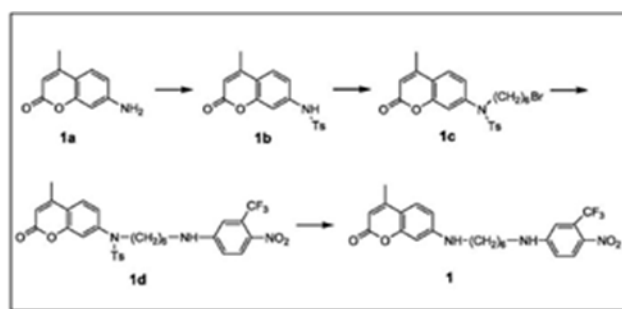


**Figure 1.** Schematic synthesis of 7-[Hexyl(4-nitro-3-(trifluoromethyl)phenyl)amine-amino]-4-methylcoumarin.

7-[6-Bromohexyl-(4-methanesulfonyl-phenyl)-amino]-4-methyl-coumarin (1c). Compound 1b (0.50 g, 1.52 mmol) was dissolved in CH<sub>3</sub>CN (100 mL). Then Cs<sub>2</sub>CO<sub>3</sub> (0.54 g, 2.28 mmol) and excess of 1,6-dibromohexane (3.7 g, 0.015 mol) were added to the solution under confined conditions, and the reaction was refluxed for 3 h. After filtration, the solution was evaporated and purified by means of silica gel column chromatography (EtOAc/hexane 1 : 2) to give a colourless solid 1c (0.72 g, 95% yield), R<sub>f</sub> = 0.75 (EtOAc/hexane 1 : 2). <sup>1</sup>H NMR (CDCl<sub>3</sub>, 500 MHz): δ = 7.60 (d, J = 8 Hz, 1H), 7.47 (d, J = 8.5 Hz, 2H), 7.28 (d, J = 8 Hz, 2H), 7.26 (dd, J = 8.5, 2 Hz, 1H), 6.87 (d, J = 2 Hz, 1H), 6.30 (s, 1H), 3.56 (t, J = 6.5 Hz, 2H), 3.37 (t, J = 6.5 Hz, 2H), 2.45 (s, 3H), 2.44 (s, 3H), 1.80 (m, J = 7 Hz, 2H), 1.43 (m, J = 6.5 Hz, 2H), 1.37 (m, 4H). <sup>13</sup>C NMR (50 MHz, CDCl<sub>3</sub>): 160.2, 153.4, 151.8, 143.9, 142.2, 134.4, 129.6, 127.4, 125.2, 124.9, 119.1, 115.2, 115.1, 49.8, 33.6, 32.4, 27.7, 27.4, 25.4, 21.5, 18.6 ppm.

7-[Hexyl(4-nitro-3-(trifluoromethyl)phenyl)amine-(4-methane-sulfonyl-phenyl)-amino]-4-methylcoumarin (1d). A mixture of 1c (400 mg, 0.83 mmol), 4-nitro-3-(trifluoromethyl)aniline (172 mg, 0.83 mmol) and Cs<sub>2</sub>CO<sub>3</sub> (407 mg, 1.25 mmol) was heated at reflux in acetonitrile

overnight. The reaction mixture was allowed to cool to room temperature. After filtration, the solvent was removed under vacuum and the residue was purified by column chromatography (EtOAc/hexane 70 : 30) to afford compound 1d as a yellowish powder (0.36 g, 70% yield),  $R_f = 0.6$  (EtOAc/hexane 1 : 2).  $^1\text{H NMR}$  ( $\text{CDCl}_3$ , 200 MHz):  $\delta = 8.03$  (d,  $J = 9$  Hz, 1H), 7.59 (d,  $J = 8.6$  Hz, 1H), 7.46 (d,  $J = 8.4$  Hz, 2H), 7.28 (d,  $J = 8.4$  Hz, 2H), 7.24 (dd,  $J = 8.6, 2.2$  Hz, 1H), 6.87 (d,  $J = 2.2$  Hz, 2H), 6.66 (dd,  $J = 8.8, 2.8$  Hz, 1H), 6.29 (d,  $J = 1.2$  Hz, 1H), 4.86 (broad t, 1H), 3.57 (m, 2H), 3.23 (m, 2H), 2.43 (s, 6H), 1.64 (m, 2H), 1.41 (m, 6H).  $^{13}\text{C NMR}$  (50 MHz,  $\text{CDCl}_3$ ): 160.3, 153.4, 152.0, 151.9, 144.1, 142.1, 135.8, 134.3, 129.7, 129.2, 127.3, 126.7, 124.9, 124.9, 119.1, 115.4, 115.1, 112.1, 104.9, 49.5, 42.8, 28.4, 27.4, 25.7, 25.4, 21.5, 18.5 ppm.

7-[Hexyl(4-nitro-3-(trifluoromethyl)phenyl)amine-amino]-4-methylcoumarin (1). Compound 1d (100 mg, 1.75 mmol) was added to conc. sulfuric acid (5 mL) and the solution was stirred for 12 h at room temperature. The reaction mixture was cooled and carefully poured into water. The mixture was neutralized with saturated aqueous sodium bicarbonate and extracted with EtOAc three times. The organic solution was dried and evaporated to give 1 as a yellow powder (0.76 g, 94%),  $R_f = 0.38$  (EtOAc/hexane 1 : 2).  $^1\text{H NMR}$  ( $\text{CDCl}_3$ , 200 MHz):  $\delta = 8.03$  (d,  $J = 9.2$  Hz, 1H), 7.35 (d,  $J = 8.6$  Hz, 1H), 6.87 (d,  $J = 3$  Hz, 1H), 6.66 (dd,  $J = 9, 2.6$  Hz, 1H), 6.50 (dd,  $J = 8.6, 2.2$  Hz, 1H), 6.42 (d,  $J = 2.2$  Hz, 1H), 5.97 (s, 1H), 4.66 (broad t, 1H), 4.21 (broad s, 1H), 2.33 (s, 6H), 169–144 (m, 8H).  $^{13}\text{C NMR}$  (50 MHz,  $\text{CDCl}_3$ ): 162.1, 155.9, 152.3, 151.9, 151.5, 135.9, 129.3, 126.9, 126.2, 124.9, 119.5, 112.1, 111.2, 110.3, 109.0, 97.64, 43.2, 28.9, 28.7, 26.6, 18.5 ppm.

### **2.3 Instrumentation**

UV-Vis spectra were recorded using a JascoV-560 spectrophotometer using either quartz cells with a path length of 1 cm or a specific holder for thin films. Fluorescence emission spectra were recorded using a Spex Fluorolog-2 (mod. F-111) in air-equilibrated solutions either in right angle or in front face mode for solution or film samples, respectively.  $^1\text{H NMR}$  and  $^{13}\text{C NMR}$  spectra were recorded on a VARIAN INOVA 200 spectrometer at room temperature at 200 MHz and 50 MHz, respectively, and calibrated using  $\text{SiMe}_4$  as an internal reference. Chemical shifts ( $\delta$ ) are given in parts per million (ppm) and the coupling constants ( $J$ ) in Hertz (Hz).

Irradiation conditions. Irradiation of the samples in solution was performed in a thermostated quartz cell (1 cm pathlength, 3 mL capacity) under gentle stirring, by using a continuum laser with  $\lambda_{exc} = 405 \text{ nm}$  (ca.  $3 \text{ W cm}^{-2}$ ) having a beam diameter of ca. 1.5 mm. Irradiation of the film samples was performed using a 150 W xenon lamp having a beam diameter of ca. 3.5 cm, mounting a cut-off filter at 400 nm.

Amperometric NO detection. NO release for samples in solution was measured using a World Precision Instrument, ISO-NO meter, equipped with a data acquisition system, and based on direct amperometric detection of NO with a short response time ( $< 5 \text{ s}$ ) and a sensitivity range of 1 nM–20 mM. The analog signal was digitalized using a four-channel recording system and transferred to a PC. The sensor was accurately calibrated by mixing standard solutions of NaNO<sub>2</sub> with 0.1 M H<sub>2</sub>SO<sub>4</sub> and 0.1 M KI according to the reaction:



Irradiation was performed in a thermostated quartz cell (1 cm pathlength, 3 mL capacity) using the above continuum laser with  $\lambda_{exc} = 405 \text{ nm}$ . NO measurements were carried out under stirring with the electrode positioned outside the light path in order to avoid NO signal artefacts due to photoelectric interference on the ISO-NO electrode.

#### ***2.4 Chemical detection of NO***

NO release was also measured by means of the well-known, highly sensitive (detection limit on the order of the picomoles) fluorimetric bioassay of Misko et al. (36), based on the ring closure of the nonfluorescent 2,3-diaminonaphthalene (DAN) with nitrite to form the highly fluorescent product 2,3-diamino-naphthotriazole (DANT). Pieces of PLGA films (2 cm<sup>2</sup>) were placed in a quartz cell (3 mL capacity) filled with water and were irradiated at different times or kept in the dark. Once photo-generated under aerobic conditions, NO, in the absence of other scavengers, is rapidly converted into nitrite and nitrate, its stable metabolites. Since only nitrite reacts quantitatively with DAN to give rise to DANT, the samples (1 mL) were incubated with nitrate reductase from *Aspergillus niger* and b-nicotinamide adenine dinucleotide phosphate in reduced form for 20 min at 37 °C, in order to convert nitrate to nitrite before addition of DAN. Afterwards 100 mL of 0.31 mM DAN in 0.62 M HCl were added and the solutions were stirred for 20 min at room temperature. After adding 100 mL of NaOH 2.8 M to the above solutions, the fluorescence emission and excitation spectra were recorded (Fig. S3, ESI†). A standard

calibration curve was obtained by using freshly prepared solutions of sodium nitrite in phosphate buffer 10 mM at pH 7.4.

### *2.5 Film preparation*

A polymer film integrating the compound 1 was prepared by the solvent casting method. Resomer<sup>s</sup> RG 855 (85 : 15 D,L-lactide : glycolide molar ratio, inherent viscosity 1.3–1.7 dl g<sup>-1</sup> for 0.1% solution in chloroform at 25 °C) from Boehringer Ingelheim (Germany) was used. Resomer<sup>s</sup> RG 855 (150 mg) and polyethylene glycol 400 Da (37 mg) as plasticizers were first dissolved in 5.9 mL of methylene chloride by overnight stirring. Thereafter, 100 mL of a solution of 1 in methylene chloride (7 mg mL<sup>-1</sup>) were added to the polymer solution. The mixture was then cast onto a Teflon<sup>s</sup> Petri dish (diameter 75 mm), covered with punctured Parafilm<sup>s</sup> and placed on a levelled surface under a hood for 24 h to allow solvent evaporation. The thickness and the weight of the films were measured using a digital micrometer and a digital balance (sensitivity = 0.01 mg), respectively. The film thickness was quite uniform across all the sample (0.050 ± 0.002 mm). The content of 1 in the film was 16 mg cm<sup>-2</sup>. Distribution of 1 in the polymer film was evaluated by dividing the film into 8 slices, which were singularly weighed and dissolved in 5 mL of tetrahydrofuran. The amount of 1 was quantified by UV absorption at  $\lambda = 390$  nm. A calibration curve in the range of 3–60 mg mL<sup>-1</sup> was constructed and the linearity of response was verified ( $r^2 = 0.995$ ). The amount of 1 in the film was 3.38 ± 0.018 mg mg<sup>-1</sup> film. Distribution of 1 in the polymer film was evaluated by dividing the film into 8 slices, which were singularly weighed and dissolved in 5 mL of tetrahydrofuran. The amount of 1 was quantified by UV absorption at  $\lambda = 400$  nm. A calibration curve in the range of 3–60 mg mL<sup>-1</sup> was constructed and the linearity of response was verified ( $r^2 = 0.995$ ). The amount of 1 in the film was 3.38 ± 0.018 mg mg<sup>-1</sup> film.

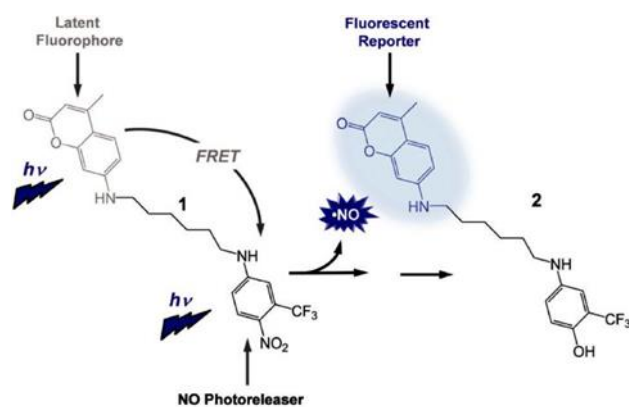
### *2.6 Antibacterial assay*

One hundred mL of a bacterial suspension (50 000 CFU per mL) of *Escherichia coli* ATCC 25922 were placed into a 96-well microplate containing at the bottom the PLGA film (circular disk, diameter = 6 mm, each containing 4.5 mg of 1) and were irradiated for 5 and 20 min by using a 470 W Xe lamp equipped with a cut-off filter  $\lambda < 400$  nm or kept in the dark. Equal aliquots of the bacterial suspension were also placed into a 96-well microplate in the absence

of the PLGA film and were irradiated under the same conditions. Afterwards, an aliquot of the bacterial suspension (20 mL) was placed on the sterile agar plate of MacConkey (Biokar diagnostics), where *Escherichia coli* grows with a typical pink color. The plates were incubated for 20 h at 37 °C to allow bacterial growth.

### 3 Results and discussion

To achieve our goal, we have designed the molecular hybrid 1 as a multifunctional component (Scheme 1). It consists of a nitroaniline-based NO photodonor developed in our group (37,38), linked to the coumarin 120 through an alkyl spacer. The working principle of 1 is sketched in Scheme 1 and the rationale behind the design of this molecular hybrid is described in the following.



**Scheme 1.** The working principle of the functional molecular hybrid 1

The coumarin component has been chosen because its intense fluorescence emission spectrum overlaps extensively the absorption spectrum of the nitroaniline NO photodonor (Fig. S1, ESI†). This condition, the close proximity of the two chromophores and the flexibility of the alkyl spacer are key prerequisites to make the fluorescence of the coumarin significantly quenched in the conjugate 1 by a Förster resonance energy transfer (FRET) mechanism. Excitation with visible light is expected to trigger NO photorelease from the nitroaniline moiety leading to a phenol derivative as a stable byproduct (37,38). In contrast to the nitroaniline chromophore this moiety is not able to accept the energy from the excited coumarin since its absorption spectrum, falling in the UV region, does not overlap any more the emission spectrum of the coumarin, making the FRET process thermodynamically not feasible. Consequently, the coumarin fluorescence is expected to be restored upon NO photorelease. The validity of our design was firstly proven by spectroscopic and photochemical experiments performed in

solution. The absorption spectrum of 1 reflects fairly well the sum absorption spectrum of the independent coumarin and nitroaniline compounds (Fig. S2, ESI†), ruling out any significant interaction between the coumarin and nitroaniline chromophores in the ground state. On the other hand, the fluorescence emission of the coumarin fluorophore is significantly quenched in the case of the conjugate 1 (Fig. S2, ESI†), suggesting a remarkable inter-action between the two chromophores in the excited state. Photoexcitation of 1 leads to a bleaching of the main absorption band (Fig. 1A).

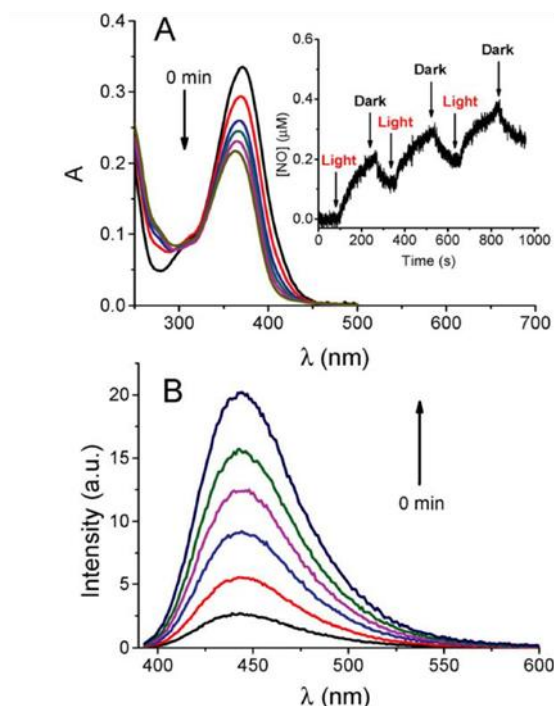


**Figure 1.** (A) Absorption spectral changes observed upon exposure of a water : methanol (20 : 80 v/v) solution of 1 (15 mM) at  $\lambda_{exc} = 405$  nm for regular intervals of 10 min.  $T = 25$  °C; the inset shows a representative NO release profile from 1. (B) Evolution of the fluorescence emission spectra corresponding to the sample of (A) and recorded at  $\lambda_{exc} = 380$  nm.

This behaviour accords with the photorelease of NO and the formation of the phenol derivative 2 as a stable photoproduct since it is in line with the photochemical pathway leading to NO release previously proposed in the case of the single NO photodonor unit.<sup>15</sup> This was confirmed by the typical NO release profile obtained by the direct amperometric detection of this species in alternating cycles of light/dark shown in the inset of Fig. 1A. Besides, the ESI-MS analysis of the crude reaction mixture carried out immediately after the photolysis experiments (ca. 20% transformation) revealed a main peak with a  $[M + 1]^+$  value of 434.2, corresponding to the structure of the conjugate 2 (see Scheme 1) in addition to that of the remaining starting compound. Fig. 1B shows the evolution of the fluorescence emission spectra corresponding to the absorption changes reported in Fig. 1A. These findings clearly indicate that

photodecomposition of 1 leads to a dramatic revival of the characteristic emission of the coumarin fluorophore which can be used as an optical reporter for the NO release. Polymeric films containing the functional conjugate 1 ( $16 \text{ mg cm}^{-2}$ ) were prepared by solvent casting using poly(lactic-co-glycolic acid) (PLGA) as a suitable polymeric matrix. PLGA is a highly biocompatible polymer approved for biomedical use, which has been recently used as a scaffold for the fabrication of NO releasing films triggered by pH changes (39,40) or chemically modified to achieve NO release under UV light irradiation (21). The film exhibited a homogeneous distribution of 1 in the polymeric matrix (see Experimental) and an excellent optical transparency which allowed us to record its UV-Vis absorption spectra in transmission mode (vide infra). The incorporation of the functional molecular hybrid into the polymeric film does not change the nature of the photochemical process. Fig. 2A and B show the absorption and fluorescence spectral changes observed upon irradiation of the film with visible light. Apart from a slight spectral shift due to a solvent effect, the behaviour observed is very similar to that exhibited by 1 in solution (see comparison with Fig. 1), since characterized by a bleaching of the main absorption band accompanied by a remarkable increase of the fluorescence intensity upon irradiation. NO photo-release from the film was detected by means of the sensitive and selective chemical method for NO detection based on the reaction between  $\text{N}_2\text{O}_3$  (formed by reaction of NO with  $\text{O}_2$ ) and 2,3-diamino-naphthalene (see ESI† and Fig. S3). As illustrated in Fig. 2C, we found an excellent linear correlation between the concentration of NO photogenerated and the increase of the fluorescence intensity of the optical reporter.

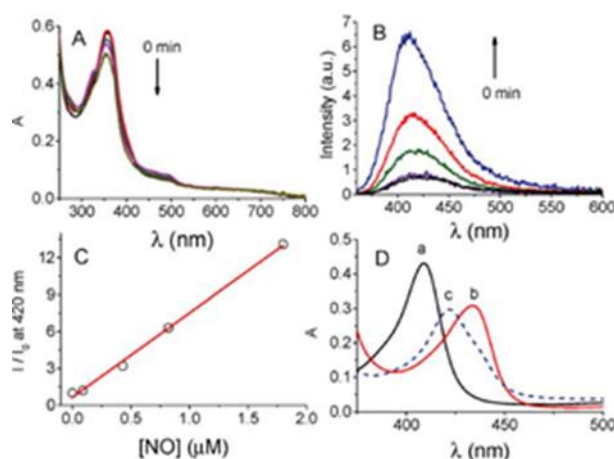


**Figure 2.** Absorption (A) and fluorescence (B) ( $I_{\text{exc}} = 350 \text{ nm}$ ) spectral changes observed upon irradiation of the PLGA film doped with 1 for 0, 1, 5, 10 and 20 min with a Xe lamp (cut-off filter 14400 nm). (C) Correlation of the fluorescence increase observed in (B) and the concentration of NO released from the film ( $I$  and  $I_0$  represent the fluorescence intensities after and before irradiation, respectively). (D) Transfer of NO from the PLGA film to reduced Mb in phosphate buffer. Absorption spectra of oxidized Mb( $\text{Fe}^{\text{III}}$ ) and reduced Mb( $\text{Fe}^{\text{II}}$ ) before (b) and after (c) 50 min of irradiation of the film.  $[\text{Mb}] = 2.5 \text{ mM}$ ; cell pathlength = 1 cm.

The doped PLGA film is a convenient NO dispenser for biological targets as demonstrated by its capability to transfer NO to a solution of equine skeletal myoglobin (Mb) (41) where the film was immersed. NO delivery to Mb can be easily monitored by absorption spectroscopy and the results obtained are illustrated in Fig. 2D. Mb exhibits its Soret absorption band at 410 nm (spectrum a). The addition of dithionite resulted in a shift of the absorption maximum at 432 nm, corresponding to the reduction of Mb (spectrum b). After irradiation of the film, the spectrum of the supernatant showed the appearance of a new Soret absorption band at 420 nm which, according to the literature (42), confirms the binding of NO to the Fe(II) of the heme group of Mb (spectrum c). Control experiments performed irradiating the solution containing the reduced Mb (i) in the absence of the film, (ii) in the presence of the film without 1 or (iii) keeping the film doped with 1 in the dark did not show any evidence for the formation of the 420 nm band. It is important to note that NO is indeed released from the film and not from molecules of 1 diffusing from the film to the supernatant solution. In fact, the leaching test performed by leaving the film immersed in a phosphate buffer solution (pH 7.4, 10 mM) at room temperature in the dark did not show any detectable absorption spectrum of 1 in the solution over a period of one week, according to the insolubility of 1 in this medium.

Interestingly, the release process with fluorescence reporting in the polymeric film is also triggered by sunlight and can be easily followed by the naked eye. The as-prepared PLGA film (Fig. 3A) was covered with a black plastic mask (Fig. 3B) and left for 30 min outdoor under sunlight. Fig. 3C shows the typical blue fluorescence of the reporter arising only from the illuminated sites, accounting for a remarkable spatial differentiation between the illuminated and non-illuminated areas. This finding clearly demonstrates that it is therefore possible to deliver NO to a specific location by either the covering of the surrounding areas or appropriately focusing the light source.



**Figure 3.** PLGA film (A) and its selective exposition to sunlight for 30 min with a black plastic mask on top (B). Fluorescence image ( $I_{exc} = 350$  nm) of the irradiated film after removing the mask (C).

Antibacterial activity of the film was tested towards Gram-negative *Escherichia coli* ATCC 25922 bacteria strain. The results in Fig. 4 show that no effect on the bacterial growth is observed both in the presence of the film in the dark (A) and under illumination in the absence of the film (B). On the other hand, a remarkable reduction of the number of colonies was observed after irradiation with visible light in the presence of the PLGA film, in a manner clearly dependent on the irradiation time (C and D).

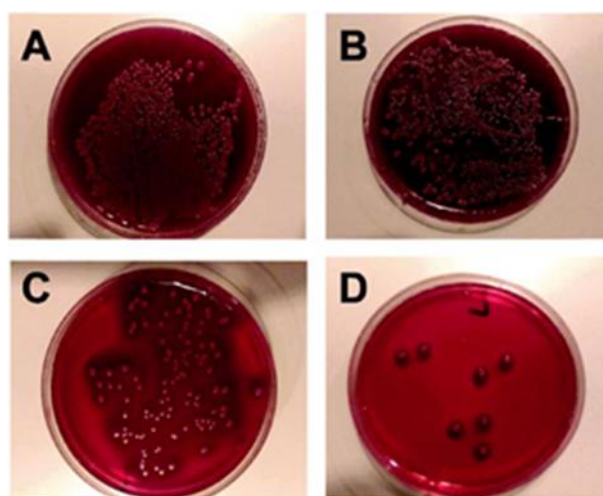


**Figure 4.** MacConkey's agar plates inoculated with 20 mL of bacterial sus-pensions of *Escherichia coli* ATCC 25922 (ca. CFU  $5 \times 10^4 \text{ mL}^{-1}$ ) after incubation with the PLGA film in the dark (A) and irradiated for 5 min (C) and 20 min (D). Control of the bacterial suspension after 20 min of irradiation in the absence of the PLGA film (B). Irradiation was performed with a 470 W Xe lamp, cut-off filter 14400 nm.

#### 4 Conclusions

We have achieved a biocompatible film of PLGA incorporating a novel tailored NO photoreleaser. The polymeric film is stable in the dark but it is able to release substantial amounts of NO with spatiotemporal control under excitation with visible light. The release process can be activated even by sunlight exposure and can be followed in real time by the intense blue fluorescence of a by-product, which acts as a convenient optical reporter of the NO concentration. To our knowledge, this is the first time that NO release with fluorescence reporting is demonstrated in film sam-ples. Once photogenerated, the NO radical promptly diffuses out of the polymeric matrix to reach biological targets. The film shows excellent and strictly light-dependent bactericidal activity against the Gram-negative *E. Coli* ATCC 25922

bacterial strain, opening intriguing possibilities for its further engineering in the perspective of coating and devices for biomedical applications. Finally, we would like to stress that the FRET mechanism occurring in compound 1 and the high two-photon cross-section of the coumarin chromophore offer, in principle, the possibility to trigger the NO photorelease and to detect the fluorescence of the reporter by two-photon excitation (TPE) of the coumarin component. In this regard, the study in progress in our laboratories is ongoing to demonstrate the possibility of the present system to eradicate biofilms with very high spatial resolution via TPE.

## **5 Acknowledgements**

We thank the Marie Curie Program (FP7-PEOPLE-ITN-2013, CYCLON-HIT 608407) for financial support to MC fellow MPL and funding of the research.

## References

1. Taubes G. The bacteria fight back. *Science*. 2008;321(5887):356-61.
2. Cohen ML. Changing patterns of infectious disease. *Nature*. 2000;406(6797):762-7.
3. Laxminarayan R, Duse A, Wattal C, Zaidi AK, Wertheim HF, Sumpradit N, et al. Antibiotic resistance-the need for global solutions. *Lancet Infect Dis*. 2013;13(12):1057-98.
4. Pittet D, Allegranzi B, Storr J, Donaldson L. 'Clean Care is Safer Care': the Global Patient Safety Challenge 2005-2006. *Int J Infect Dis*. 2006;10(6):419-24.
5. Page K, Wilson M, Parkin IP. Antimicrobial surfaces and their potential in reducing the role of the inanimate environment in the incidence of hospital-acquired infections. *Journal of Materials Chemistry*. 2009;19(23):3819-31.
6. Shlaes DM, Sahm D, Opiela C, Spellberg B. The FDA reboot of antibiotic development. *Antimicrob Agents Chemother*. 2013;57(10):4605-7.
7. Schairer DO, Chouake JS, Nosanchuk JD, Friedman AJ. The potential of nitric oxide releasing therapies as antimicrobial agents. *Virulence*. 2012;3(3):271-9.
8. Nitric oxide and infection, ed. G. Fang, Kluwer Academic/Plenum Publishers, New York, 1999..
9. Gardner PR, Gardner AM, Martin LA, Salzman AL. Nitric oxide dioxygenase: an enzymic function for flavohemoglobin. *Proc Natl Acad Sci U S A*. 1998;95(18):10378-83.
10. Fang FC. Antimicrobial reactive oxygen and nitrogen species: concepts and controversies. *Nat Rev Microbiol*. 2004;2(10):820-32.
11. Nitric Oxide: Biology and Pathobiology, ed. L. J. Ignarro, Elsevier Inc., 2010.
12. Wang PG, Xian M, Tang X, Wu X, Wen Z, Cai T, et al. Nitric oxide donors: chemical activities and biological applications. *Chem Rev*. 2002;102(4):1091-134.
13. Nitric Oxide Donors for Pharmaceutical and Biological Applications, ed. P. G. Wang, T. B. Cai and N. Taniguchi, Wiley-VCH Verlag GmbH & Co. KGaA, Weinheim, Germany, 2005.

14. Riccio DA, Schoenfisch MH. Nitric oxide release: part I. Macromolecular scaffolds. *Chem Soc Rev.* 2012;41(10):3731-41.
15. Seabra AB, Duran N. Nitric oxide-releasing vehicles for biomedical applications. *Journal of Materials Chemistry.* 2010;20(9):1624-37.
16. Halpenny GM, Heilman B, Mascharak PK. Nitric oxide (NO)-induced death of gram-negative bacteria from a light-controlled NO-releasing platform. *Chem Biodivers.* 2012;9(9):1829-39.
17. Sortino S. Light-controlled nitric oxide delivering molecular assemblies. *Chem Soc Rev.* 2010;39(8):2903-13.
18. Sortino S. Photoactivated nanomaterials for biomedical release applications. *Journal of Materials Chemistry.* 2012;22(2):301-18.
19. Ford PC. Photochemical delivery of nitric oxide. *Nitric Oxide.* 2013;34:56-64.
20. Fry NL, Mascharak PK. Photoactive ruthenium nitrosyls as NO donors: how to sensitize them toward visible light. *Acc Chem Res.* 2011;44(4):289-98.
21. Joslin JM, Neufeld BH, Reynolds MM. Correlating S-nitrosothiol decomposition and NO release for modified poly(lactic-co-glycolic acid) polymer films. *RSC Advances.* 2014;4(79):42039-43.
22. Roveda AC, de Fazio Aguiar H, Miranda KM, Tadini CC, Franco DW. Light-triggered and cysteine-mediated nitric oxide release from a biodegradable starch-based film. *Journal of Materials Chemistry B.* 2014;2(41):7232-42.
23. Dolanský J, Henke P, Kubát P, Fraix A, Sortino S, Mosinger J. Polystyrene Nanofiber Materials for Visible-Light-Driven Dual Antibacterial Action via Simultaneous Photogeneration of NO and O<sub>2</sub>(1Δg). *ACS Applied Materials & Interfaces.* 2015;7(41):22980-9.
24. Mosinger J, Lang K, Kubát P. Photoactivatable Nanostructured Surfaces for Biomedical Applications. *Top Curr Chem.* 2016;370:135-68.
25. Bishop A, Anderson JE. NO signaling in the CNS: from the physiological to the pathological. *Toxicology.* 2005;208(2):193-205.

26. Veldhuyzen WF, Nguyen Q, McMaster G, Lawrence DS. A light-activated probe of intracellular protein kinase activity. *J Am Chem Soc.* 2003;125(44):13358-9.
27. Pellois J-P, Hahn ME, Muir TW. Simultaneous Triggering of Protein Activity and Fluorescence. *Journal of the American Chemical Society.* 2004;126(23):7170-1.
28. Weinstain R, Segal E, Satchi-Fainaro R, Shabat D. Real-time monitoring of drug release. *Chemical Communications.* 2010;46(4):553-5.
29. Fry NL, Wei J, Mascharak PK. Triggered Dye Release via Photodissociation of Nitric Oxide from Designed Ruthenium Nitrosyls: Turn-ON Fluorescence Signaling of Nitric Oxide Delivery. *Inorganic Chemistry.* 2011;50(18):9045-52.
30. Zheng Q, Bonoiu A, Ohulchanskyy TY, He GS, Prasad PN. Water-Soluble Two-Photon Absorbing Nitrosyl Complex for Light-Activated Therapy through Nitric Oxide Release. *Molecular Pharmaceutics.* 2008;5(3):389-98.
31. Vittorino E, Sciortino MT, Siracusano G, Sortino S. Light-activated release of nitric oxide with fluorescence reporting in living cells. *ChemMedChem.* 2011;6(9):1551-4, 34.
32. Kirejev V, Kandoth N, Gref R, Ericson MB, Sortino S. A polymer-based nanodevice for the photoregulated release of NO with two-photon fluorescence reporting in skin carcinoma cells. *Journal of Materials Chemistry B.* 2014;2(9):1190-5.
33. Fraix, A. and Sortino, S. (2015), Photoactivable Platforms for Nitric Oxide Delivery with Fluorescence Imaging. *Chem. Asian J.*, 10: 1116–1125. doi:10.1002/asia.201403398
34. Fraix A, Marino N, Sortino S. Phototherapeutic Release of Nitric Oxide with Engineered Nanoconstructs. *Top Curr Chem.* 2016;370:225-57.
35. Q. Lin, C. Bao, G. Fan, S. Cheng, H. Liu, Z. Liu and L. Zhu, *J. Mater. Chem.*, 2012, 22, 6680.
36. Misko TP, Schilling RJ, Salvemini D, Moore WM, Currie MG. A fluorometric assay for the measurement of nitrite in biological samples. *Anal Biochem.* 1993;214(1):11-6.

37. Caruso EB, Petralia S, Conoci S, Giuffrida S, Sortino S. Photodelivery of Nitric Oxide from Water-Soluble Platinum Nanoparticles. *Journal of the American Chemical Society*. 2007;129(3):480-1.
38. S. Conoci, S. Petralia and S. Sortino, EP2051935A1/US20090191284, 2006
39. Cai W, Wu J, Xi C, Meyerhoff ME. Diazeniumdiolate-doped poly(lactic-co-glycolic acid)-based nitric oxide releasing films as antibiofilm coatings. *Biomaterials*. 2012;33(32):7933-44.
40. Brisbois EJ, Bayliss J, Wu J, Major TC, Xi C, Wang SC, et al. Optimized polymeric film-based nitric oxide delivery inhibits bacterial growth in a mouse burn wound model. *Acta Biomater*. 2014;10(10):4136-42.
41. Møller JKS, Skibsted LH. Nitric Oxide and Myoglobins. *Chemical Reviews*. 2002;102(4):1167-78.
42. R. W. Romberg and R. J. Kassner, *Biochemistry*, 1979, 18, 5387

## **ANNEX-II**

### **Evolution of the scientific literature on drug delivery: A 1974-2015 bibliometric study**

Published as:

Claude Robert, CS Wilson , Alessandro Venuta , Mauro Ferrari and CD Arreto

**J Control Release. 2017;260:226-33.**

## **Abstract**

This study charts the growth of the drug delivery literature published during 1974-2015 from journals indexed in the Science Citation Index Expanded database. The growth of publications on drug delivery paralleled the total scientific publications for three decades (1974-2003); however, from 2004 to 2015 it exploded fourfold, while the total increased only 1.75 fold. Industrialized countries (USA, UK, Germany, Japan, Italy, France and Canada) were the most prolific during the first decades, but in 2014-2015 China, India and South Korea ranked 1st, 3rd and 4th respectively among the productive countries. The number of participating countries increased fivefold (from 19 to 96). During the last 15 years, the journals targeted by drug delivery research increased nearly 2.4 fold (416 to 1001) and three journals (Journal of Controlled Release, Advanced Drug Delivery Reviews, and International Journal of Pharmaceutics) published nearly one-fifth of the drug delivery research in 2014-2015.

## 1. Introduction

Drug delivery (D.D.) concerns a large spectrum of approaches, formulations, technologies, and systems used to achieve and optimize the transport of pharmaceutical compounds in the human body by increasing their quantity and half-life in biological fluids while minimizing their adverse effects. One of the main benefits of D.D. systems is the opportunity to select the anatomical route through which drugs can be administered to the human body on the basis of the desired effect, the disease, and the type of molecule. The first D.D. devices were developed in the nineties and solely consisted of transdermal and oral delivery systems based on improving the drug release kinetics in order to obtain a constant rate over a certain period of time to enhance drug bioavailability, patient compliance, and decrease therapy costs [1]. Interestingly, since diseases such as cancer have been addressed as transport issues [2], there has been an increase in the exploitation of nanoparticles for medical applications. As a result, nanotechnology, whose conceptual foundations were laid down by Richard Feynman [3], has become one of the fastest growing research areas [4]. In particular, nanotherapeutics (i) improve the properties of drugs without affecting the carried molecules, (ii) provide the drugs with the ability to overcome several biological barriers that normally reduce the accumulation of therapeutics in the target area (iii) can consist in nanovectors loaded with various compounds such as two different drugs or a drug with an imaging agent in order to track the particles, (iv) increase the therapeutic impact by interacting with specific tissues and cells through surface functionalization and, (v) permit potential clinical application. Several types of nanovectors such as liposomes [5–7], polymeric nanoparticles [8], micelles [9,10], and iron based nanoparticles [11] have been exploited. Unfortunately, nanotechnology did not achieve the expected results, in fact a recent work showed that only a small portion of the injected dose accumulated at the target site [12] due to the presence of multiple biological barriers in the body that represent the main obstacles of D.D [13]. New technologies arise from a multidisciplinary approach that involves biology, chemistry, physics, and engineering based on the micro scale. Multistage discoidal vectors are an example of the next generation D.D. systems, and can be loaded with nanotherapeutics thereby overcoming biological barriers in a sequential manner to promote the accumulation at the site of interest [14,15]. In addition to injectable D.D. systems, other devices must be mentioned. Examples include the transdermal drug D.D., which is an effective alternative to the oral administration of various compounds [16], osmotic D.D. systems, that are suitable for implantation as well as for oral delivery by exploiting the movement of water through a selectively permeable membrane driven by a difference in

osmotic pressure [17], and mucoadhesive D.D. systems which are tablets, polymer gels, and films that remain in close contact with the tissue such as the oral cavity, the eye, and the nasal cavity resulting in high drug accumulation at the site of release [18]. In addition, implantable D.D. systems are based on microfluidics and can exploit both micro- and nano-scale technologies. Such systems display some disadvantages such as higher cost and the necessity to be implanted with surgery, but at the same time they provide therapeutic drug concentrations over the whole treatment, even if it requires continuous or repeated administration [19–21]. External Medical devices play an important role in several therapies such as the therapies for pulmonary diseases. On the market there are several devices working with passive and active mechanisms such as dry powder inhalers (DPI) that make up a large part of the market [22]. It is important to stress that all these approaches, formulations, technologies, and systems arise from basic science or bench research and can potentially be translated into clinical applications. During the last decades, qualitative evaluations of the progress in D.D. are available through the publication of numerous reviews [23,24]. Although such literature reviews provide readers updated and synthesized subject information, to our knowledge there is an absence of quantitative data describing the scientific publishing pattern of D.D. over time thus preventing scientists, physicians, decision-makers, politicians, and others a global view of scholarly communication in this field. The aim of this study is to use bibliometric techniques to provide a 40+ year longitudinal view (1974 to 2015) of the evolution of the scientific literature on D.D. without focusing on a specific area. Two indicators were chosen to follow this evolution: the publishing outputs of D.D. research by countries, and the journals used to publish research on D.D.

## **2. Method**

The data were collected between 20th October and 10th November 2016 from the Science Citation Index Expanded (SCI-E), a multidisciplinary index to the journal literature of science and technology, through the ISI Web of Knowledge™ (<http://www.isiwebofknowledge.com/>) – a part of the Web of Science (WoS) database. The search strategy consisted of: • all documents published in journals with at least one of the following keyphrases in the title: drug deliver\*, drug release\*, drug carr\*, sustained release\*, controlled release\*, intranasal administra\*, sustained deliver\*, intelligent delivery system, pulsatile releas\*, transdermal deliver\*, drug nanocarr\*, nasal deliver\*, rectal deliver\*, oral deliver\*, buccal deliver\*, drug nanopart\*, nanopart\* deliv\*, nanopart\* releas\*, nanoparticle drug, with asterisks replacing characters following the word-stems; • all documents published in the following journals: Journal of

Controlled Release, Advanced Drug Delivery Reviews, Expert Opinion on Drug Delivery, Drug Delivery, Journal of Drug Delivery Science and Technology, Current Drug Delivery, Critical Reviews in Therapeutic Drug Carrier Systems, Drug Delivery and Translational Research, Journal of Aerosol Medicine and Pulmonary Drug Delivery, Polymeric Drug Delivery I Particulate Drug, Cancer Drug Delivery, Polymeric Drug Delivery II Polymeric Matrix, Polysaccharides for Drug Delivery and Pharmaceutical Applications, Advances in Controlled Drug Delivery Science Technology and Products, Filled Elastomers Drug Delivery Systems. Only journal article and journal review-type publications (as defined in the SCI-E database) published during 1974–2015 were considered. The 2015 impact factors (IF) were collected using the Thomson Scientific Journal Citation Reports. Downloaded documents were then analyzed by countries, and for each two-year period from 1974 to 2015 the following parameters were considered: • the total number of publications authored or co-authored by researchers in each country – publications issued from more than one country were assigned equally to each contributing country – and, • the top-10 most prolific journals publishing drug delivery research. Publications originating from England, Wales, Scotland and Northern Ireland were assigned to the United Kingdom (UK), and the European Union (EU) was defined as the official member States registered on the 1st of January for each of the two year-periods considered. The set of BRICS countries includes Brazil, Russia, India, China and South Africa.

### 3. Results and discussion

#### 3.1. Evolution of the drug delivery research

During the past 40+ years the scientific literature on D.D. emerged and has grown rapidly (Figure 1). The global evolution of D.D. literature can be split into 2 parts. From 1974 to the start of the 2000s, the D.D. scientific literature grew slowly (from 63 publications published in 1974–1975 to 1750 publications in 2000–2001) paralleling the growth of the total WoS literature. However, from 2002 to 2015, the growth exploded: there was a fourfold increase of the D.D. literature (1848 D.D. publications published in 2002–2003 vs. 7823 in 2014–2015), while the total for the WoS literature only increased 1.75 fold.

#### 3.2. Evolution of countries publishing drug delivery research

As shown in Table 1, from 1974 to 2015 the number of countries involved in D.D. research increased fivefold: 19 countries in the 1974–1975 period, 36 in 1984–1985, 52 in 1994–1995, 72 in 2004–2005, and 96 countries in 2014–2015. In the first four of the five two-year periods analyzed the USA was by far the most productive country with a lead of 43.6% of the total share in 1984–1985; however, it ranked second in 2014–2015 with only 21.4% of the total publications. Some industrialized countries (UK, Japan, Germany, France, Netherlands and Canada) that were present among the leading countries in 1984–1985 slowly lost their high ranking positions, but remained among the leading countries in 2014–2015. These observations

are in line with the domination (in terms of the number of publications) of these countries in various fields of Biology [25], Medicine [26,27], and in research fields more closely allied to D.D. research such as Nanotechnologies [28] and Liposomes

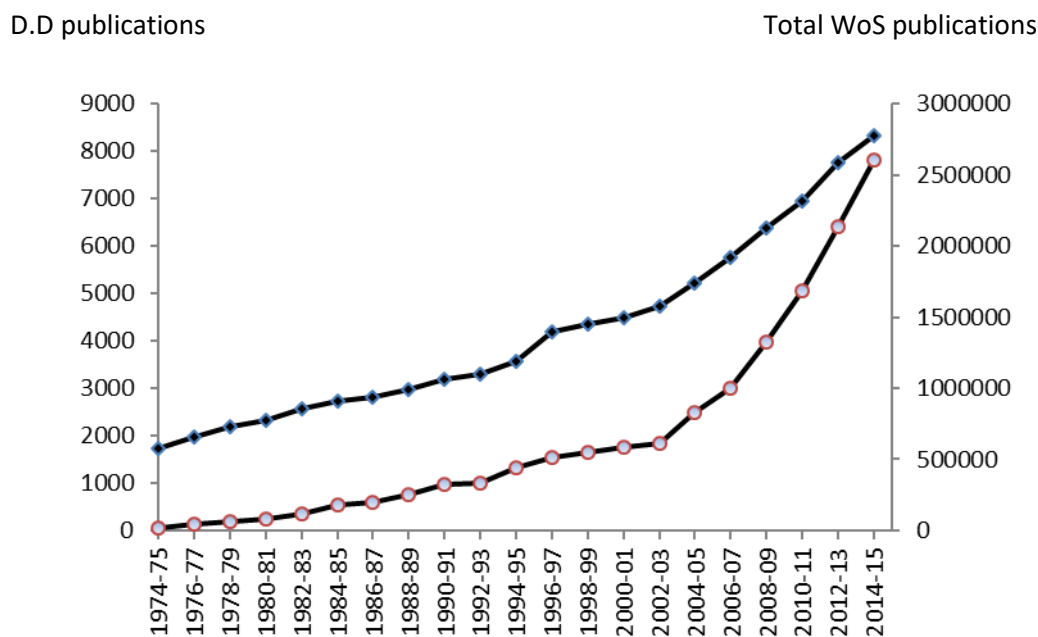


**Figure 1.** Number of Drug Delivery and total WoS research articles and review publications: 1974-2015

**Table 1.** The number of drug delivery research articles and review publications by countries, the EU countries, BRICS countries, and the World: 1974–1975, 1984–1985, 1994–1995, 2004–2005 and 2014–2015.

Countries/Territories	1974-1975		
	#publications	%	Rank
World	63	100.0	
EU	18	28.5	
USA	22	34.9	1
UK	12	19.0	2
Canada	4	6.3	3
Norway	3	4.7	4
Fed Rep Germany	2	3.1	5
Germany Dem Rep	2	3.1	5
Sweden	2	3.1	5
United Arab Rep	2	3.1	5
Belgium	1	1.6	9
Bulgaria	1	1.6	9
Denmark	1	1.6	9
Finland	1	1.6	9
India	1	1.6	9
Ireland	1	1.6	9
Israel	1	1.6	9
Netherlands	1	1.6	9
New Zealand	1	1.6	9
Switzerland	1	1.6	9
Trinidad & Tobago	1	1.6	9

Countries/Territories	1984-1985		
	# publications	%	Rank

**Table 1 continued**

World	527	100.0	
EU	169	32.0	
USA	230	43.6	1
UK	80	15.1	2
Japan	33	6.2	3
Fed Rep Germany	26	4.9	4
France	21	3.9	5
Netherlands	18	3.4	6
Canada	16	3.0	7
Israel	13	2.4	8
Denmark	11	2.0	9
Austria	10	1.8	10
India	10	1.8	10
Italy	10	1.8	10
Belgium	8	1.5	13
Australia	6	1.1	14
Switzerland	6	1.1	14
Egypt	5	0.9	16
Finland	4	0.7	17
Sweden	4	0.7	17
Turkey	4	0.7	17
Czechoslovakia	3	0.5	20
New Zealand	3	0.5	20
Poland	3	0.5	20
South Africa	3	0.5	20
Taiwan	3	0.5	20
Germany Dem Rep	2	0.3	25
Ireland	2	0.3	25
Jordan	2	0.3	25
Norway	2	0.3	25
Thailand	2	0.3	25
Argentina	1	0.1	30
Bahamas	1	0.1	30
Hungary	1	0.1	30
Kenya	1	0.1	30
Nigeria	1	0.1	30
Peoples R China	1	0.1	30

**Table 1 continued**

P hilippines	1	0.1	30
1994-1995			
Countries/Territories	# publications	%	Rank
World	1329	100.0	
BRICS	67	5.0	
EU	411	30.9	
USA	533	40.1	1
Japan	173	13.0	2
UK	150	11.2	3
France	62	4.6	4
Germany	60	4.5	5
Italy	57	4.2	6
Canada	52	3.9	7
Netherlands	42	3.1	8
Israel	41	3.0	9
India	36	2.7	10
Belgium	31	2.3	11
Sweden	23	1.7	12
Switzerland	17	1.2	13
Spain	17	1.2	13
Denmark	17	1.2	13
Finland	15	1.1	16
P eoples R China	15	1.1	16
Turkey	15	1.0	18
Australia	14	<1	19
Egypt	12	<1	20
Taiwan	12	<1	20
South Africa	10	<1	22
New Zealand	9	<1	23
Austria	8	<1	24
Czech Rep	7	<1	25
Norway	6	<1	26
Russia	6	<1	26
South Korea	6	<1	26
Saudi Arabia	5	<1	29

Yh T

Greece	4	<1	30
Hungary	4	<1	30
Iceland	4	<1	30
Argentina	3	<1	33
Bulgaria	3	<1	33
Chile	3	<1	33
Croatia	3	<1	33
Hong Kong	2	<1	37
Malaysia	2	<1	37
Mexico	2	<1	37
Nigeria	2	<1	37
Portugal	2	<1	37
Singapore	2	<1	37
Thailand	2	<1	37
Bangladesh	1	<1	44
Estonia	1	<1	44
Ireland	1	<1	44
Jordan	1	<1	44
Philippines	1	<1	44
Poland	1	<1	44
Romania	1	<1	44
Slovenia	1	<1	44
Ukraine	1	<1	44

2004-2005

Countries/Territories	#publications	%	Rank
World	2485	100.0	
BRICS	373	15.0	
EU	833	33.5	
USA	746	30.0	1
Japan	262	10.5	2
UK	222	8.9	3
Peoples R China	169	6.8	4
Germany	153	6.1	5

India	146	5.8	6
South Korea	137	5.5	7
Italy	126	5.0	8
France	126	5.0	9
Canada	98	3.9	10
Spain	57	2.2	11
Switzerland	56	2.2	12
Netherlands	55	2.2	13
Australia	47	1.8	14
Belgium	46	1.8	15
Singapore	45	1.8	16
Taiwan	44	1.7	17
Israel	38	1.5	18
Turkey	36	1.4	19
Austria	33	1.3	20
Sweden	33	1.3	20
Brazil	31	1.2	22
Finland	23	<1	23
Iran	23	<1	23
Ireland	21	<1	25
Denmark	17	<1	26
Egypt	17	<1	26
New Zealand	17	<1	26
Russia	17	<1	26
Portugal	16	<1	30
Thailand	15	<1	31
Czech Rep	13	<1	32
South Africa	12	<1	33
Norway	11	<1	34
Romania	11	<1	34
Argentina	8	<1	36
Greece	8	<1	36
Mexico	8	<1	36
Malaysia	7	<1	39
Croatia	6	<1	40
Kuwait	6	<1	40
Slovenia	6	<1	40
Iceland	4	<1	43

Philippines	4	<1	43
Poland	4	<1	43
Cuba	4	<1	43
Hungary	3	<1	47
Jordan	3	<1	47
Nigeria	3	<1	47
Pakistan	3	<1	47
Saudi Arabia	3	<1	47
Yugoslavia	3	<1	47
Bulgaria	2	<1	53
Estonia	2	<1	53
Indonesia	2	<1	53
U Arab Emirates	2	<1	53
Bahrain	1	<1	57
Chile	1	<1	57
Kazakhstan	1	<1	57
Latvia	1	<1	57
Lebanon	1	<1	57
Lithuania	1	<1	57
Malta	1	<1	57
Myanmar	1	<1	57
Nepal	1	<1	57
Rep Of Georgia	1	<1	57
Serbia Montenegro	1	<1	57
Slovakia	1	<1	57
Tanzania	1	<1	57
Tunisia	1	<1	57
Ukraine	1	<1	57
Uruguay	1	<1	57

2014-2015

Countries/Territories	# publications	%	Rank
World	7824	100.0	
BRICS	3153	40.2	
EU	1924	20.5	
Peoples R China	2042	26.0	1
USA	1675	21.4	2

India	872	11.1	3
South Korea	408	5.2	4
UK	383	4.8	5
Germany	341	4.3	6
Japan	290	3.7	7
Italy	252	3.2	8
France	236	3.0	9
Iran	229	2.9	10
Spain	219	2.7	11
Australia	208	2.6	12
Canada	190	2.4	13
Brazil	146	1.8	14
Taiwan	144	1.8	15
Saudi Arabia	140	1.7	16
Egypt	139	1.7	17
Netherlands	123	1.5	18
Portugal	121	1.5	19
Singapore	119	1.5	20
Switzerland	113	1.4	21
Belgium	95	1.2	22
Malaysia	94	1.2	23
Israel	83	1.0	24
Denmark	71	<1	25
Turkey	69	<1	26
Thailand	65	<1	27
Pakistan	62	<1	28
Poland	61	<1	29
Sweden	61	<1	29
Russia	60	<1	31
Romania	59	<1	32
South Africa	54	<1	33
Finland	52	<1	34
Austria	48	<1	35
Greece	48	<1	35
Argentina	42	<1	37
Ireland	42	<1	37
Czech Rep	34	<1	39
Hungary	34	<1	39

Norway	34	<1	41
New Zealand	29	<1	42
Serbia	23	<1	43
Slovenia	23	<1	43
Mexico	22	<1	45
Nigeria	22	<1	45
Jordan	18	<1	47
Chile	17	<1	48
Vietnam	16	<1	49
U Arab Emirates	11	<1	50
Estonia	10	<1	51
Bulgaria	8	<1	52
Croatia	8	<1	52
Indonesia	8	<1	52
Bangladesh	6	<1	55
Colombia	6	<1	55
Iceland	6	<1	55
Slovakia	6	<1	55
Algeria	5	<1	59
Cuba	5	<1	59
Syria	5	<1	59
Iraq	4	<1	62
Mauritius	4	<1	62
Tunisia	4	<1	62
Cyprus	3	<1	65
Lebanon	3	<1	65
Luxembourg	3	<1	65
Morocco	3	<1	65
Philippines	3	<1	65
Qatar	3	<1	65
Rep of Georgia	3	<1	65
Byelarus	2	<1	72
Ghana	2	<1	72
Montenegro	2	<1	72
Oman	2	<1	72
Tanzania	2	<1	72
Yemen	2	<1	72
Azerbaijan	1	<1	78

Benin	1	<1	78
Brunei	1	<1	78
Burkina Faso	1	<1	78
Cameroon	1	<1	78
Costa Rica	1	<1	78
Ecuador	1	<1	78
Ethiopia	1	<1	78
Kenya	1	<1	78
Kuwait	1	<1	78
Libya	1	<1	78
Macedonia	1	<1	78
Myanmar	1	<1	78
Nepal	1	<1	78
Sudan	1	<1	78
Uganda	1	<1	78
Ukraine	1	<1	78
Venezuela	1	<1	78
Zimbabwe	1	<1	78

In the first four of the five two-year periods analyzed the USA was by far the most productive country with a lead of 43.6% of the total share in 1984-1985; however, it ranked second in 2014-2015 with only 21.4% of the total publications. Some industrialized countries (UK, Japan, Germany, France, Netherlands and Canada) that were present among the leading countries in 1984-1985 slowly lost their high ranking positions, but remained among the leading countries in 2014-2015. These observations are in line with the domination (in terms of the number of publications) of these countries in various fields of Biology [25], Medicine [26, 27], and in research fields more closely allied to D.D. research such as Nanotechnologies [28] and Liposomes [29]. Contrariwise, two Asian newcomers, China and South Korea, along with the continuous presence of India among the productive countries have progressively joined the industrialized countries in their D.D. research efforts: China from ranked 17th in 1994-1995, 4th in 2004-2005, to 1st in 2014-2015; and South Korea from ranked 28th in 1994-1995, 7th in 2004-2005, to 4th in 2014-2015.

The increasingly leading position of China is also supported by the fact that five of the ten most productive institutions in D.D. research are located in China (data not shown). The recent increase of Chinese D.D. publication (see Figure 2) can be correlated to the explosion of publications authored by Chinese scientists in Pharmacology and Pharmacy journals [30]. More globally, it can be seen as a consequence of the recent increase of China's total expenditure on Research and Development – on average 23% per annum over the last decade [31]. Additionally, the recent ascendancy of China over the USA was predicted in a report of the Royal Society [32].

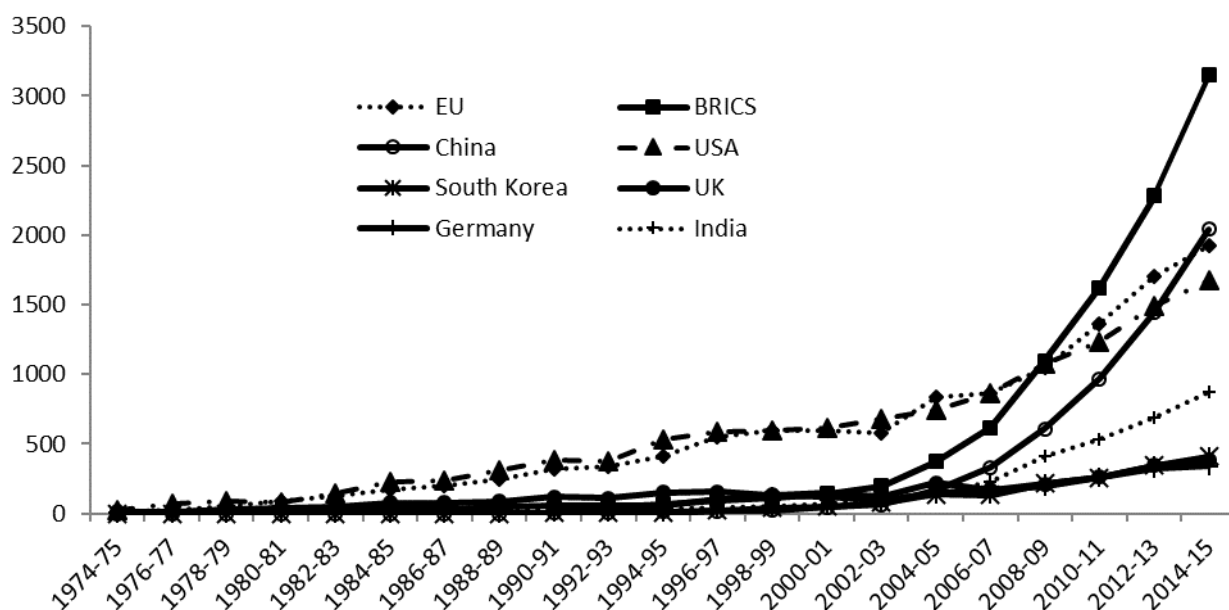


**Figure 2.** Number of Drug Delivery research articles and review publications for top-producing countries, the EU countries and BRICS countries: 1974-2015

While the share of D.D. publications among the EU countries remained stable from 1994 to 2005 (30.9% in 1994-1995, and 33.5% in 2004-2005) but decreased to 20.5% in 2014-2015; the share of the BRICS countries increased continuously (mainly due to the D.D. research output of China and India): 5.0% in 1994-1995, 15.0% in 2004-2005 and 40.2% in 2014-2015. As noted earlier, three members of BRICS (China, India and South Korea) were present in the top-ranking countries in 2004-2005 and in 2014-2015.

### 3.3. Evolution of journals publishing drug delivery research

During the 40+ years studied, the number of journals targeted by D.D. researchers increased in two trajectories (Figure 3). From 1974 to the beginning of the 2000s, the increase of D.D. journals more or less paralleled that of the SCI-E database; however, from 2002 to 2015, the number of D.D. journals increased 2.4 fold (416 journals in 2002-2003 and 1,001 for 2014-2015) while the total number of journals indexed in the SCI-E increased only 1.2 fold (7,822 journals for 2002-2003 and 9,550 for 2014-2015).

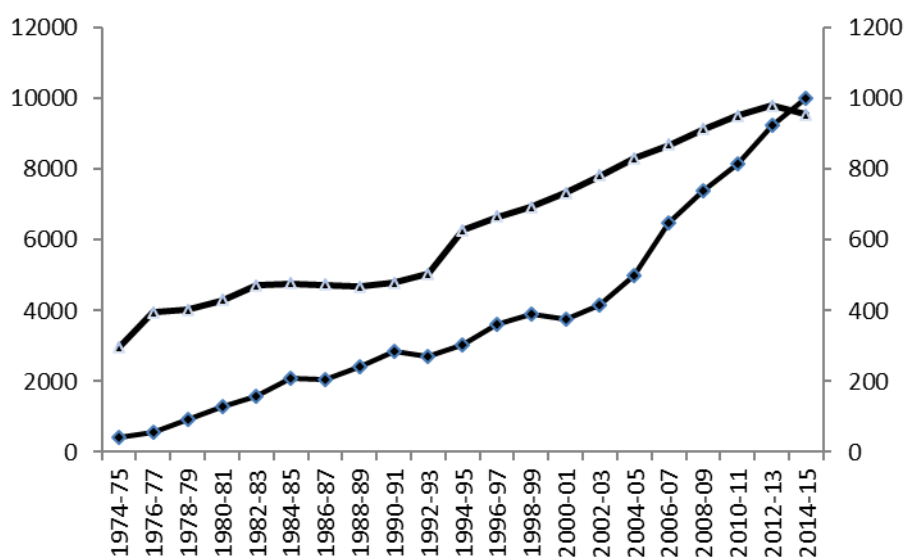


**Figure 3.** Number of journals publishing Drug Delivery research articles and review publications: 1974-2015

The top-10 most productive journals on D.D. research in each of the last four time periods are presented in Table 2. During the last three periods analyzed (1994-1995, 2004-2005 and 2014-2015) three journals (Journal of Controlled Release, Advanced Drug Delivery Reviews, and International Journal of Pharmaceutics) were ranked among the top-4 most productive journals; two other journals (Drug Delivery and Journal of Drug Delivery Science and Technology) were present among the top-10 most productive journals in the two most

recent rankings (2004-2005 and 2014-2015). For the last time period studied, eight of the top-10 ranked journals had an IF >3.00 with a maximum IF of 15.60 for the journal *Advanced Drug Delivery Reviews*.

**Table 2.** The top-10 journals publishing Drug Delivery research articles and review publications: 1984-1985, 1994-1995, 2004-2005 and 2014-2015 (including 2015 IFs)

Source Titles	# publications	% of 527	WoS category
<i>Cancer Drug Delivery</i>	53	10.0	n.a.
<i>International Journal of Pharmaceutics</i>	29	5.5	Pharmacology & Pharmacy
<i>Drug Development and Industrial Pharmacy</i>	18	3.4	Chemistral, Medicinal; Pharmacology & Pharmacy
<i>Journal of Pharmaceutical Sciences</i>	17	3.2	Chemistry, Multidisciplinary; Chemistry, Medicinal; Pharmacology & Pharmacy
<i>British Journal of Clinical Pharmacology</i>	15	2.8	Pharmacology & Pharmacy
<i>Journal of Pharmacy and Pharmacology</i>	11	2.0	Pharmacology & Pharmacy
<i>International Journal of Clinical Pharmacology and Therapeutics</i>	11	2.0	Pharmacology & Pharmacy
<i>Chemical Pharmaceutical Bulletin</i>	11	2.0	Chemistry, Multidisciplinary; Chemistry, Medicinal; Pharmacology & Pharmacy
<i>American Journal of Medicine</i>	8	1.5	Medicine, General & Internal
<i>Pharmacy International</i>	7	1.3	n.a.
<i>Biopharmaceutics Drug Disposition</i>	7	1.3	Pharmacology & Pharmacy
<i>Annals of the New York Academy of Sciences</i>	7	1.3	n.a.

Source Titles	# publications	% of 1329	WoS category
<i>Journal of Controlled Release</i>	325	24.4	Chemistry, Multidisciplinary Pharmacology & Pharmacy
<i>Advanced Drug Delivery Reviews</i>	107	8.0	Pharmacology & Pharmacy
<i>International Journal of Pharmaceutics</i>	96	7.2	Pharmacology & Pharmacy
<i>Drug Development and Industrial Pharmacy</i>	65	4.8	Chemistral, Medicinal; Pharmacology & Pharmacy
<i>Journal of Pharmaceutical Sciences</i>	47	3.5	Chemistry, Multidisciplinary; Chemistry, Medicinal; Pharmacology & Pharmacy
<i>Pharmaceutical Research</i>	45	3.3	Chemistry, Multidisciplinary Pharmacology & Pharmacy
<i>Chemical Pharmaceutical Bulletin</i>	19	1.4	Chemistry, Multidisciplinary; Chemistry, Medicinal; Pharmacology & Pharmacy
<i>STP Pharma Sciences</i>	17	1.2	Pharmacology & Pharmacy
<i>Journal of Pharmacy and Pharmacology</i>	16	1.2	Pharmacology & Pharmacy
<i>Journal of Drug Targeting</i>	15	1.0	Pharmacology & Pharmacy
<i>Journal of Clinical Pharmacology</i>	15	1.0	Pharmacology & Pharmacy
<i>Critical Reviews in Therapeutics Drug Carrier System</i>	15	1.0	n.a.

Source Titles	# publications	% of 2485	WoS category
<i>Journal of Controlled Release</i>	678	27.2	Chemistry, Multidisciplinary Pharmacology & Pharmacy
<i>Advanced Drug Delivery Reviews</i>	217	8.7	Pharmacology & Pharmacy
<i>Journal of Drug Delivery Science and Technology</i>	134	5.3	Pharmacology & Pharmacy
<i>International Journal of Pharmaceutics</i>	127	6.1	Pharmacology & Pharmacy
<i>Drug Delivery</i>	85	3.4	Pharmacology & Pharmacy
<i>Biomaterials</i>	46	1.8	Engineering, Biomedical; Materials Science, Biomaterials
<i>Drug Development and Industrial Pharmacy</i>	41	1.6	Chemistral, Medicinal; Pharmacology & Pharmacy
<i>European Journal of Pharmaceutics and Biopharmaceutics</i>	40	1.6	Pharmacology & Pharmacy
<i>Pharmaceutical Research</i>	31	1.2	Chemistry, Multidisciplinary Pharmacology & Pharmacy
<i>Journal of Applied Polymer Science</i>	31	1.2	Polymer Science

Source Titles	# publications	% of 7823	IF (2015)	WoS Category
<i>Journal of Controlled Release</i>	962	12.2	7.44	Chemistry, Multidisciplinary Pharmacology & Pharmacy
<i>Advanced Drug Delivery Reviews</i>	280	3.5	15.60	Pharmacology & Pharmacy
<i>International Journal of Pharmaceutics</i>	277	3.5	3.99	Pharmacology & Pharmacy
<i>Expert Opinion on Drug Delivery</i>	251	3.2	5.43	Pharmacology & Pharmacy
<i>RSC Advances</i>	228	2.9	3.28	Chemistry, Multidisciplinary
<i>Journal of Drug Delivery Science and Technology</i>	217	2.7	0.62	Pharmacology & Pharmacy
<i>Journal of Materials Chemistry B</i>	186	2.3	4.87	Materials Science, Biomaterials
<i>Drug Delivery</i>	179	2.2	4.84	Pharmacology & Pharmacy
<i>Colloids and Surfaces B Biointerfaces</i>	141	1.8	3.90	Biophysics; Chemistry, Physical; Materials Science, Biomaterials

Furthermore, during the same three time periods the distributions of publications in journals were markedly skewed:

- in 1994-1995, 1% (3 journals) of D.D journals concentrated 39.7% of the 1,329 publications, while 91.3% (276 journals) of D.D. journals had  $\leq 5$  publications;
- in 2004-2005, 1% (5 journals) of D.D. journals concentrated 50% of the 2,485 D.D. publications, while 91.5% (457 journals) of D.D. journals had  $\leq 5$  publications; and finally
- in 2014-2015, 1% (10 journals) of the journals concentrated 36.4% of the 7,823 D.D. publications, while 81.9% (820 journals) of D.D. journals had  $\leq 5$  publications.

With the rapid growth of the scientific literature, review publications are essential updating tools for researchers [33]. During the last fifteen years, the number of D.D. review publications increased 3.5 fold (347 reviews in 2000-2001 vs. 1,220 in 2014-2015) while the total number of reviews in the SCI-E database only increased 2.6 fold (60,394 in 2000-2001 vs. 155,926 in 2014-2015). As in numerous scientific disciplines, a review journal, *Advanced Drug Delivery Reviews*, specifically dedicated to the field of D.D., was launched in 1987. This journal publishes approximately 150 publications per year, has a 2015 JCR impact factor of 15.60, and ranked 3rd (of 255) among the leading journals in the Pharmacology & Pharmacy WoS category. Although this journal published most of the D.D. review publications, other

review publications were scattered among a broad range of journals: prestigious journals such as The Lancet [34], Nature [35], Nature Reviews Drug Discovery [36] and more specialized journals [37, 38]. Additionally, the increasing ratio of review publications / review+non-review publications from 1974 to 2000 and the stabilization since 2001 to 2015 from between 15% to 20% are indications of the evolving and maturing of the D.D. field.

Although two emblematic journals targeted by D.D. researchers began in the mid-1980s (The Journal of Controlled Release in 1984 and Advanced Drug Delivery Reviews in 1987), the recent explosion of the D.D. literature was accompanied by the launching of six more journals dedicated to D.D. in the 2000s: The Journal of Drug Delivery Science Technology (launched in 2004), Expert Opinion on Drug Delivery (2004), Current Drug Delivery (2004), Drug Delivery (2007), Journal of Aerosol Medicine and Pulmonary Drug Delivery (2008) and Drug Delivery and Translational Research (2011).

From 1974 to 2015 the scientific literature on D.D. spread among a broad range of scientific fields (WoS subject categories): 24 in 1974-1975; 70 in 1984-1985, 100 in 1994-1995; 124 in 2004-2005; and 144 in 2014-2015. During this period, the WoS subject category Pharmacology & Pharmacy was the most targeted field; some of the top-leading WoS fields (Ophthalmology and Dermatology) disappeared while other fields gained in importance: Biochemistry Molecular Biology in 1984-1985, Materials Science Biomaterials, Polymer Science, or Engineering Biomedical in 1994-1995, and Nanoscience Nanotechnology and Chemistry Physical in 2004-2005.

## **4. Conclusion**

This brief bibliometric investigation on the evolution of the scientific literature on during 40+ years reveals three major trends: an explosion of D.D.-related publications (63 publications for 1974-1975 vs. 7,824 for 2014-2015); the spread and distribution of publications among publishing countries (19 countries in 1974-1975 vs. 96 in 2014-2015); and an increase of the number of journals involved in D.D. publications (42 journals in 1974-1975 vs. 1,001 in 2014-2015). Despite an overall increase in publications that seem to result in a rapid advancement of the field after an initial success achieved by the first D.D. systems, production of approved D.D. systems for clinical use slowed down in the following years. This happens because overcoming the physiochemical and biological barriers is still a challenge [39]. The development of new delivery systems that are able to address current challenges in medicine was often driven by discoveries in basic science. Specifically, biology gave a huge boost to the development of nanotechnologies with discoveries such as the enhanced permeability and retention (EPR) effect [40]. Likewise, chemistry and material sciences have had a tremendous impact on the development of all D.D. systems, while physics and mathematics have added to the understanding of transport through the organism. Therefore, it is easy to understand how the collaboration among different disciplines is fundamental and that it is critical to maintain a detached view from the major scientific trend to keep up with new scientific discoveries [41]. Overcoming such limits will have a great impact also on the healthcare economy by introducing new technologies. As an example, the commercialization of Doxil [42], the first approved nanoformulated drug, decreased the cost of treatment and hospitalization [43]. Furthermore, the economic investments play a critical role in the translation of basic research into the clinic. In particular, the funding management varies among countries. For example, there is a substantial difference in the funding approaches between the U.S. and China, which are the two leading countries in D.D. research. U.S. governmental agencies that provide research funding, such as

the National Institutes of Health (NIH), promote the development of projects in which the translational aspect is a major component, thereby making the U.S. the leader in translational research. On the other hand, in the last few decades China has been investing most of its funds in basic sciences, which has led to a massive production of scientific publications less focused on translational science.

In the years to come there will be an increase in the development and the commercialization of D.D. systems thereby resulting in increased research activities worldwide and consequentially in an increased production of related scientific publications, probably with a similar trend observed in the last two decades among the countries considered.

We hope that our study will arouse interest in scientists, physicians, decision-makers, and politicians in extending this bibliometric study of the D.D. field.

D.D.

## References

1. A.S. Hoffman, The origins and evolution of "controlled" drug delivery systems, *J Control Release*, 132 (2008) 153-163.
2. F. Michor, J. Liphardt, M. Ferrari, J. Widom, What does physics have to do with cancer?, *Nat Rev Cancer*, 11 (2011) 657-670.
3. R.P. Feynman, There's plenty of room at the bottom, *Engineering and Science*, 23:5 (1960).
4. O.C. Farokhzad, R. Langer, Impact of nanotechnology on drug delivery, *ACS Nano*, 3 (2009) 16-20.
5. T.M. Allen, P.R. Cullis, Liposomal drug delivery systems: from concept to clinical applications, *Adv Drug Deliv Rev*, 65 (2013) 36-48.
6. V.P. Torchilin, Recent advances with liposomes as pharmaceutical carriers, *Nat Rev Drug Discov*, 4 (2005) 145-160.
7. A. Puri, K. Loomis, B. Smith, J.H. Lee, A. Yavlovich, E. Heldman, R. Blumenthal, Lipid-based nanoparticles as pharmaceutical drug carriers: from concepts to clinic, *Crit Rev Ther Drug Carrier Syst*, 26 (2009) 523-580.
8. K.S. Soppimath, T.M. Aminabhavi, A.R. Kulkarni, W.E. Rudzinski, Biodegradable polymeric nanoparticles as drug delivery devices, *J Control Release*, 70 (2001) 1-20.
9. S.R. Croy, G.S. Kwon, Polymeric micelles for drug delivery, *Curr Pharm Des*, 12 (2006) 4669-4684.
10. A. Mandal, R. Bisht, I.D. Rupenthal, A.K. Mitra, Polymeric micelles for ocular drug delivery: From structural frameworks to recent preclinical studies, *J Control Release*, 248 (2017) 96-116.
11. R. Tietze, J. Zaloga, H. Unterweger, S. Lyer, R.P. Friedrich, C. Janko, M. Pottler, S. Durr, C. Alexiou, Magnetic nanoparticle-based drug delivery for cancer therapy, *Biochem Biophys Res Commun*, 468 (2015) 463-470.

12. S. Wilhelm, A.J. Tavares, Q. Dai, S. Ohta, J. Audet, H.F. Dvorak, W.C.W. Chan, Analysis of nanoparticle delivery to tumours, *Nat Rev Mater*, 1 (2016), doi:10.1038/natrevmats.2016.14.
13. E. Blanco, H. Shen, M. Ferrari, Principles of nanoparticle design for overcoming biological barriers to drug delivery, *Nat Biotechnol*, 33 (2015) 941-951.
14. J. Wolfram, H. Shen, M. Ferrari, Multistage vector (MSV) therapeutics, *J Control Release*, 219 (2015) 406-415.
15. A. Venuta, J. Wolfram, H. Shen, M. Ferrari, Post-nano strategies for drug delivery: multistage porous silicon microvectors, *J Mater Chem B*, 5 (2017) 207-219.
16. M.R. Prausnitz, R. Langer, Transdermal drug delivery, *Nat Biotechnol*, 26 (2008) 1261-1268.
17. R.A. Keraliya, C. Patel, P. Patel, V. Keraliya, T.G. Soni, R.C. Patel, M.M. Patel, Osmotic drug delivery system as a part of modified release dosage form, *ISRN Pharm*, 2012 (2012) 528079.
18. B.M. Boddupalli, Z.N. Mohammed, R.A. Nath, D. Banji, Mucoadhesive drug delivery system: An overview, *J Adv Pharm Technol Res*, 1 (2010) 381-387.
19. E. Meng, T. Hoang, Micro- and nano-fabricated implantable drug-delivery systems, *Ther Deliv*, 3 (2012) 1457-1467.
20. O.M. Sabek, M. Farina, D.W. Fraga, S. Afshar, A. Ballerini, C.S. Filgueira, U.R. Thekkedath, A. Grattoni, A.O. Gaber, Three-dimensional printed polymeric system to encapsulate human mesenchymal stem cells differentiated into islet-like insulin-producing aggregates for diabetes treatment, *J Tissue Eng*, 7 (2016), doi: 10.1177/2041731416638198.
21. M. Farina, A. Ballerini, G. Torchio, G. Rizzo, D. Demarchi, U. Thekkedath, A. Grattoni, Remote magnetic switch off microgate for nanofluidic drug delivery implants, *Biomed Microdevices*, 19 (2017) 42.
22. J.S. Patil, S. Sarasija, Pulmonary drug delivery strategies: A concise, systematic review, *Lung India*, 29 (2012) 44-49.
23. G. Tiwari, R. Tiwari, B. Sriwastawa, L. Bhati, S. Pandey, P. Pandey, S.K. Bannerjee, Drug delivery systems: An updated review, *Int J Pharm Investig*, 2 (2012) 2-11.

24. J.Z. Hilt, N.A. Peppas, Microfabricated drug delivery devices, *Int J Pharm*, 306 (2005) 15-23.
25. C. Robert, C.S. Wilson, J.F. Gaudy, W. Hornebeck, C.D. Arreto, Trends in matrix metalloproteinase research from 1986-2007: a bibliometric study, *Biochem Cell Biol*, 88 (2010) 843-851.
26. C. Boudry, F. Mouriaux, Eye neoplasms research: a bibliometric analysis from 1966 to 2012, *Eur J Ophthalmol*, 25 (2015) 357-365.
27. C. Robert, C.S. Wilson, R.B. Lipton, C.D. Arreto, Growth of Headache Research: A 1983-2014 bibliometric study, *Cephalalgia*, (2016).
28. M.H. Biglu, F. Eskandari, A. Asgharzadeh, Scientometric Analysis of Nanotechnology in MEDLINE, *Bioimpacts*, 1 (2011) 193-198.
29. X.D. Zhou, G.H. Zhao, Global liposome research in the period of 1995-2014: a bibliometric analysis, *Scientometrics*, 105 (2015) 231-248.
30. G. Li, L.H. Hu, Z. Liao, H.C. Cui, Z.S. Li, Scientific Publications in Pharmacology and Pharmacy Journals from Chinese Authors in Various Parts of North Asia: a 10-year Survey of the Literature, *J Int Med Res*, 38 (2010) 750-759.
31. J.E. Qiu, China goes back to basics on research funding, *Nature*, 507 (2014) 148-149.
32. L. Clark, A. Plume et al., Knowledge, networks and nations: Global scientific collaboration in the 21st century, London, The Royal Society, 2011.  
<https://royalsociety.org/topics-policy/projects/knowledge-networks-nations/report/> (accessed on December 27th, 2016).
33. C.M. Ketcham, J.M. Crawford, The impact of review articles, *Lab Invest*, 87 (2007) 1174-1185.
34. M.B. Dolovich, R. Dhand, Aerosol drug delivery: developments in device design and clinical use, *Lancet*, 377 (2011) 1032-1045.
35. H. Hoag, DRUG DELIVERY Brain food, *Nature*, 510 (2014) S6-S7.
36. V.P. Torchilin, Multifunctional, stimuli-sensitive nanoparticulate systems for drug delivery, *Nat Rev Drug Discov*, 13 (2014) 813-827.

37. L. Costantino, Drug delivery to the CNS and polymeric nanoparticulate carriers, *Future Med Chem*, 2 (2010) 1681-1701.
38. V. Linko, A. Ora, M.A. Kostianen, DNA Nanostructures as Smart Drug-Delivery Vehicles and Molecular Devices, *Trends Biotechnol*, 33 (2015) 586-594.
39. Y.H. Yun, B.K. Lee, K. Park, Controlled Drug Delivery: Historical perspective for the next generation, *Journal Control Release*, 219 (2015) 2-7.
40. Y. Matsumura, H. Maeda, A New Concept for Macromolecular Therapeutics in Cancer-Chemotherapy - Mechanism of Tumoritropic Accumulation of Proteins and the Antitumor Agent Smancs, *Cancer Res*, 46 (1986) 6387-6392.
41. K. Park, Drug delivery of the future: Chasing the invisible gorilla, *Journal Control Release*, 240 (2016) 2-8.
42. Y. Barenholz, Doxil (R) - The first FDA-approved nano-drug: Lessons learned, *Journal Control Release*, 160 (2012) 117-134.
43. D.H. Smith, J.R. Adams, S.R. Johnston, A. Gordon, M.F. Drummond, C.L. Bennett, A comparative economic analysis of pegylated liposomal doxorubicin versus topotecan in ovarian cancer in the USA and the UK, *Ann Oncol*, 13 (2002) 1590-1597.